SANDIA REPORT
SAND2016-8077
Unlimited Release
Printed August 2016

Lens and Camera Arrays for Sky Surveys and Space Surveillance

Mark R. Ackermann, David D. Cox, John T. McGraw, Peter C. Zimmer

Prepared by
Sandia National Laboratories
Albuquerque, New Mexico 87185 and Livermore, California 94550

Sandia National Laboratories is a multi-program laboratory managed and operated by Sandia Corporation, a wholly owned subsidiary of Lockheed Martin Corporation, for the U.S. Department of Energy's National Nuclear Security Administration under contract DE-AC04-94AL85000.

Issued by Sandia National Laboratories, operated for the United States Department of Energy by Sandia Corporation.

SAND2016-8077
Unlimited Release
Printed August 2016

Lens and Camera Arrays for Sky Surveys and Space Surveillance

Mark R. Ackermann
System Analysis Group

David D. Cox
MD/SSA/SC Programs

Sandia National Laboratories
P.O. Box 5800
Albuquerque, NM 87185-0757

John T. McGraw and Peter C. Zimmer
J.T. McGraw & Associates
Placitas, NM 87043

Abstract

In recent years, a number of sky survey projects have chosen to use arrays of commercial cameras coupled with commercial photographic lenses to enable low-cost, wide-area observation. Projects such as SuperWASP, FAVOR, Raptor, Lotis, PANOPTES, and Dragonfly rely on multiple cameras with commercial lenses to image wide areas of the sky each night. The sensors are usually commercial astronomical change coupled devices (CCD) or digital single reflex (DSLR) cameras, while the lenses are large-aperture, high-end consumer items intended for general photography. While much of this equipment is very capable and relatively inexpensive, this approach comes with a number of significant limitations that reduce sensitivity and overall utility of the image data. The most frequently encountered limitations include lens vignetting, narrow spectral bandpass, and relatively large point spread function. Understanding these limits helps to assess the utility of the data, and identify areas where advanced optical designs could significantly improve survey performance.

Acknowledgments

The authors wish to thank John Tonry (University of Hawaii, Institute for Astronomy) and Valery Terebizh (Crimean Astrophysical Observatory) for useful conversations, data, and insight that helped in the preparation of this report.

Contents

Figures

Tables

Executive Summary

Astronomers watch the sky, but not all astronomers are alike, and what they watch for varies significantly from one group to another. Following the invention of the refractor in 1608, early astronomers studied point targets with their telescopes but surveyed the skies with their eyes. Eventually portrait lenses were adapted for use as wide-field cameras for a variety of activities such as survey and star mapping work, meteor photography, asteroid and comet searches, active satellite tracking, and characterizing space debris.

While the precise tools and techniques for such endeavors have changed some over the past century, the advantage of a wide-field optical system is that a small number of instruments can survey large parts of the sky. Lens arrays offer many small observing programs the opportunity to put significant quantities of equipment into operation at a very low cost. As a result, we have seen a proliferation of observing projects using arrays of commercial cameras equipped with commercial photographic lenses. These systems perform well, but the convenience of low initial price and rapid availability comes with limitations. Understanding these limits is important for assessing the utility of the data and identifying areas where advanced optical designs could significantly improve survey performance.

Unlike apochromatic refractors, photographic lenses are not designed for the special demands of astrophotography. Instead, the designs are optimized for the many demands of general photography. Design compromises—including vignetting, bandpass narrowing, and chromatic weighting—make the lenses lighter, less expensive, and easier to manufacture, but also reduce sensitivity. Yet a significant advantage of lens systems is their ability to image fields wider than most, if not all, reflecting telescopes.

One alternative to commercial photographic lenses is to develop custom lenses specifically optimized for wide-field astronomical observation. These lenses can be designed with higher image quality, larger apertures, smaller relative apertures, and overall wider fields of view. Combining these improvements in a single optical system results in a significant improvement in sensitivity, with only a modest increase in cost.

While lens systems are attractive due to their small size and relative ruggedness, they are not the solution for all observing missions. When high sensitivity is required and continuous surveillance is not, arrays composed of smaller numbers of telescopes based on either catadioptric or medial designs appear to provide the most cost-effective solution. Specifically, many of the Russian designs for the International Scientific Optical Network program offer very wide fields of view with apertures larger than available commercial lens systems. Designs like these provide higher sensitivity without a significant increase in the number of systems necessary to cover the celestial region of interest.

Acronyms

APO	Apochromat or Apochromatic
CCD	Charge Coupled Device
DOE	US Department of Energy
DSLR	Digital Single Lens Reflex
EF	Electro-Focus
GEO	Geosynchronous Earth Orbit
ISON	International Scientific Optical Network
MTF	Modulation Transfer Function
NASA	National Aeronautics and Space Administration
NNSA	National Nuclear Security Administration
PSF	Point Spread Function
RMS	Root Mean Square
RSO	Resident Space Objects
SLR	Single Lens Reflex
SNL	Sandia National Laboratories
SNR	Signal to Noise Ratio
UD	Ultra-low Dispersion
USM	UltraSonic Motors
WASP	Wide Angle Search for Planets

1 Introduction

Astronomers watch the sky, but not all astronomers are alike, and what they watch for varies significantly from one group to another. Following Lippershey's invention of the refractor in 1608, early astronomers studied point targets with their telescopes, but surveyed the skies with their eyes. Eventually portrait lenses were adapted for use as wide-field cameras for survey and star mapping work, followed by meteor photography, asteroid and comet searches, tracking active satellites, watching for the afterglow of gamma ray bursts, looking for transiting exoplanets, and characterizing space debris [1]. While the precise tools and techniques for such endeavors have changed some over the past century, the advantage of a wide-field optical system is that a small number of instruments can survey large parts of the sky. More importantly, the low cost of these smaller instruments allows for greater numbers to be employed for longer periods of time, pushing sky surveillance into the realm of near continuous monitoring.

Today, a multitude of sky survey projects rely on arrays of low-cost, commercial camera lenses equipped with charge coupled device (CCD) imaging sensors. While inexpensive and readily available, the commercial optics have performance limitations that result from design trades intended to make the lenses lighter, less expensive, and easier to manufacture. The limitations reduce sensitivity and introduce other concerns for the quality of scientific knowledge that can be gained from the image data.

This report presents a brief overview of survey projects using arrays of camera lenses, explores the limitations of these systems, and discusses potential gains that might be achieved through the use of custom lens systems designed specifically for wide-field astronomical applications rather than general purpose photography.

2 Astronomical Lens Arrays

In recent years, astronomers have increasingly turned to low-cost camera lenses to collect images over wide areas of the sky, and in many cases, over wide temporal windows. The camera lens-based instruments are inexpensive, therefore allowing astronomers to increase sensitivity by dedicating multiple apertures to monitoring the same part of the sky, or they use multiple apertures to simultaneously cover a larger portion of the visible sky. Some classify these instruments as telescopes, while others consider them to be astrographs. Here we simply call these small, multiple-aperture instruments "lens arrays" to distinguish them from single and double aperture refractive astrographs such as the Red Lens Astrograph at the US Naval Observatory [2] and the Carnegie Double Astrograph at the Lick Observatory [3].

The widely published use of commercial lens-based instruments with CCD sensors dates back to the early 1990s when a distributed network of all-sky cameras was used to watch for meteors and fireballs. In the mid-1990s, other instruments were used for imaging the tails of comets Hyakutake and Hale Bopp [4]. Table 1 presents a list of lens-based survey projects. The list is not represented as being complete and the start dates are derived from published papers, which may, or may not, report the actual start date of the project. What is striking about this list is how extensively these systems are in use at present.

Of the lens array projects in Table 1, we highlight four that demonstrate some of the dominant features and the range of design space for lens arrays.

- The miniWASP survey is somewhat unique as it is an amateur project and combines commercial camera lenses and apochromatic (APO) refractors within the same small array [5].
- The RAPTOR-Q system, part of the "Thinking Telescope" project of Los Alamos National Laboratory, combines five small, but very wide angle, lenses to form an integrated all-sky monitoring system [6].
- DragonFly is a relatively new project, combining ten large, 400mm focal length lenses on a single mount [7].
- The lens array of the Honghe Station of the Purple Mountain Observatory in China appears to combine approximately 100 apertures mounted through the surface of a dome to provide a complete view of the visible sky [8].

Figure 1 presents pictures of the hardware used for the miniWASP survey (Figure 1a), the RAPTOR-Q system (Figure 1b), and the DragonFly instrument (Figure 1c). Figures 2a and 2b present exterior and interior views of the lens array system at Honghe Station in China.

Table 1. List of survey projects using arrays of commercial camera lenses

Project	Start	Name	Description	Ref.
AROMA-W	2010	**A**GU **R**obotic **O**ptical **M**onitor for **A**strophysical objects, **W**ide-field	Active galactic nuclei	9
ASAS	1997	**A**ll **S**ky **A**utomated **S**urvey	Photometric monitoring of the entire sky	10
ASAS-SN	2013	**A**ll **S**ky **A**utomated **S**urvey for **S**uper**N**ovae	Supernova search	11
AWCam	2012	**A**rctic **W**ide-Field **Cam**era	Exoplanet search from high latitudes	12
BOOTES	1997	**B**urst **O**ptical **O**bserver and **T**ransient **E**xploring **S**ystem	Follow up observation of Gamma Ray Bursts	13
CAMS	2010	**C**ameras for **A**llsky **M**eteor **S**urveillance	Minor meteor shower observation	14
CATS	2012	**C**ompound **A**rctic **T**elescope **S**urvey	10,000 square degree transient and transit search	15
CoCam & CoCam2	1997	**Co**met **Cam**era	Wide-field comet tail photography	4
COLD	2012	**C**ommercial **O**ptics for **L**EO **D**ebris	Wide-field search for space debris in LEO	16
ConCam	2003	**Con**(tinuous) **Cam**(era)	All-sky camera for monitoring transient phenomena	17
DragonFly	2014	Dragonfly Telephoto Array	Low surface brightness objects	7
EvryScope	2014	Wide Seer, full-sky gigapixel-scale telescope	Time-domain all sky observation for exoplanets, supernova etc.	18
FAVOR	2005	**FA**st **V**ariability **O**ptical **R**egistration	Subsecond time domain, wide-field imaging	19
FlyEye	2013	Fly's Eye Camera System	Large etendue time-domain survey	20
HAT	1999	**H**ungarian-made **A**utomated **T**elescope	Extra solar planet detection	21
Honge	unk	Honge Station Lens Array	LEO Satellite Tracking?	8
ISON VT-53e	2003	**I**nternational **S**cientific **O**ptical **N**etwork	Satellites in Low Earth Orbit	22
KELT	2007	**K**ilodegree **E**xtremely **L**ittle **T**elescope	Transiting exoplanets	23
LOTIS	1996	**L**ivermore **O**ptical **T**ransient **I**maging **S**ystem	Gamma ray burst follow-on observation (similar to ROTSE-1)	24
MASCARA	2014	**M**ulti-Site **A**ll **S**ky **Cam**e**ra**	Finding key targets for exoplanet atmosphere studies	25
MASTER-VWF	2009	**M**obile **A**stronomical **S**ystem of the **TE**lescope **R**obot - **V**ery **W**ide **F**ield	Prompt GRB observations	26
miniMegaTortora	2010	**T**elescopio **O**ttimizzato per la **R**icerca dei **T**ransienti **O**ttici **RA**pidi	Rapid transients, meteors, satellites in LEO	27
MMT-6	2012	miniMegaTortora - 6-lens system	Rapid transients, meteors, satellites in LEO	28
MMT-9	2014	miniMegaTortora - 9-lens system	Rapid transients, meteors, satellites in LEO	29
miniWASP	2012	mini **W**ide-**A**rea **S**earch for **P**lanets	Amateur exoplanet search similar to WASP	5
PANOPTES	2014	**P**anoptic **A**stronomical **N**etworked **OP**tical observatory for **T**ransiting **E**xoplanets **S**urvey	Transiting exoplanets	30
PASS	2001	**P**ermanent **A**ll **S**ky **S**urvey	Transiting exoplanets	31
PhotopicSkySurvey	2012	Photopic Sky Survey	All sky, high resolution, full color image	32
Pi of Sky	2009	Pi of the Sky	Search for short duration optical transients	33
QES	2010	**Q**atar **E**xoplanet **S**urvey	Exoplanet discovery	34
RAPTOR	2002	**RAP**id **T**elescopes for **O**ptical **R**esponse	Detect and track transient objects	6
ROTSE-1	1996	**R**obotic **O**ptical **T**ransient **S**earch **E**xperiment	Robotic search for optical afterglow of gamma ray bursts	35
Sentinel	1993	Sentinel Fireball All-Sky Camera Network	Continuous monitoring of the night sky for meteors	36
Sova-5	2014	Sight - part of the Pritsel system	Satellites in Low Earth Orbit	37
Starbrook (UK)	2010	United Kingdom Satellite Surveillance	Space situational awareness - satellite tracking	38
SuperWASP	1999	**Super W**ide **A**ngle **S**earch for **P**lanets	Photometry of planetary transits	39
TASS	1996	**T**he **A**mateur **S**ky **S**urvey	All sky survey	40
TrES	2004	**Tr**ansAtlantic **E**xoplanet **S**urvey	Exoplanet search	41
SSA	2012	Lens Array Demo	Space situational awareness - satellite tracking	
WASP0	2000	**W**ide-**A**ngle **S**earch for **P**lanets	Search for exoplanets	42
WIDGET	2004	**WID**efield telescope for **G**amma-ray burst **E**arly **T**iming	Gamma-ray burst optical afterglow monitoring	43
XO	2003	**XO** Project	Detection and Characterization of Transiting Extrasolar Planets	44

(a) miniWASP (b) RAPTOR-Q (c) DragonFly

Figure 1. Three modern lens array projects.

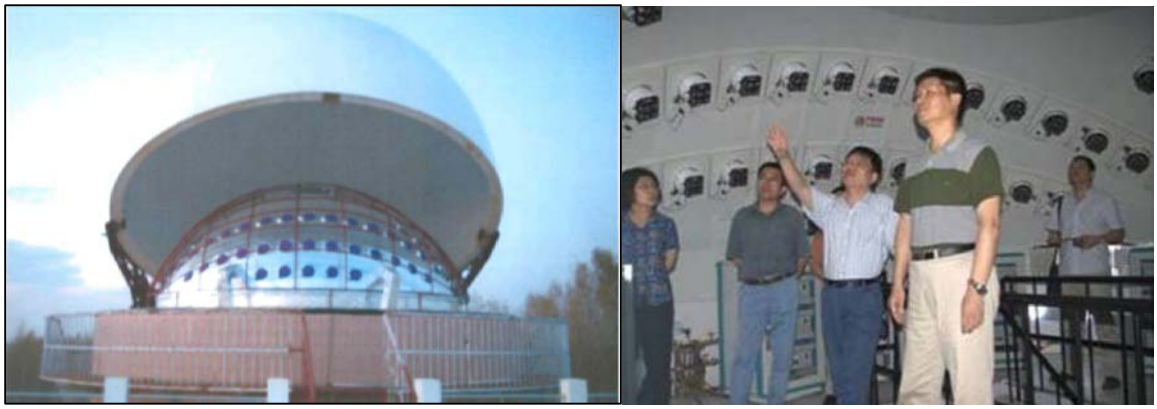

(a) exterior view (b) interior view

Figure 2. The lens array at Honghe Station, China.

While astrograph arrays made with commercial lenses and cameras are rapidly increasing in popularity, it is interesting to note that the use of lens arrays for astronomical observations is by no means a recent development. The literature contains multiple examples of camera lenses being used to build custom wide-field astronomical instruments for sky mapping and meteor photography, but these are normally single aperture instruments.

The first recorded use of a camera lens for dedicated astrophotography (not solar or lunar photography) is credited to William Simpson of the U. P. School in Aberdeen, Cape Province, South Africa [45]. On October 3, 1882, Simpson captured an image of the “Great Comet of 1882” and sent it to David Gill, then director of the Royal Observatory at the Cape of Good Hope. The image was of no scientific value due to camera motion [46], but it demonstrated to Gill, the potential for wide-field astrophotography. A reproduction of Simpson’s comet image is seen in Figure 3. A few weeks later, Gill used an f/4.4 Ross rapid portrait lens (built by Dallmeyer), to capture an image of the great comet of 1882 [47]. In the finished photograph Gill noticed that the lens and film were sufficiently sensitive to record many stars, which gave him the idea that portrait lenses could be used to develop star catalogs. A reproduction of Gill’s original photograph is seen in Figure 4.

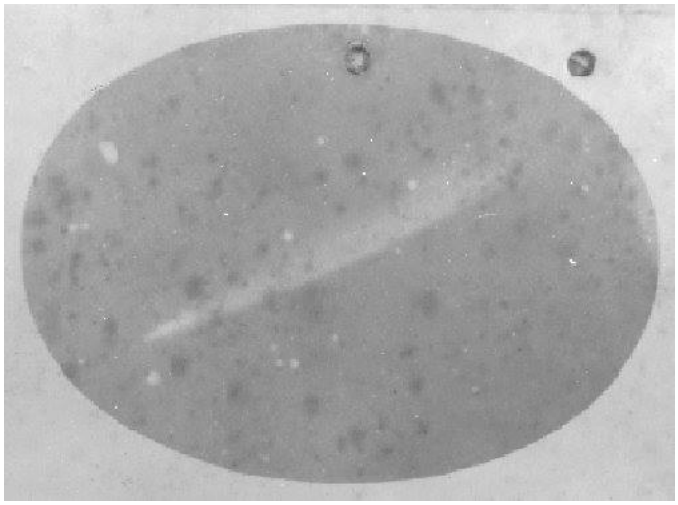

Figure 3. Simpson's image of the Great Comet of 1882 [48].

Figure 4. The great comet of 1882, by David Gill.
Image credit: Wikimedia Commons.

Perhaps the most famous portrait lens astrograph was known as the "Willard Lens." This was a Petzval-type portrait lens made by Charles Unser in New York City in the 1850s, and distributed by Willard & Company [49]. The lens had a 5.85-inch aperture and 31-inch focal length. The Petzval optical system is important in astronomy as it has been used both for astrograph lenses and apochromatic refractors. Figure 5 shows the layout of a Petzval portrait lens. The legendary astronomer, E.E. Barnard began experimenting with the Willard lens in 1889. Later, the lens was mated to a mount and drive mechanism and became known as the Croker Telescope, seen in Figure 6. An image of Messier object #31, then believed to be a nebula, as captured by Barnard in 1889, is seen in Figure 7.

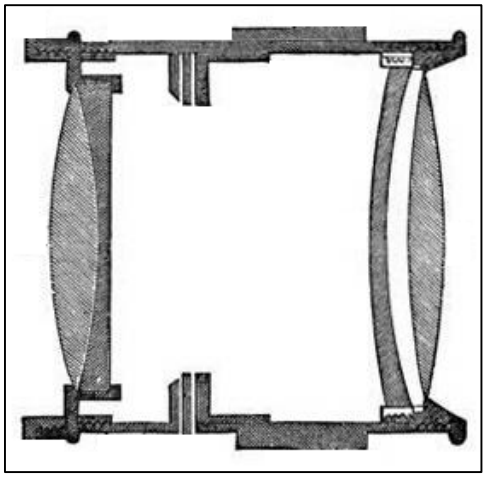

Figure 5. Layout of Petzval-type portrait lens.

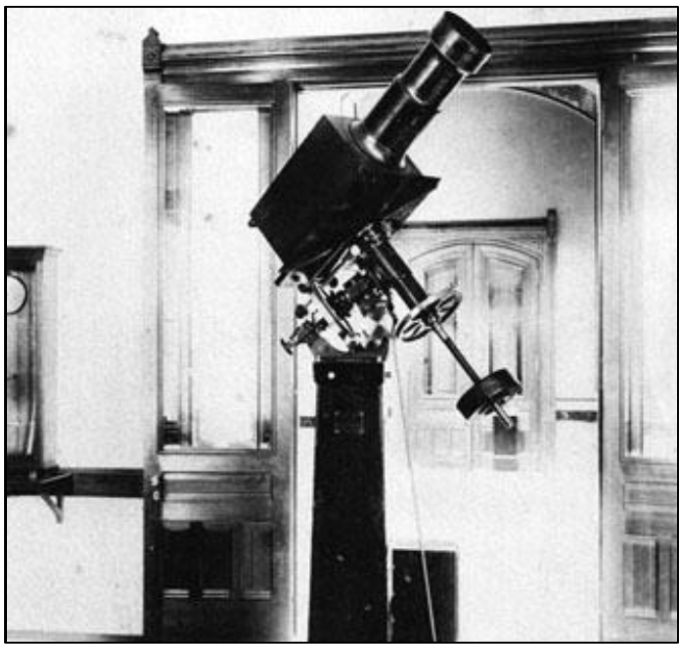

Figure 6. The Crocker Telescope featuring the Willard lens [50].

Figure 7. Image of M31, by E.E. Barnard, 1889 [51].

While there are numerous examples of commercial camera lenses being used for astrophotography since 1882, there are also multiple examples of wide-field lens systems being purposely built to support astrophotography. Two of the better-known examples of such lenses are the 24-inch Bruce Telescope and various examples of the Ross-type lens astrograph. The Bruce Telescope was a 24-inch aperture Petzval-type lens built specifically for astrophotography [52]. It was ordered in 1889 but not completed until 1893 when it was installed at the Cambridge Observatory of the Harvard College. At 24 inches of aperture, the Bruce Telescope was enormous. Clearly, no commercial camera lenses of this size were available. Compared to smaller Petzval-type lenses, the field of view was reduced significantly to accommodate available glass plates. The narrower field also allowed for better correction of aberrations and higher overall image quality. An image of the Bruce Telescope is seen in Figure 8.

Figure 8. 24-inch aperture Bruce Telescope of the Harvard Observatory [53].

In 1918, Frank Ross, then working for the Eastman Kodak company, modified the World War I era Hawkeye aerial camera lens to improve image quality for astronomical photography [54]. This work was not simply to repurpose an existing aerial camera lens for astrophotography. Ross actually reformulated the lens design to reduce aberrations and improve the field of view. The lens consisted of four separated elements, but unlike the Petzval design, the Ross lens was symmetric about the aperture stop, which resulted in reduced distortion with similar improvements in coma and astigmatism. Various versions of the Ross lens were built for astronomical research, ranging in aperture from 3 inches to as large as 20 inches. One example of large Ross-type astronomical lenses is the double astrograph of the Yale Southern Observatory [3]. A picture of the twin lenses is seen in Figure 9.

Figure 9. Twin lenses of Yale Southern Observatory double astrograph [55]

Similar to the Bruce Telescope, a custom lens design for the Yale astrograph was sought to improve utility for astronomical research. Multiple commercial designs similar to the Ross lens layout were available as early as 1898 [56], but the Ross lens was specifically formulated to improve image quality beyond that which was available from these commercial alternatives.

In the late 1890s, the famous Yale astronomer, Edward Pickering, used an array of six cameras with portrait lenses, all on a common mount, to photograph meteor showers. The instrument was called the Yale Meteorgraph [57]. Eventually a second system with six lenses was built and located a few miles away. At one point, both instruments were equipped with a large rotating shutter in an attempt to obtain timing information to determine meteor velocities. Each lens could image an area of 600 square degrees with the complete instrument covering 2400 square degrees (accounting for image frame overlap). A picture of the Yale Meteorgraph is shown in Figure 10 [58].

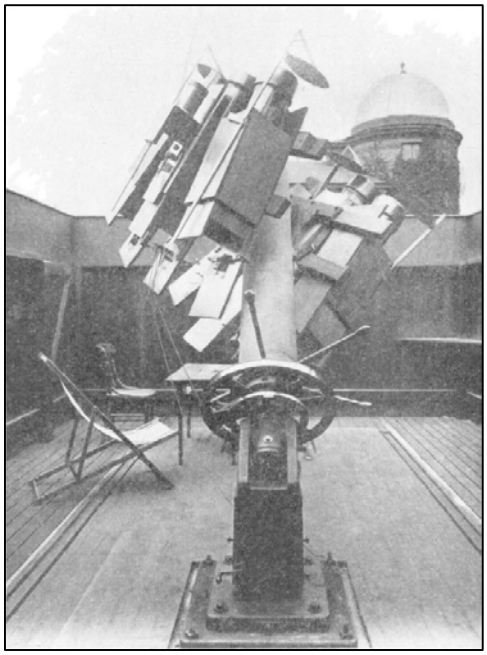

Figure 10. The Yale Meteorgraph.

Decades later saw the development of the Remeis camera for the Bamberg Southern Sky Patrol. Various partial descriptions of this instrument exist with different configurations, but the most common design featured six cameras mounted three each in two boxes, all on a common tracking mount. A later configuration increased the lens count to ten cameras with two boxes containing two cameras each added to the common mount. Two separate systems were operated to cover the northern and southern skies. The northern sky patrol operated from 1928-1939, while the southern survey operated from 1963-1976 [59]. A picture of the Remeis camera with ten apertures is shown in Figure 11.

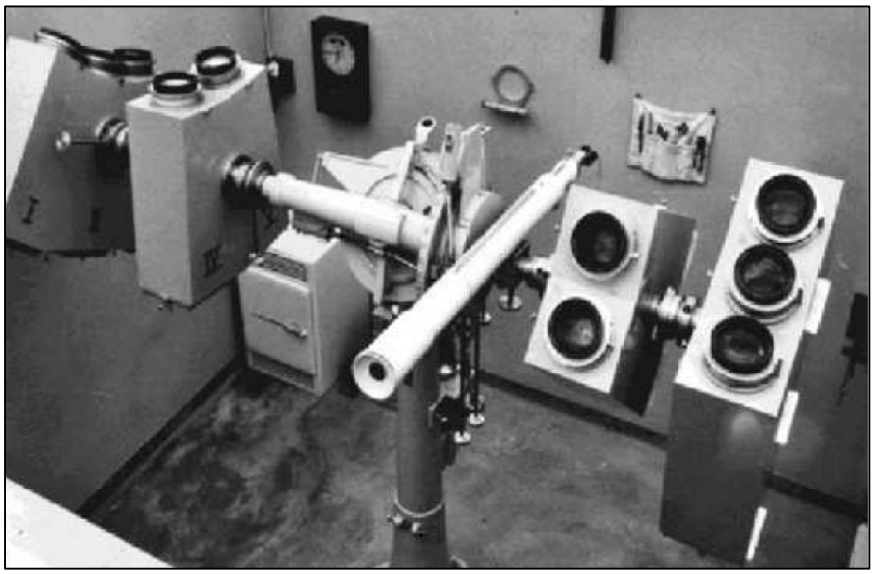

Figure 11. The Remeis camera of the Bamberg Southern Sky Patrol.

The Harvard Observatory built the Damon Telescope in the early 1960s and operated them at two sites from 1965 to 1990. The telescopes were actually three small cameras that recorded wide-field images onto photographic plates, with all three cameras imaging the same area of the sky. Each site was equipped with three cameras, with one each dedicated to red, blue, and yellow wavelengths [60]. A picture of the Damon cameras at the South African observing site is shown in Figure 12. In recent years these plates have been digitized to enable continued exploitation of these data.

Figure 12. The Damon Telescope (cameras) in South Africa.

Lens arrays for wide-field imaging were not solely the pursuit of major universities and observatories. Beginning in the mid-1980s, the Dutch Meteor Society began fielding an array of up to eleven 35mm, single lens reflex (SLR) film cameras [61]. Several versions of the array were fielded over the next decade. The camera array, combined with the wide-field lenses covered most of the visible sky, thereby ensuring images of streaks during meteor showers. An image of the Dutch camera array is shown in Figure 13. A similar concept was pursued by Reeves during the 1990s, but his array consisted of only eight SLR film cameras [63]. A picture of Reeve's array is seen in Figure 14.

Figure 13. Camera array of the Dutch Meteor Society [62].

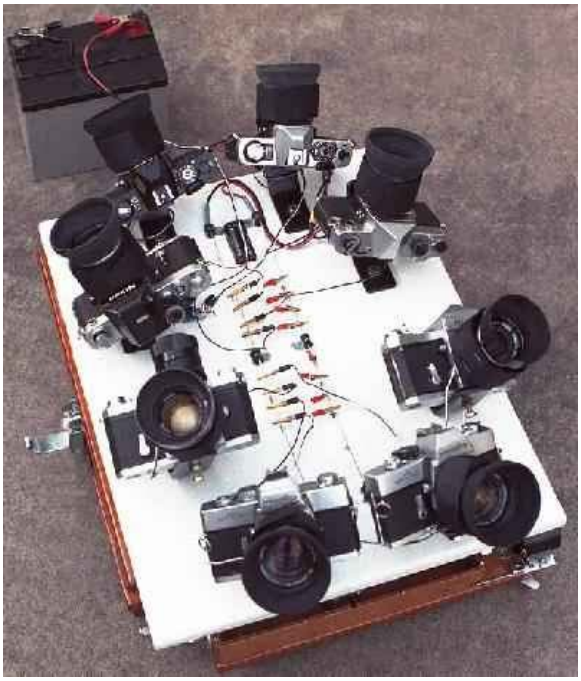

Figure 14. Meteor camera array of Reeves.

3 Limitations of Commercial Lens Systems Used for Astronomy

3.1 Photographic Objectives

Commercial camera lenses have a long history of use for recording wide-field images of the sky. Their primary attractiveness results from their short focal length, large numerical aperture, wide field of view, small size, and light weight. Low cost and relative abundance only add to their attractiveness.

Modern commercial photographic objectives are available from many manufacturers in myriad combinations of focal length and relative aperture. They are inexpensive, relatively lightweight, have good image quality for general photography, and are readily available. These lenses all, however, have a number of characteristics that potentially limit their utility for astrophotography and space surveillance work. These limitations stem from the availability of optical glass, the desire to keep the lenses small and light, and the need to keep the lenses affordable for their targeted consumer group. Simply put, commercial photographic lenses do not require the same level of image quality traditionally seen in images for astronomical research. However, as was true in the late 19th century, these lenses can play an important role in astronomy and sky survey work provided their limitations are understood. For situations where such limitations would pose a problem, the solution is, again, to turn to custom optical lens designs.

The primary limitations found in commercial camera lenses include the following:

- vignetting
- wavelength bandpass narrowing
- wavelength bandpass weighting
- center of field weighting of image quality
- an overall relaxing of image quality to achieve wider fields
- thermal stability.

Each limitation is discussed below. Another issue to consider is the annoying tendency of manufacturers and vendors to obscure the true performance of commercial lenses by providing data that are incomplete and potentially misleading. Examples of such behavior are spot diagrams without wavelength references; tiny spots shown in the center of huge square boxes such that it is impossible to tell how large the spots really are; modulation transfer function plots showing medium to high performance at low resolution; and almost no discussion regarding the range of wavelengths the lens was designed to cover. While these advertising strategies are annoying, here we limit our discussion to limitations of the lens systems themselves.

3.1.1 Vignetting

Vignetting is the apparent darkening of an image, which increases the further one looks off the optical axis. Some refer to this as the darkening of the corners in photographic images. For our purposes, we shall consider two types of vignetting: natural and design induced. An example of photographic vignetting can be seen in Figure 15.

Figure 15. Example of vignetting.
Image credit: Wikimedia Commons.

Natural vignetting results from geometric factors of the lens and the object being photographed [64]. When one considers a point in the object plane located at an angle of θ degrees off the optical axis, the apparent size, or projected area, of the physical aperture decreases as the cosine of θ. Similarly, an element of area on the object decreases in projected area, and hence, projected luminance, by the same cos(θ). Finally, the intensity of light from this element of object area decreases according to the inverse square law. Since the distance to an off axis point increases proportional to 1/cos(θ), the intensity decreases proportional to $1/\cos(\theta)^2$. Combining all the factors yields a natural vignetting function proportional to $\cos(\theta)^4$. Note that this derivation applies to objects imaged at a finite conjugate.

When imaging point sources at an infinite distance, it is likely that the $\cos(\theta)^4$ law breaks down and is replaced by something closer to a simple cos(θ) dependence as it makes no sense to account for projected area of the source or variation in solid angle with field angle.

Design-induced vignetting exists in most photographic lenses and is generally much more pronounced than natural or geometric vignetting. When purchasing a lens for low-light photography, consumers look for the product with the largest numerical aperture, or smallest f-number that meets their budget and needs. Manufacturers advertise lenses by their speed, or largest relative aperture. For example, lenses with a maximum aperture of f/1.4 are relatively common, but more expensive than slower optics. The problem is that these lenses are almost always only f/1.4 in the center of the field, with the effective relative aperture decreasing rapidly as one moves off the optical axis. This effect can be seen in Figure 16, which shows the vignetting for a 16mm f/1.4 lens at five different aperture settings [65]. Note the significant falloff in relative illumination at f/1.4 as one approaches the edges of the images. This dependence on

field angle is well in excess of the simple $\cos(\theta)^4$ dependence that would normally be expected for images of extended objects.

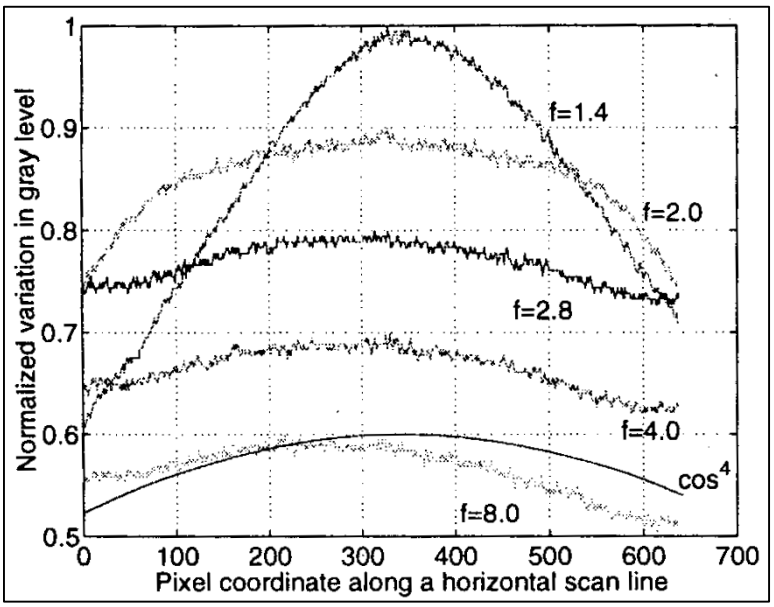

Figure 16. Measured vignetting data for a 16mm, f/1.4 lens [65].

Design-induced vignetting results from a number of factors that all conspire to limit the diameter of lenses both in front of and behind the physical aperture stop in commercial lens designs. One factor is the types of glass available for simultaneous correction of chromatic and geometric aberrations. Some glass types that provide good correction also result in significant curvature of individual lens elements. This curvature limits the physical diameter of the lens to help avoid very thick lenses, zero or negative lens edge thickness, and curves that result in off-axis light rays striking lens elements at extreme angles.

As an example, consider the 100mm, f/1 lens designed by Angenieux for the National Aeronautics and Space Administration (NASA), as described in US Patent 2,701,982 [66]. The lens was used to photograph the dark side of the moon during the Apollo 8 mission prior to the first manned landing. The lens did not perform as NASA had hoped, which led to development of the Zeiss 50mm, f/0.7 lens made famous by the legendary film director, Stanly Kubrick [67]. The layout for the Angenieux lens, as described in the patent, is shown in Figure 17.

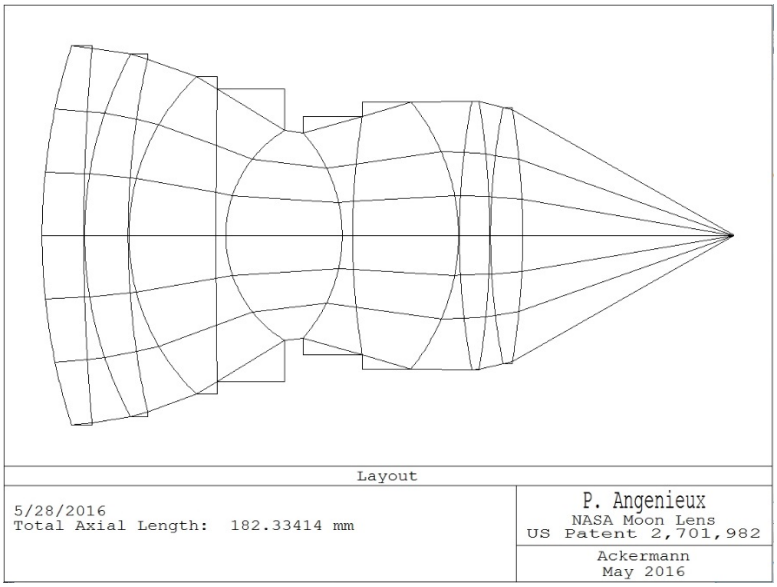

Figure 17. Angenieux moon lens, optical layout.

The lens is described as having six components, but it actually has eight lens elements arranged into six groups. The design, as seen in Figure 17, only shows optical rays for a point on the optical axis. The design was adjusted by Angenieux to provide lens diameters that gave 100% relative illumination on axis, and lens element thickness values were adjusted so that each lens could actually be realized. The problem with this design, however, becomes apparent when we examine the effect of off-axis light rays. In Figure 18, we see the effect of light rays for a point 10 degrees off axis. To fully accommodate these light rays, the various lens elements need to increase in diameter to the point where there are negative edge thickness values and adjacent lenses growing into one another. Clearly this is not possible, so the designer limited the element diameters such that the overall objective has an effective aperture of f/1 only in the center, with light transmission falling off towards the edges of the field as seen in Figure 19. The vignetting plot is shown in Figure 20. Note that this vignetting plot only covers a field the size of a 35mm single lens reflex camera. If the lens were to be used for larger format cameras, the field angles would be wider and the light falloff would be greater. Many commercial lenses suffer far greater vignetting than the Angenieux design.

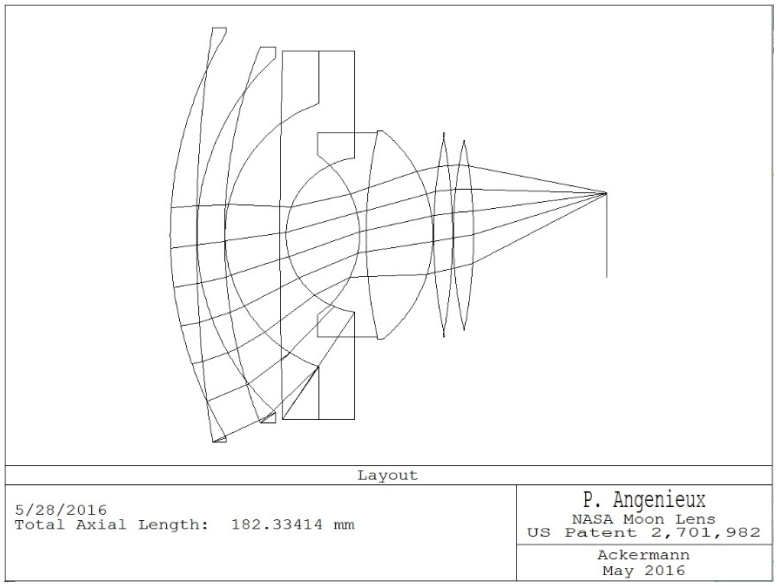

Figure 18. Angenieux design with light rays for 10 degrees off axis.

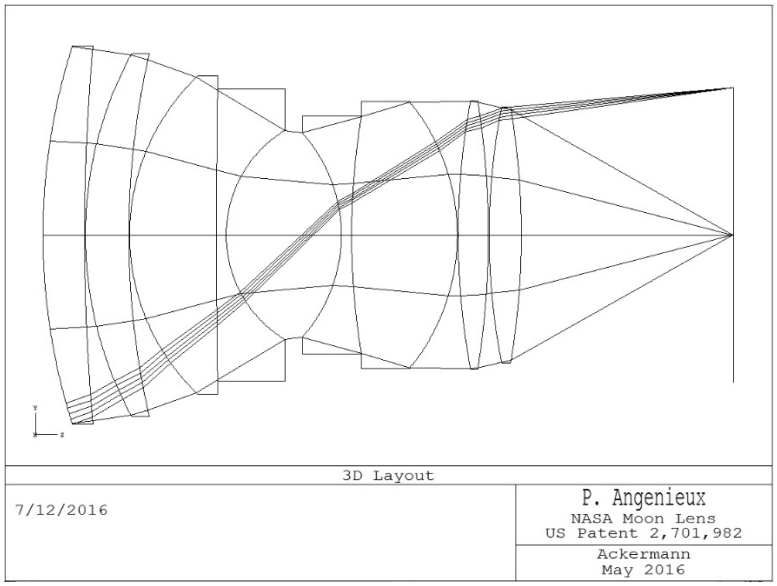

Figure 19. Angenieux design with light rays for center of field, and 23 degrees off axis.

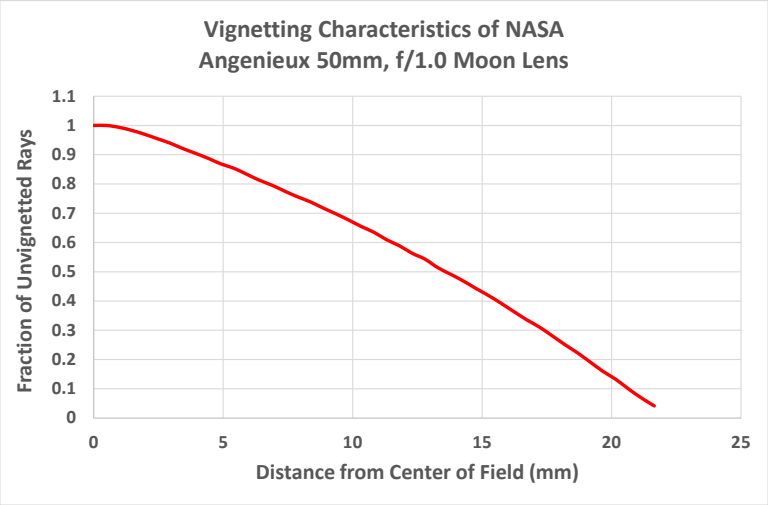

Figure 20. Vignetting of the Angenieux lens across a 35mm SLR image.

Astute readers will note that the Angenieux lens was actually a custom design for NASA and not a commercial product. It is however, a valid example, as the Angenieux design is very similar to many patented designs that ended up as commercial objectives for high-end 35mm SLR camera systems, such as those offered by Nikon, Canon, Leica, Minolta, and Olympus.

3.1.2 Wavelength Bandpass Narrowing

The most difficult part of designing refractive optical systems with positive or negative power, as opposed to afocal systems, is the correction of chromatic aberration. Most systems have sufficient degrees of freedom to achieve highly corrected images for monochromatic light, but correction across a broad band of wavelengths quickly becomes difficult. As a result, refractive systems are designed only for the range of wavelengths required for their application and, frequently, this band is narrowed somewhat from what would be required for normal operation. The narrower range of wavelengths helps to simplify the optical design and improve correction, but only over the specific range of wavelengths used to drive the design.

The human eye is sensitive to light in the range of 400 to 700 nm. The first refractive telescopes had a simple lens and could bring only a single wavelength of light to focus at a time. The first color-corrected refractors were known as achromats. They were designed to bring two colors of light to a common focus. Frequently, the early achromatic refractors would bring the spectrographic C (656 nm) and F (486 nm) lines to a common focus [68]. The wavelengths in between the C and F lines were close to focus, but not in focus, thereby resulting in star images that appeared slightly out of focus. A plot of the chromatic focus shift for a simple f/10 achromat illustrates this, as seen in Figure 21. Human operators would frequently adjust focus to give the best visual image, which would place the wavelengths of best focus somewhere in between the C and F lines. The net result is that wavelengths longer than the C line, or shorter than the F line, are significantly out of focus.

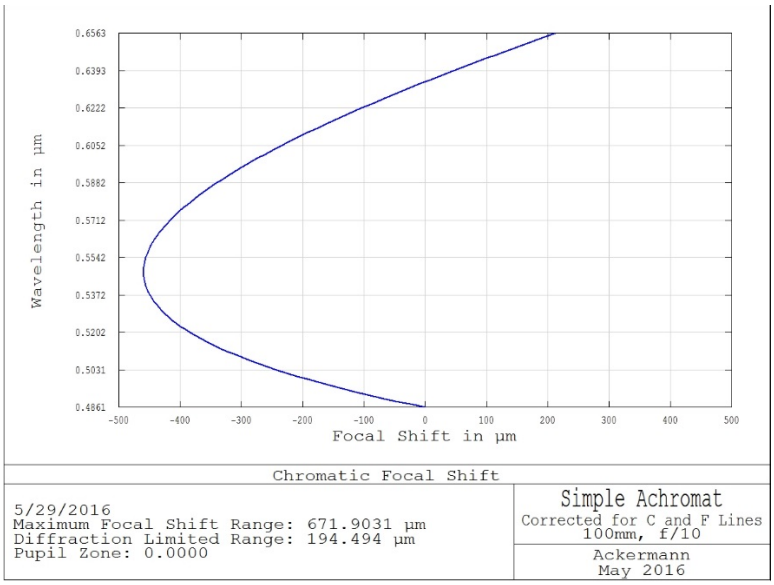

Figure 21. Chromatic focus shift for an f/10 achromatic objective.

While the earliest photographic lenses were corrected for blue wavelengths to match the sensitivity of the available photographic emulsions, for more than 100 years common camera lenses have been designed to operate across most of the visible spectrum. However, to ease the design process, the range of wavelength is narrowed with less expensive lenses corrected for the C, d (586 nm), and F lines. The resulting optical system performs well across this range but begins to lose definition towards both the red and blue ends of the spectrum. Most designers believe this to be a reasonable compromise as the eye and many films are most sensitive to the middle portion of the visible spectrum and less sensitive at either limit.

More expensive modern lenses are often corrected for the C, d, F, and g (436 nm) lines, thereby improving performance for blue wavelengths. Very few lenses are corrected for a wider range of wavelengths. When using CCD photon sensors, these wavelength limitations can become problematic as most CCDs are sensitive from wavelengths less than 400 nm on the blue end, to 1100 nm on the red end. The quantum efficiency varies significantly across this range, but most CCDs retain significant sensitivity in the 700 to 850 nm range. When used with commercial camera lenses, one must either accept a loss of image quality due to the poor focusing of wavelengths outside the design range, or limit the sensor with a bandpass filter.

As an example, consider the 50mm, f/1.2 camera objective described in US Patent 4,364,643 [69]. Canon originally optimized this lens for the C, d, F, and g lines. Simulating this design, with adjustments and reoptimization to account for currently available glass results in root mean square (RMS) spot radius ranging from 25 to 50 µm across most of a 43-degree full field, as shown in Figure 22. If instead, the lens is used for typical astronomical imaging with wavelengths ranging from 390 to 900 nm, the RMS spot radius range increases to approximately 100 µm across most of the field, as shown in Figure 23. The important point is that most commercial lenses were never intended to be used over such an extensive range of wavelengths, yet astronomers will, at times, operate these lenses well outside their designed performance envelope.

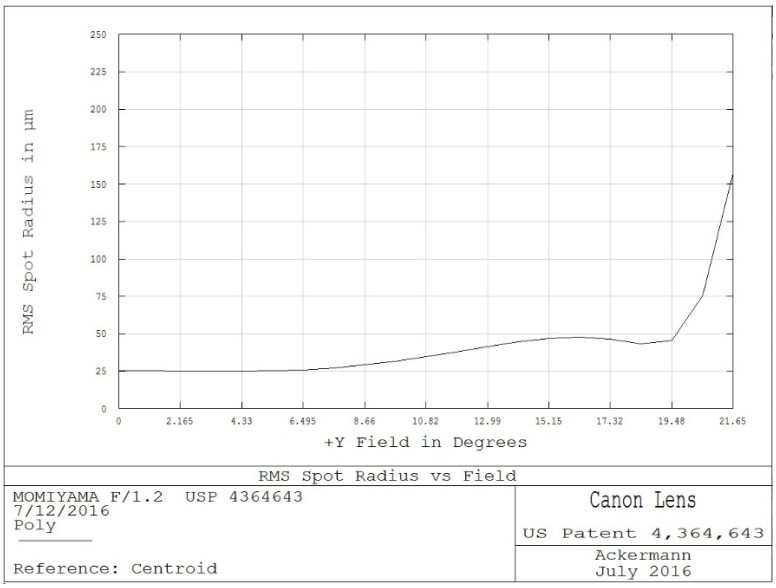

Figure 22. RMS spot radius for Canon 50mm f/1.2 lens, 436-656 nm.

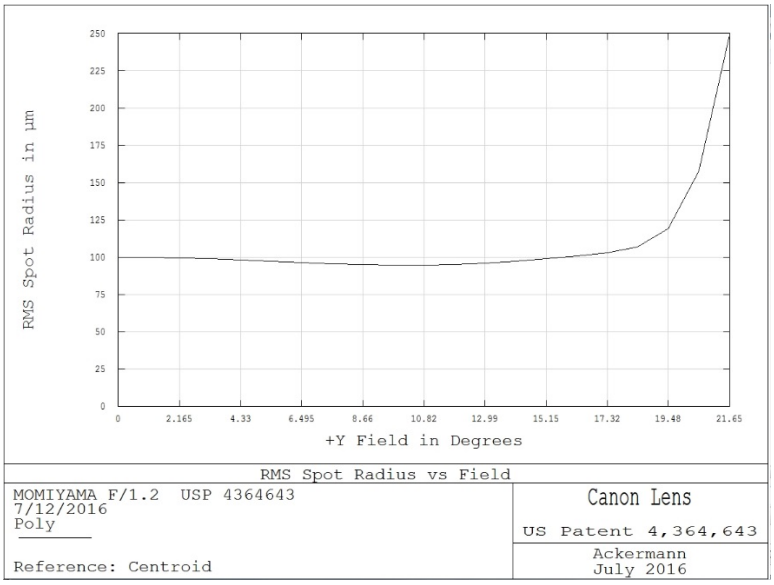

Figure 23. RMS spot radius for Canon 50mm f/1.2 lens, 390-900 nm.

3.1.3 Wavelength Bandpass Weighting

Another trick used by optical designers, apparently to improve the performance of refractive optical systems, is to adjust the weighting across the wavelength bandpass to reduce the influence of colors at the red and blue end of the spectrum. This well-known but not well-documented practice is used by many, but not all, optical designers.

In optical design programs such as the well-known Zemax [70], the user specifies a number of discrete wavelengths over which the design will be simulated and optimized. Along with each wavelength, the

operator can enter a relative weight. Some designers use uniform weighting [71] while other designers weight the individual wavelengths to account for variations in the solar illumination spectrum [72], or variations in quantum efficiency of CCDs as a function of wavelength. The thought is that if the eye, or electronic sensor, is less sensitive at a given wavelength, the impact of larger spot diameters at those wavelengths is reduced. Since many optical designs prove to be most difficult at the outer limits of their chromatic bandpass, reducing the importance of these wavelengths helps to improve overall performance of the optical system at the central, and more easily sensed, wavelengths.

Consider the quantum efficiency curve for the KAF-50100 front-illuminated CCD as shown in Figure 24 (upper trace for the microlens configuration). The quantum efficiency at 420, 550, and 680 nm is 42%, 62%, and 47%, respectively. For an optical design optimized at these same wavelengths, some designers choose to assign weights to the wavelengths of 0.677 at 420 nm, 1.0 at 550 nm, and 0.76 at 680 nm. This approach produces a better design for 550 nm light while allowing the spot diameters to relax slightly at 420 and 680 nm.

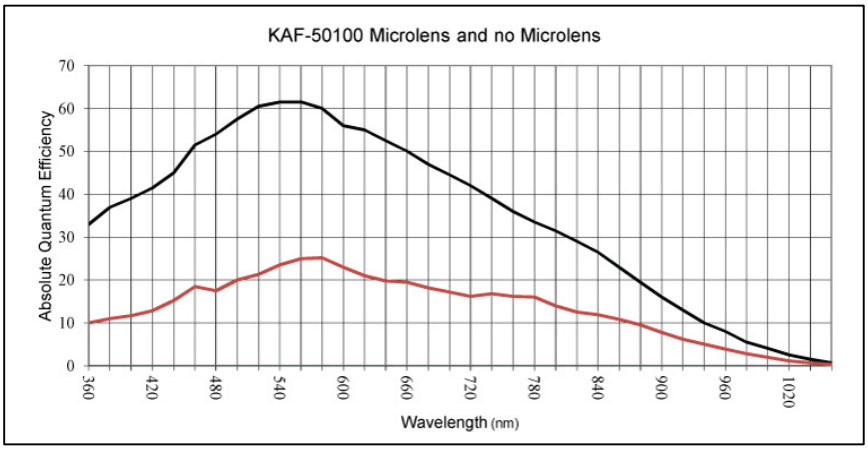

Figure 24. Quantum efficiency of KAF-50100 front-illuminated CCD [73].

Another school of thought suggests that inverse weighting of wavelengths in the design process is more appropriate. Since CCDs and the human eye are generally less sensitive at both the blue and red end of the spectrum, one should overweight these wavelengths to force smaller spot diameters. The tighter concentration of light at these wavelengths, in theory, should partially offset the reduced sensitivity of the sensor. In the case of the sensor from Figure 24, the weighting would be 1.477 at 420 nm, 1.0 at 550 nm, and 1.316 at 680 nm.

The final option is simply to use uniform weighting for all wavelengths. This is the approach preferred by the authors. The various options for wavelength weighting are plotted in Figure 25.

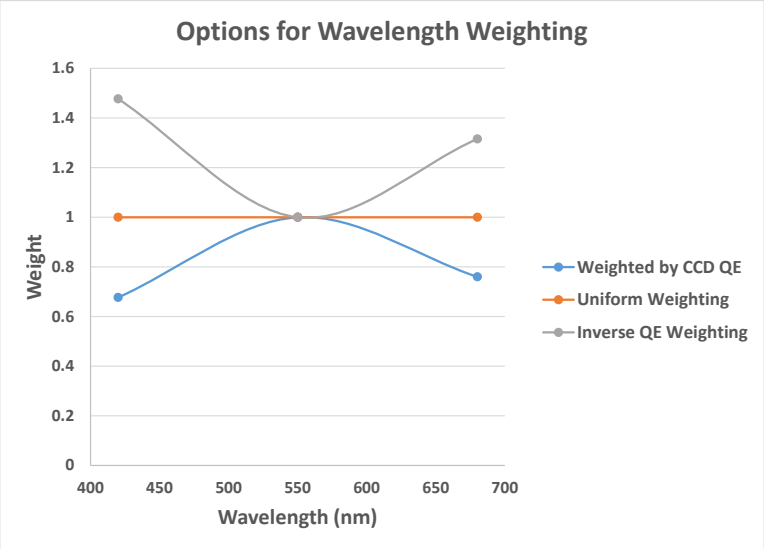

Figure 25. Options for weighting wavelengths in lens design.

3.1.4 Image Quality Center Weighting

Most photographic objectives are designed to have higher resolution in the center of the image than towards the corners. The usual rationale is that the subject of the photograph will normally be located somewhere near the center. Since the eye will be drawn to the center of the image, that is where the highest image quality should reside. While this may be true in many cases, it is also true that it is easier to design optical systems with higher image quality on-axis than off-axis.

The image quality of most commercial lenses is reported by their modulation transfer function (MTF), which reports the modulation, or contrast ratio, as a function of resolution (line pairs per mm on the sensor or film) as a position of field angle, or location on the image plane. The MTF curves for the Leica Noctilux-M 50mm f/0.95 Aspheric commercial camera lens are shown in Figure 26 [74]. This lens is the finest, high-speed, normal focal length lens available for 35mm photography. One problem with published MTF curves is that manufacturers frequently make it difficult to interpret the data presented, by omitting a legend for each curve plotted. Fortunately Leica has not done this and the data in Figure 26 are of use. The curves are for 5, 10, 20, and 40 line pairs per millimeter, with the lowest resolution having the highest modulation, on axis. The solid and dashed lines correspond to sagittal and tangential resolution. The horizontal axis corresponds to the location on the image plane in millimeters from the center.

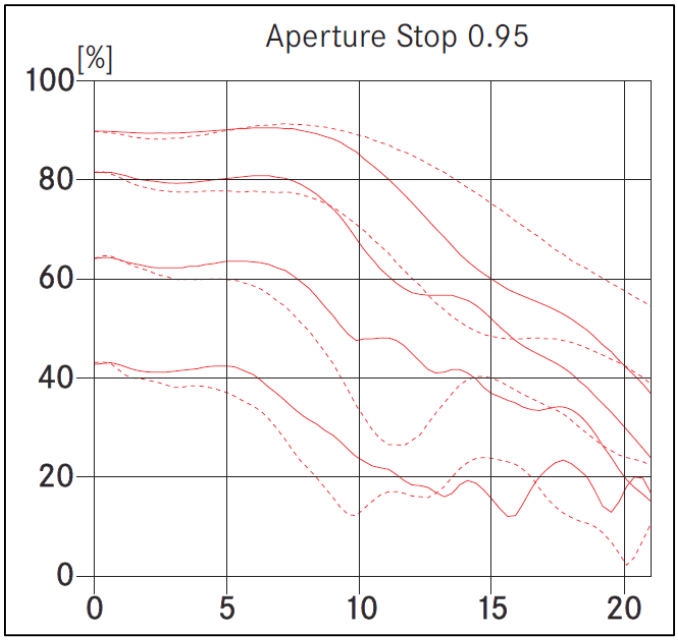

Figure 26. MTF curves for Leica Noctilux-M, 50mm f/0.95 Aspheric lens [74].
(See text for explanation.)

Figure 26 clearly shows the effect of center weighting image performance. The modulation at each resolution degrades from the center of the field to the edge (corners). Lower resolution corresponds to larger spot diameters. While center-weighting image performance might be acceptable for photographic purposes, in astronomical applications, high image quality across the entire frame is most desirable.

MTF curves have their use, but when calculating the sensitivity of an optical system for detecting faint sky targets, the RMS diameter of the point spread function (PSF) is actually more useful. This practice introduces some errors as one must assume a shape for the distribution of energy across the PSF and the shape, as seen in the MTF plot for the Noctilux lens, is more than likely quite complex and not accurately described by a single Gaussian distribution function. If however, we assume that the PSF of this lens can be approximated by a Gaussian distribution, then we can use the MTF curve to calculate an approximate RMS spot size as shown in Figure 27. This single curve combines sagittal and tangential spot characteristics into a single RMS-averaged spot diameter. Figure 27 clearly shows that image quality is center weighted for this lens.

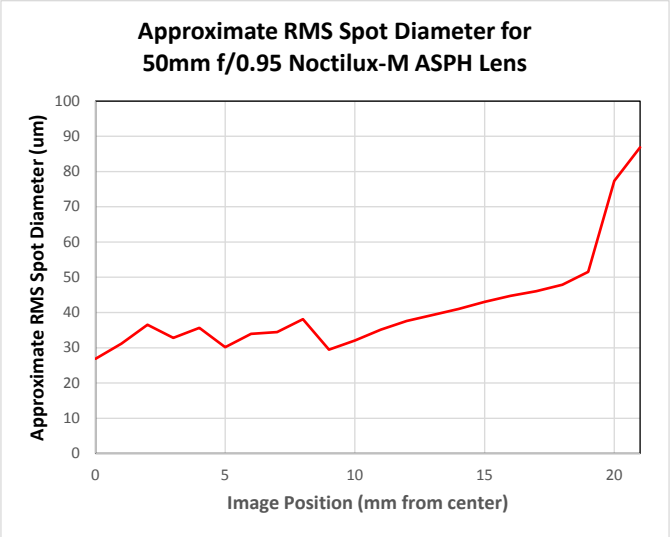

Figure 27. Approximate averaged RMS spot diameter for Noctilux lens.

3.1.5 Overall Relaxing of Image Quality

With lower cost commercial camera lenses, there is a tendency of the manufacturers to reduce the lens element count to help meet a desired price point. The net result is usually an overall loss of image quality across the entire image field. High-end optics, such as the premium fixed focal length lenses by Nikon, Canon, and Leica still require design trades but usually feature a higher overall image quality. This increase in performance often comes at the expense of greater complexity, higher lens element count, and a correspondingly higher price. For example, the Canon EF 50mm f/1.0 objective includes 11 lens elements and 2 aspheric surfaces. The image quality is very high, but the lens is complex and expensive. When used for astronomical applications, one finds that this lens still includes all the limitations mentioned in Sections 3.1.1 to 3.1.4.

To further illustrate the point, we compare two Nikon designs for lenses of 135mm focal length. The first example is an older design, dating to 1977, with a maximum aperture of f/2.0 as described in US Patent 4,062,630 [75]. The design is fairly simple and should have been a moderately priced optic in its day. It has six elements arranged in four groups and is optimized for the C, d, F, and g lines. The optical layout is shown in Figure 28, with the approximate ray-traced spot diagram performance shown in Figure 29. The optical performance is good, but by no means spectacular. Image quality is lower across the entire field when compared to the latest high-dollar commercial lenses available today.

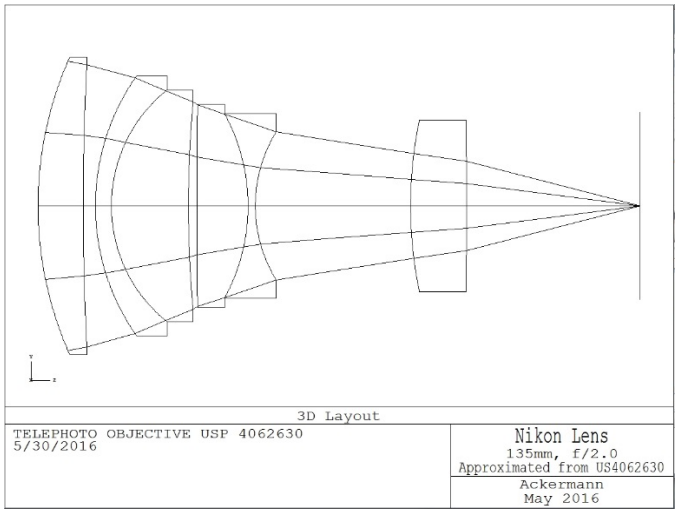

Figure 28. Nikon 135mm, f/2.0 lens layout.

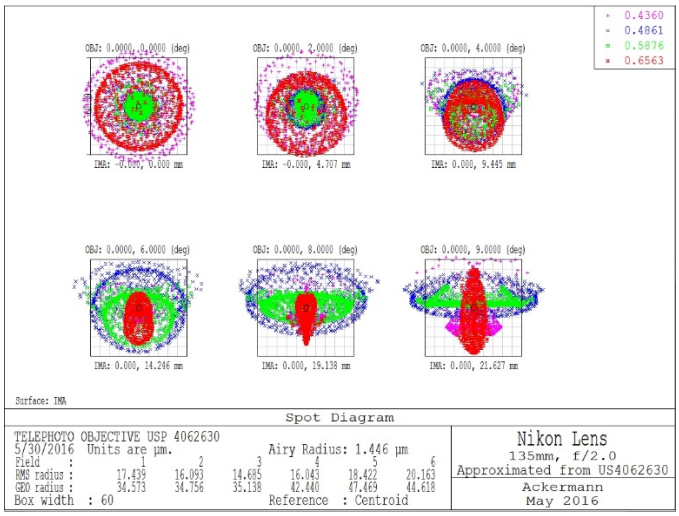

Figure 29. Approximate performance of Nikon 135mm, f/2.0 lens.

The second example is a newer design, dating to 2012, with a maximum aperture of f/1.8 as described in US Patent Application Publication 2012/0050872 [76]. The design is rather complex and would represent a high-end optic in today's market. It has 15 elements arranged in 9 groups and is also optimized for the C, d, F, and g lines. The optical layout is shown in Figure 30, with the approximate ray-traced spot diagram performance shown in Figure 31. What cannot be seen in the figures is that the newer design also includes four elements made from two different types of low dispersion glass. The older design contained no special types of glass. Image quality for the newer design is very high across the entire field. To make a direct comparison of the two lenses less difficult, the image scale in Figures 29 and 31 are the same.

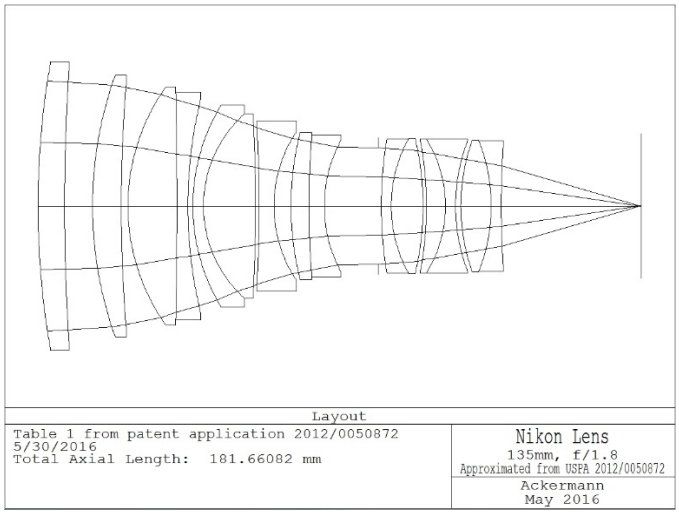

Figure 30. Nikon 135mm, f/1.8 lens layout.

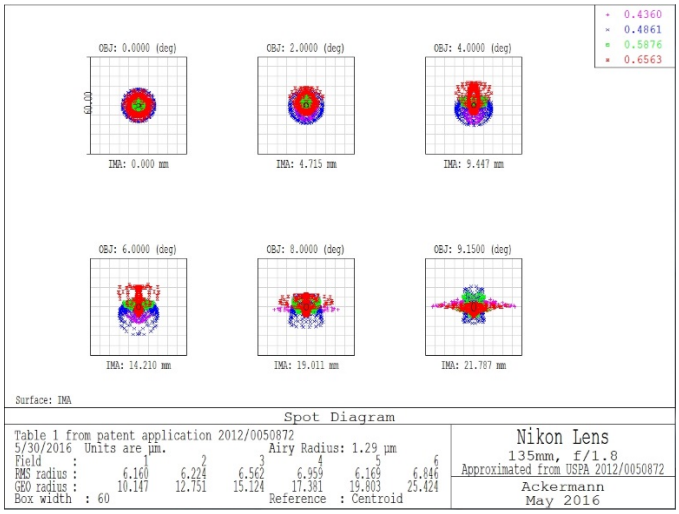

Figure 31. Approximate performance of Nikon 135mm, f/1.8 lens.

3.1.6 Thermal Stability

Commercial camera lenses are intended primarily for hand-held photography, which normally requires shutter speeds greater than 1/30th of a second. The photographer focuses the lens and then fires the shutter. Essentially there is no chance that the lens focus will shift due to temperature fluctuations within the time that the lens is focused and the shutter fired. In astronomical applications, it is not uncommon for the shutter to remain open for seconds to hours. The more common imaging cadence is for a series of 10- to 60-second images to be made over the course of hours. The astronomers would like to focus the system and then let it collect images without additional attention. Unfortunately, as the night temperature changes, the lenses experience a subtle but important change in focus. Sky surveys using commercial lenses often need to continuously check focus, house the lens in thermal blankets or temperature-controlled enclosures, or have computer-controlled drive mechanisms that continuously adjust focus [77]. The heaters on the Canon 200mm f/1.8 lenses for the SuperWASP survey can be seen in Figure 32.

Figure 32. Lens heaters used on Canon lenses for SuperWASP [78].

3.2 Apochromatic Refractor Objectives

While apochromatic (APO) refractors are not commonly encountered in sky survey and space surveillance work, they are also not entirely unknown. A small number of surveillance and survey projects at least partially rely on APO refractors. Therefore, we will briefly include a discussion of APO refractors and their limitations.

Historically, APO objectives and camera lenses have been somewhat different in design and function, but when upon closer examination, they are actually more similar than different. The first APO was developed by Taylor in 1895 [79-80]. The objective was described as being perfectly achromatic as the term, “apochromat,” had not yet been given to such lens systems. The significant difference between an APO and an achromat is that the APO is designed to bring three wavelengths to a common focus, rather than only two as is typical for an achromat. At the time the apochromat was developed, astronomers were using separate refracting telescopes for photographic and visual applications [81] as the visual systems were not corrected in the blue and violet wavelengths where photographic plates were sensitive. At the same time, other astronomers were experimenting with extra lenses that could be added to a visual achromat to shift the color correction into the blue [82], and unusual refractor designs where reversing the front lens would convert the system from visual to photographic correction [83]. A single instrument that could be used equally for photographic and visual applications should have been an instant success, but technology and history conspired against the apochromat. As a result, large reflectors became the instrument of choice [84] and APOs were never much more than an expensive curiosity.

Refractors have traditionally been long-focus instruments as chromatic aberration would become significant in faster systems. The APO instantly allowed the development of shorter focus refractors, but focal ratios faster than about f/7 were typically the limit for traditional three-lens objectives. At the same time, camera lenses of the Cooke Triplet design were easily achieving focal ratios of at least f/6 [85]. The camera lens had lesser image quality as it would cover a wide field of view and was required to form the image on a flat surface (although many Cooke Triplets required curved photographic plates). The APO, on the other hand, was a relatively narrow field instrument, intended for visual use and as a result, could produce higher quality images. Color correction in the APO was usually better than the Cooke Triplet, but

more complex lens designs, such as the Tessar (four elements), Heliar (five elements) and Planar (six elements), would both improve image quality and color correction.

Modern APO telescopes come in a very wide variety of configurations with lens counts ranging from two elements to six elements (at present). These more complex designs are beginning to rival camera lenses in complexity, but they are not constructed to be as robust as a camera lens, and as such, these systems are believed to be difficult to collimate and keep in collimation [86].

Traditional APOs have all their lens elements up front in a common lens cell. There are countless examples of two-lens and three-lens APOs, making them quite common. Quadruplet APOs where all lenses are in a common cell are much less common, but such designs do exist. In the current market, four-lens APOs with the lenses arranged in two separated groups are more usual. For the purpose of this section on APO refractors, a group is loosely defined as two or more lenses in a common cell, even if they include small air spaces. Lenses do not need to be in contact to count as a group. Common quadruplet designs have two and three lens groups with configurations including 2+2-lenses (Televue Petzval, Figure 33), 2+1+1-lens (Takahashi FSQ-106, Figure 34), and 3+1-lens (TS Imaging Star, Figure 35). All three of these design variations feature a flat image field without the need for add-on field-flattening optics. The Petzval design is derived from the Petzval photographic objective. A key feature is that the telescope is normally longer than its focal length. The Takahashi system is loosely based on the circa-1900 traditional telephoto lens design by Dallmeyer [87]. The optical system is normally shorter than its focal length. The TS Imaging Star uses a single, nearly afocal, lens to correct and flatten the field of a more traditional triplet APO objective. This design is similar to the color correcting lenses used for achromatic refractors beginning as early as 1865 [88].

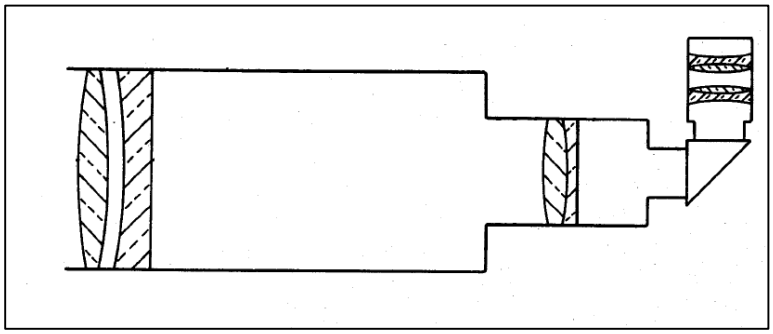

Figure 33. Televue Petzval APO configuration [89].

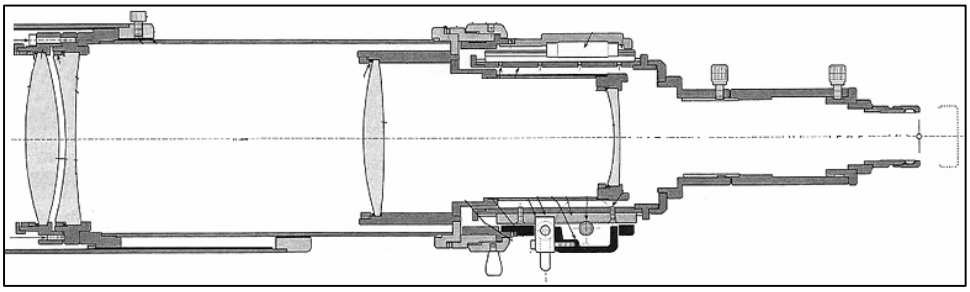

Figure 34. Takahashi telephoto APO configuration [90].

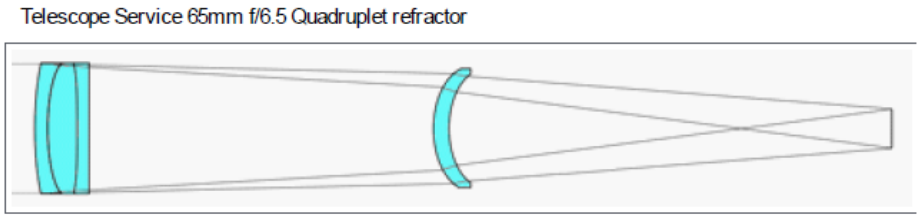

Figure 35. TS Imaging Star dialyte APO configurations [91].

The recent trend in APO refractor design is to push for faster optical systems and wider fields of view. The necessary result is that the optical systems are becoming more complex. While four-lens systems were considered somewhat exotic 40 years ago, today they are commonplace while seen as having limited potential. Five- and even six-lens APOs are now the norm, and APOs are slowly becoming indistinguishable from camera lenses.

Three recent five-lens systems are the Takahashi FSQ-130 (2+1+1+1-lens, Figures 36 and 37), the Vixen VSD100 (2+3-lenses, Figure 38) and the Sky Watcher Esprit 100ED (3+1+1-lens, Figure 39). The Takahashi design is new and little has been published about the actual optics. The Vixen system appears to be based on a now discontinued Pentax four-lens design. Vixen correctly advertises their telescope as having five lenses in five groups, but the first two lenses reside in one cell while the remaining three are in a second cell. The optical configuration of each scope can be seen in the figures below.

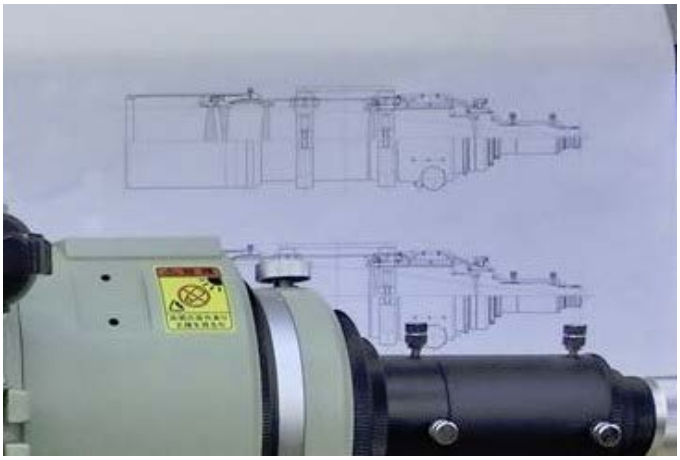

Figure 36. Takahashi FSQ-130 [92].

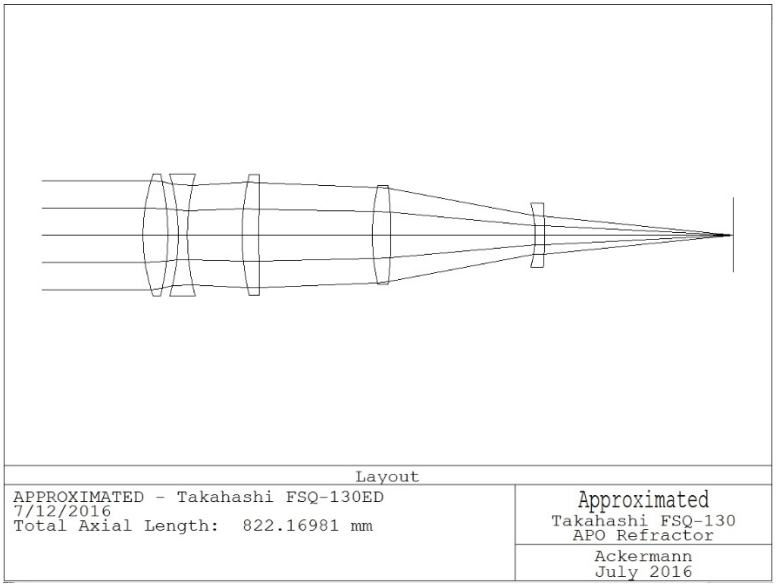

Figure 37. Approximate Zemax layout for FSQ-130ED APO.

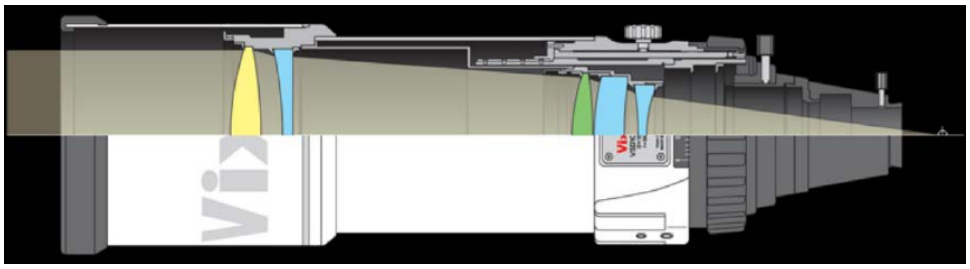

Figure 38. Vixen VSD100 [93].

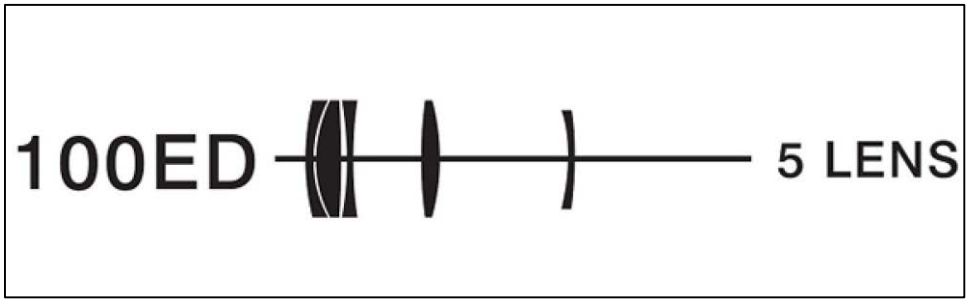

Figure 39. Sky Watcher Esprit 100ED [94].

Six-lens APOs are much less common, but at least four systems are available on the commercial market. Borg sells a four-lens focal reducer and field flattener for their more conventional two-lens APO [95]. The optical system has a 2+2+2-lens configuration, as shown in Figure 40, and operates near f/4. Both Sky Rover [96] and Stellarvue [97] market sextuplet APOs, but no details of either optical configuration are available. Finally, TAL sells a slower six-lens APO that is intended for visual use, but might work for narrow-field imaging [98]. The TAL system is quite unusual in that it uses a simple lens for the objective,

followed by a triplet and then a doublet corrector arranged in a 1+3+2-lens configuration, as shown in Figure 41. More unusual still is that the entire system can be realized with only Schott-type BK7 and F2 glasses.

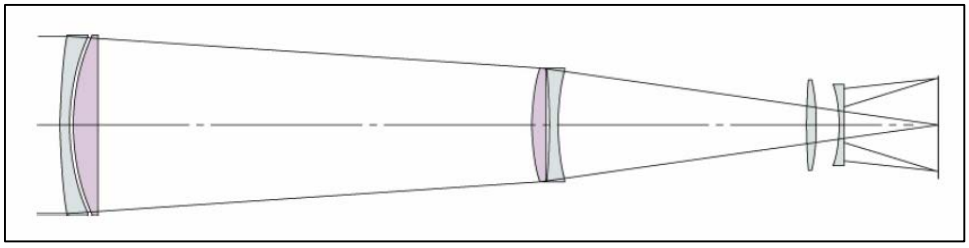

Figure 40. Borg six-lens APO astrograph [95].

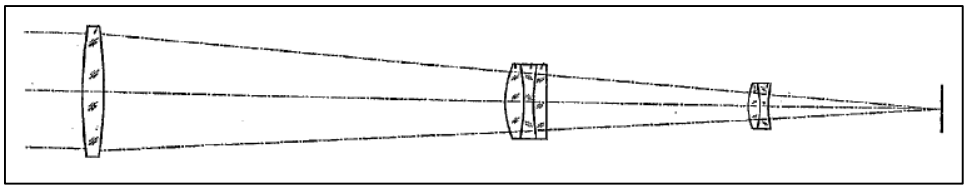

Figure 41. TAL APO refractor configuration [98].

The limitations of wide-field APOs are not unlike those of similar camera lenses. Most systems will have some vignetting, though not as pronounced as seen in photographic lenses. Most systems are designed for a narrowed range of wavelengths, and most systems sacrifice some image quality to achieve wider fields. In general, the image quality from these APOs is quite high, but surprisingly, only about equal to high-end camera lenses of similar aperture and focal ratio, as was demonstrated in recent system-to-system comparisons [99-100].

4 Performance of Commercial Lens Systems Used for Astronomy

Table 2 presents a list of the commercial lenses most frequently encountered in wide-field sky survey and space surveillance projects. The table does not include all of the survey efforts from Table 1, but most are represented. The most common lenses in use are the 50mm, f/1.2; 85mm, f/1.2; 200mm, f/1.8; and the 400mm, f/2.8. It would be interesting to examine each of their optical systems in detail, but it is only necessary to study one to understand how the limitations discussed above impact performance when used for astronomical purposes. Rather than choose one of the four common lenses, we instead select the 135mm, f/2.0 lens as it sits roughly in the middle of this group, and nicely images a field of 10 x 15 degrees onto a standard, full-frame 35mm DSLR. As lenses by Canon seem to be slightly more popular among astronomers than those from other manufacturers, we will closely examine the Canon EF 135mm, f/2.0L USM lens.

Table 2. Lenses in use with various survey projects

Focal Length (mm)	f/#	Survey Projects Using this Lens
24	1.4	MASCARA, WIDGET-1
28	1.4	RAPTOR-Q, BOOTES
35	1.4	WIDGET-1.5
50	1.2	AWCam, WIDGET-2, BOOTES-1, MASTER-VWF
50	2.0	PASS
50	4.0	ASAS-4
80	1.9	KELT
85	1.2	AWCam, CATS, EvryScope, FlyEye, Pi of Sky, RAPTOR A&B
85	1.4	PANOPTES
85	2.8	PhotopicSkySurvey
100	2.0	AROMA-W
135	1.8	ASAS-1, ASAS-2
135	2.0	Multiple
180	1.2	FAVOR
180	2.8	HAT-1
200	1.8	HAT, HAT-S, LOTIS, QES, RAPTOR-K, ROTSE-1, SuperWASP, XO, COLD
200	2.0	Starbrook, ASA-3N
200	2.8	AROMA-W, ASAS-3
280	2.8	TrES
300	2.8	TrES
400	2.8	DragonFly, QES, RAPTOR-A&B, RAPTOR-P, ASAS-SN, Bootes-1A, Starbrook
400	4.0	TASS

4.1 The Canon 135mm f/2.0 Lens

The Canon 135mm f/2.0 lens has a mass of 750 g, a maximum diameter of 83 mm, and a length of 112 mm. The lens was introduced to the market in 1996. It features ten glass elements arranged into eight groups. The optical cross section of the lens is seen in Figure 42. Lenses two and three appear to be a doublet but are, in fact, air spaced. Lenses two and four are made from a low dispersion glass. Some call this SD glass, others call it ED glass, while Canon literature refers to this as ultra-low dispersion (UD)

glass. The optical performance, as described by a plot of the lens MTF, is shown in Figure 43. The black traces correspond to 10 and 30 line pairs per millimeter at full aperture (f/2.0) while the cyan traces correspond to f/8.0.

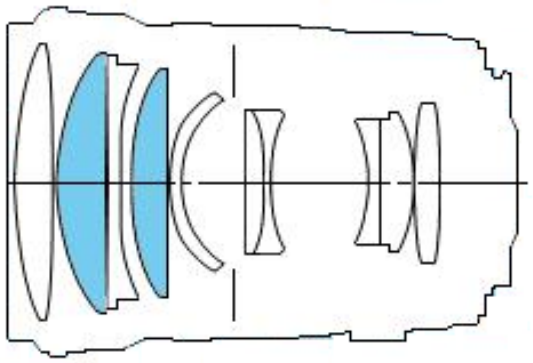

Figure 42. Optical configuration for the Canon EF 135mm, f/2.0L USM lens [101].

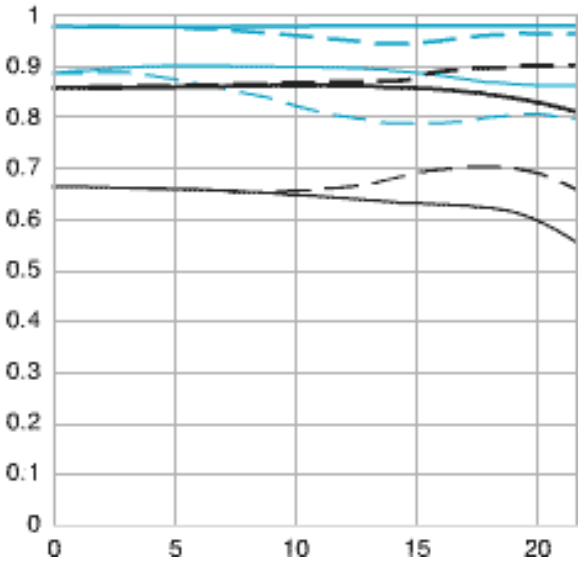

Figure 43. MTF plot for Canon EF 135mm f/2.0L USM lens [101].

4.2 Optical Performance

An approximate optical design for the Canon 135mm lens was developed from examples found in the patent literature [102]. This optical design is shown in Figure 44, with the corresponding RMS spot radius plotted in Figure 45. Canon has not published a spot diagram for this lens, but using the MTF curves, we can back-calculate an approximate spot size as shown in Figure 46.

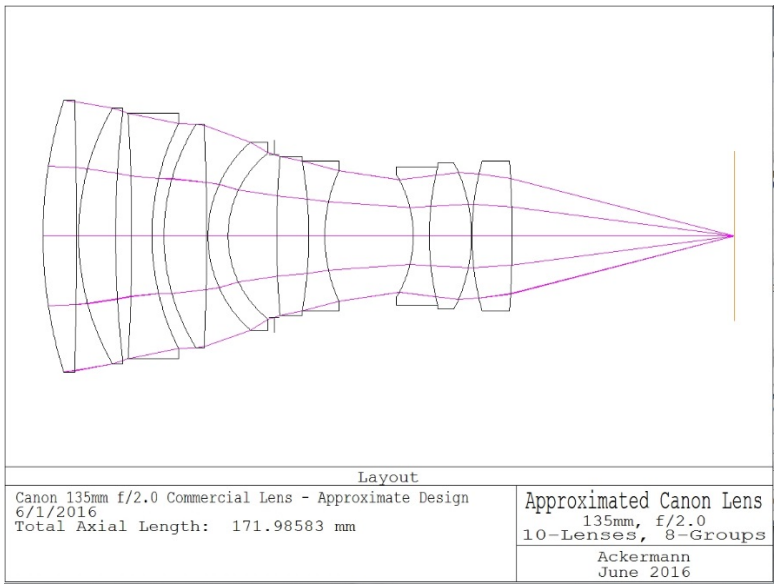

Figure 44. Approximate optical design for Canon EF 135mm f/2.0L USM lens [103].

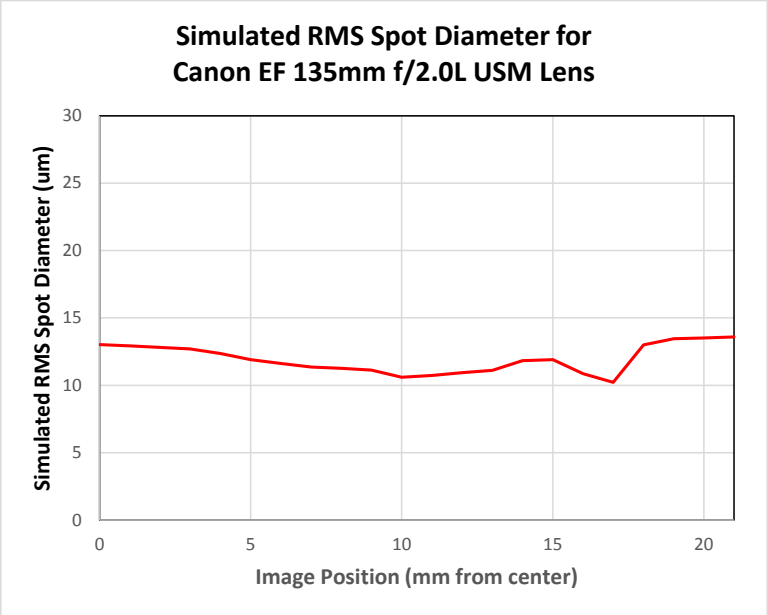

Figure 45. Simulated RMS spot radius for Canon EF 135mm f/2.0L USM lens [103].

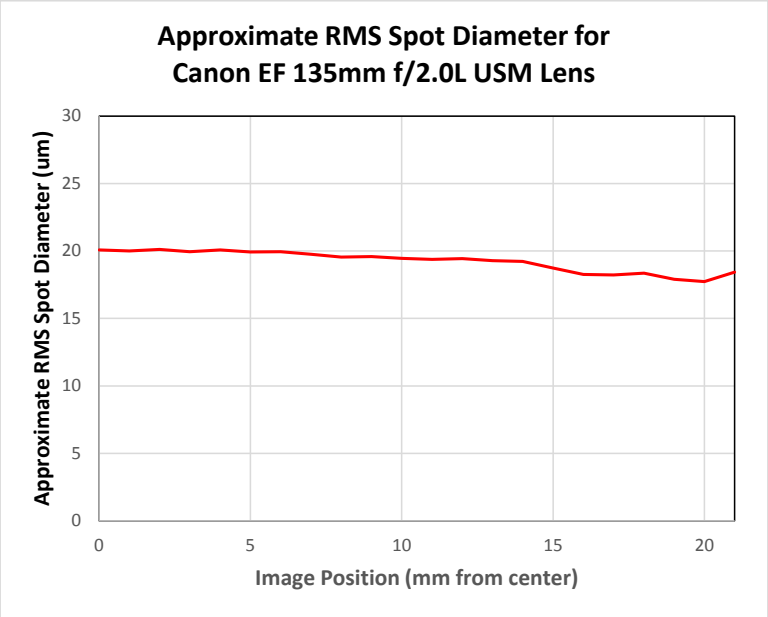

Figure 46. RMS spot radius for Canon EF 135mm f/2.0L USM lens, back-calculated from published MTF data.

The approximate geometric vignetting characteristics of this lens are in Figure 47. Similar to published Canon designs for other lens systems, the approximated design for the 135mm, f/2.0 lens was optimized for the C, d, F, and g line wavelengths. Figure 48 shows the ray-traced spot diagram, as it is, at times, more useful and more intuitive than an MTF plot, which is seen in Figure 49.

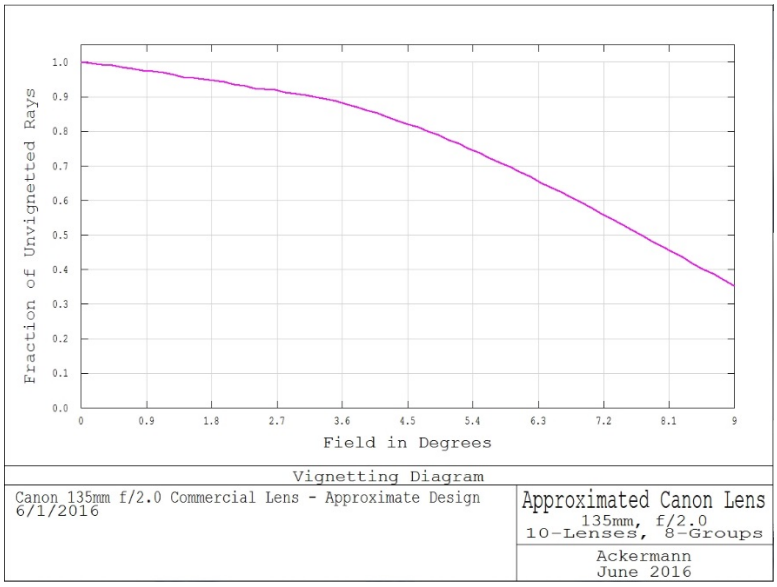

Figure 47. Simulated geometric vignetting plot for Canon EF 135mm f/2.0L USM lens [103].

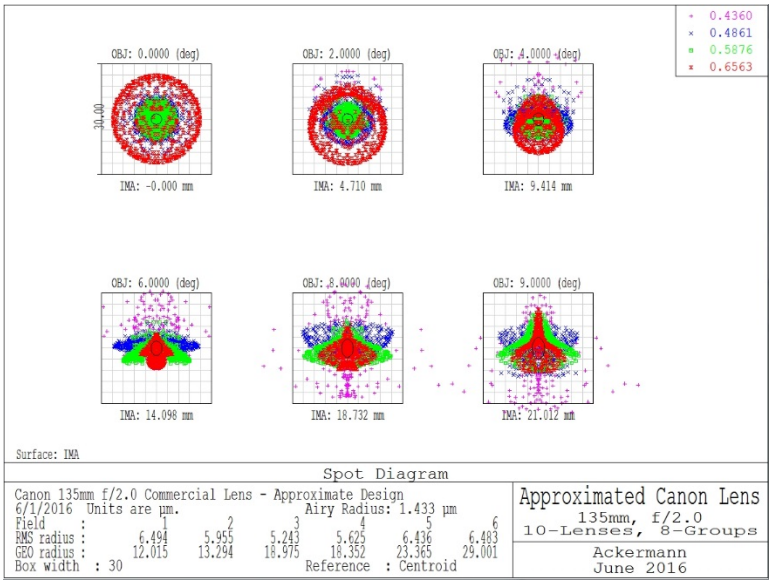

Figure 48. Ray-traced spot diagram for Canon EF 135mm f/2.0L USM lens [103].

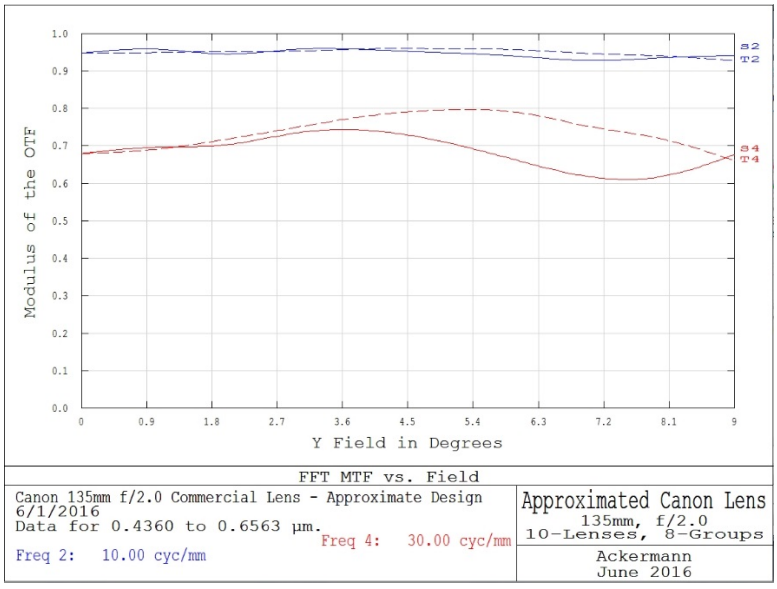

Figure 49. Simulated MTF plot for Canon EF 135mm f/2.0L USM lens [103].

While simulations provide useful insight into the design and function of an optical system, measured data are invaluable for providing confidence in the results of such calculations. Figure 50 presents the image of a star field seen behind the line of geosynchronous earth orbit (GEO) satellites, as observed from the state of Hawaii [104]. The image was captured with a Canon DSLR with an image sensor of 5760 x 3840 pixels. The background stars appear as streaks, as the 30-second exposure was made without tracking. This observation method does, however, result in GEO satellites appearing as fixed spots and several can be seen in the full resolution image. For convenience, the negative of this image is seen in Figure 51.

Figure 50. Streaking star field image made with Canon DSLR and Canon EF 135mm f/2.0L USM lens [104].

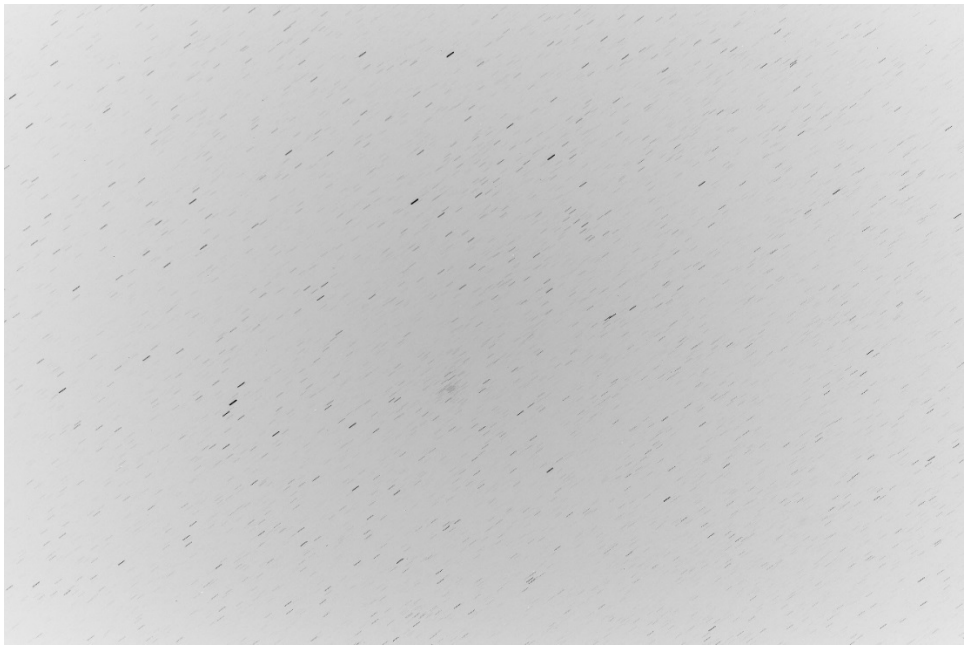

Figure 51. Negative of image seen in Figure 50.

The sample image combined with MTF data from the manufacturer and results from the approximate lens design is useful for a number of quantitative, and qualitative purposes. First, by examining the width of the star streaks across the image, we find that the image quality is very consistent from the center to the edge of the field. This is as expected since the MTF plot seen in Figure 43 shows almost no variation

across the image. Next, the width of the star trails is approximately three pixels across. With a pixel size of approximately 6 µm, this suggests the PSF is on the order of 18-µm diameter, also as expected from both MTF data and ray-traced spot data. Finally, if we plot Figure 50 in false color and adjust the contrast, as shown in Figure 52, we can clearly see the vignetting characteristics of the lens. Extracting the intensity on a diagonal line through the sample image and then normalizing, we can extract the actual, measured vignetting characteristics as shown in Figure 53. The calculated vignetting resulting from the ray-trace simulation, as shown in Figure 47, compares well with actual measured data in Figure 53.

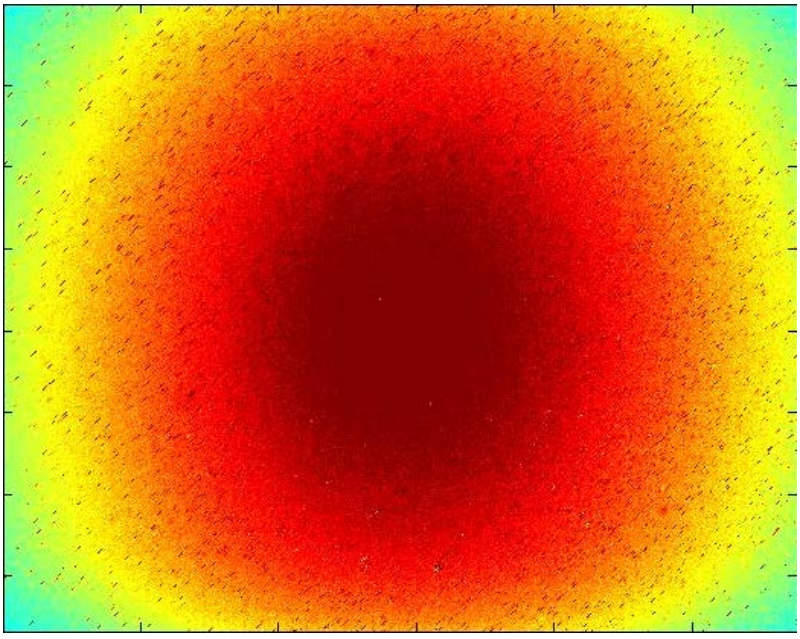

Figure 52. False color representation of the image seen in Figure 50.

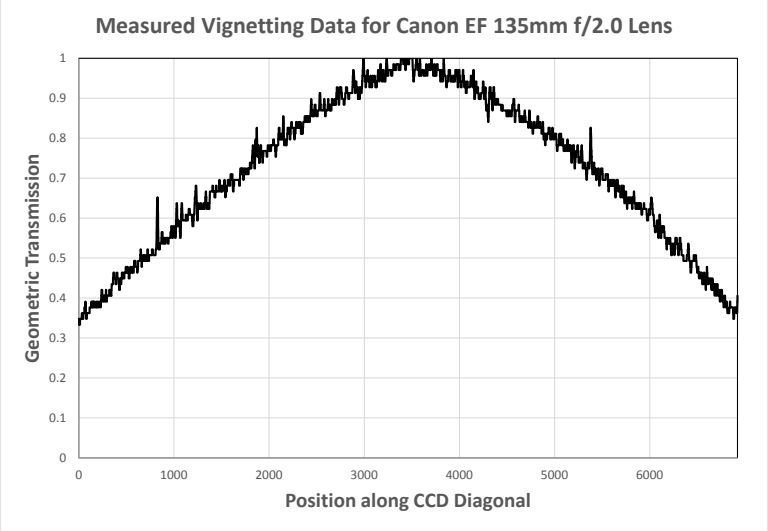

Figure 53. Measured vignetting of Canon EF 135mm f/2.0L USM lens.

4.3 Sensitivity

While optical designs, point spread functions, and a catalog of survey efforts are all interesting items to consider, the important characteristics for any sky survey effort are search rate and sensitivity. Search rate is primarily dependent upon the system's field of view but has a secondary dependence on integration time. Longer integration times provide greater sensitivity but also reduce the attainable search rate. Sensitivity, on the other hand, is primarily dependent upon aperture with a strong secondary dependence upon integration time, which itself is influenced by the optical system focal ratio and the observation mode. Sensitivity and integration time are directly related for tracked targets, but there is a more complex relationship when targets are in motion.

Sensitivity requires one to be able to sense a desired signal in the presence of noise. The key performance parameter is the signal to noise ratio (SNR). With low SNR targets, there is a high probability of false alarms and missed targets. With an SNR equal to or greater than six, one has high confidence of properly identifying targets and rejecting false targets. SNR is directly dependent upon the signal strength and integration time, and inversely dependent upon the noise terms expressed as the square root of the sum of the factors contributing to sensor output variance. The method of calculating SNR for astronomical and orbital targets is well documented and will not be reproduced here [105].

To increase sensitivity, one must increase signal relative to the noise, or decrease noise relative to the signal. The only options for increasing signal are integration time and the target photon flux. Since the targets are essentially fixed, the only method of increasing photon flux is to increase the collection aperture. Increasing integration time is slightly more complex and highly dependent upon the type of target each particular survey is attempting to detect.

Essentially all modern wide-field sky surveys are looking for time-dependent targets. The transit of an exoplanet across a star is a fairly slow-motion event. The system operators can increase integration time without much thought and the sensitivity will be dominated by the background sky brightness and the resulting noise term. When looking for comets, asteroids, and potentially hazardous near-earth objects, the astronomers must deal with the problem that the targets move relative to the star background. In almost all cases, this motion is relatively slow and long integrations, typically 60 seconds or more, are easily made without concern for diminishing returns. The detection of earth-orbiting satellites and debris is another matter as the angular rates can be very high and the orientation of the motion relative to the rotation of the earth must be considered. For satellite detection and tracking, simply increasing integration time provides no guarantee of detecting more faint targets.

When looking for resident space objects (RSOs) in low and medium altitude orbits, the objects move at high angular rates relative to the stellar background, with each target's rate highly dependent upon its orbital characteristics. For such objects, the observer has the choice of tracking the object to increase integration time, tracking the stars to provide a fixed stellar background for positional reference, or not tracking and letting everything streak.

One can track individual targets to improve SNR, but that requires knowing where the object is in the first place, which defeats the intended use of wide-field surveillance optics for blind search. Tracking the stars is an efficient approach as then only the targets streak and the star positions can be useful in extracting position information to determine orbital parameters. The final option allows everything to streak. This

saves on the expense of a tracking mount but can significantly complicate data reduction. However, if exposures are sufficiently short that stars only move a few pixels, the problem is manageable.

Targets that move more than a pixel during an integration period produce streaks. The SNR in each pixel containing target photons reaches a maximum when the integration is limited to the time required for the target image spot to cross a single pixel. Longer integration times continue to add noise from the sky background, but do not add additional signal photons, which results in a decrease in SNR.

The focal ratio of an optical system has an interesting influence on integration time and SNR. Traditional photographers and astrophotographers who specialize in recording extended space objects where low surface brightness is a concern, understand how a smaller focal ratio allows them to decrease exposure time. When searching for rapidly moving satellites and space debris, a smaller focal ratio actually allows you to increase the exposure time as the smaller focal ratio necessarily translates to a shorter focal length, which in turn results in target image spots moving more slowly across individual pixels. This is one reason why the Space Surveillance Telescope was built with an f/1 focal ratio [106].

If we consider the Canon EF 135mm f/2.0L USM lens and restrict our observations to collection of optical signals of satellites in GEO, we find there are two basic observation modes to consider. As mentioned above, we can track the stars, or simply point at the sky and track nothing. With the second option, GEO stationary satellites will move with the camera and form distinct dots. GEO satellites in inclined orbits will form short streaks. For either approach, sensitivity is calculated using standard approaches, combining characteristics of the optical system, detector, atmosphere and targets.

For the sensitivity calculations presented below, we have assumed the

- light loss of 1% per air-glass interface through the lens
- chromatic bandpass from 400 to 700 nm
- CCD quantum efficiency as depicted in the upper curve of Figure 24
- observatory location at 2 km above sea level
- look angle through the atmosphere of 40 degrees from zenith
- atmospheric seeing of 2 arc sec
- 7 days to/from full moon
- SNR=6.0

A typical sensitivity plot is seen in Figure 54. These particular data are for the 135mm f/2.0 Canon lens discussed above. The graph plots the limiting magnitude as a function of exposure time. Two traces are presented; one for an object that moves at the tracking rate (red), and the other for an object that is moving at a rate of 15 arc sec/sec relative to the tracking rate (black). As the plot in Figure 54 is for a system that is tracking the stars, the red trace shows the limiting magnitude as a function of integration time for a star, or some small object in the solar system, such as an asteroid or a comet. The black trace is for a geostationary satellite. Note that limiting magnitude for the satellite first increases with integration

time, then decreases. This is because it requires approximately three seconds for the image spot for the satellite to cross a single pixel. Hence, the optimum integration time for objects moving at 15 arc sec/sec is 3 seconds.

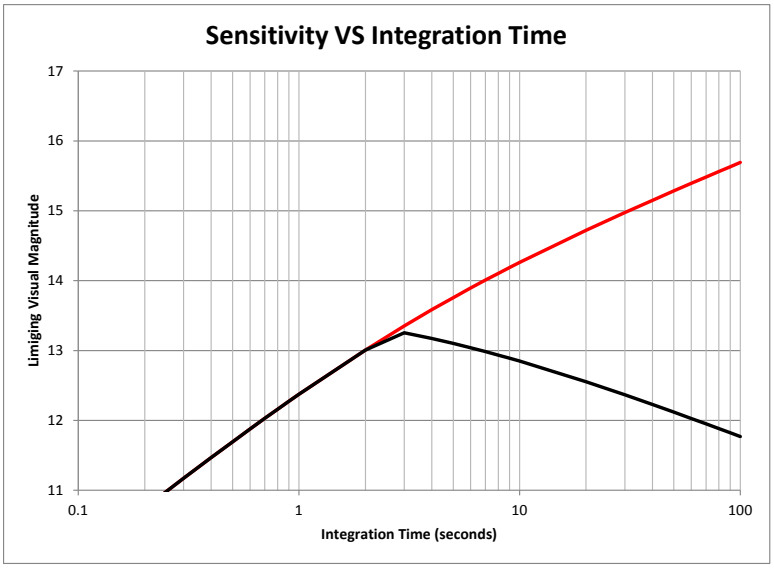

Figure 54. Canon EF 135mm f/2.0L USM, averaged aperture – sidereal tracking

In general, this optimum integration time is a complex function of optical system focal length, image spot size, pixel size, and the location of the spot center relative to a single pixel. If the centroid of a target PSF is centered over a single pixel, as seen in Figure 55, we achieve higher sensitivity than if the PSF is centered perfectly on four pixels, as seen in Figure 56. The data plotted in Figure 54 assume the target PSF is perfectly centered on a pixel at its optimum position.

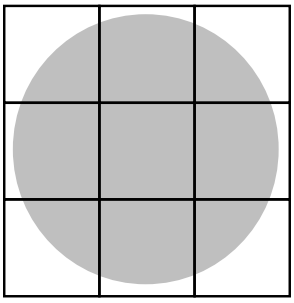

Figure 55. PSF centered on a single pixel.

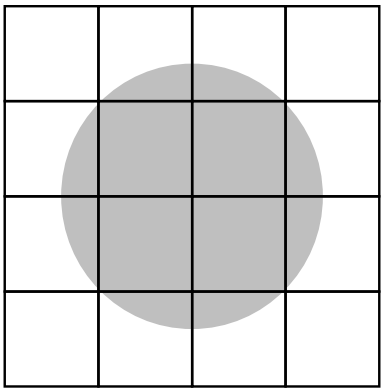

Figure 56. PSF centered on four pixels.

The impact of having the target PSF centered on one pixel as opposed to four pixels can be seen in Figure 57. There, we have plotted the system sensitivity similar to that seen in Figure 54, but we have included plots for both centered (the higher plot), and shared over four pixels (the lower plot). Note that the change in sensitivity is almost an entire visual magnitude for this lens. These data are again for a system tracking at the sidereal rate. In real applications, targets will be randomly positioned relative to pixel boundaries, but examining the ideal and worst case positions provides insight into the limits of sensitivity for the system.

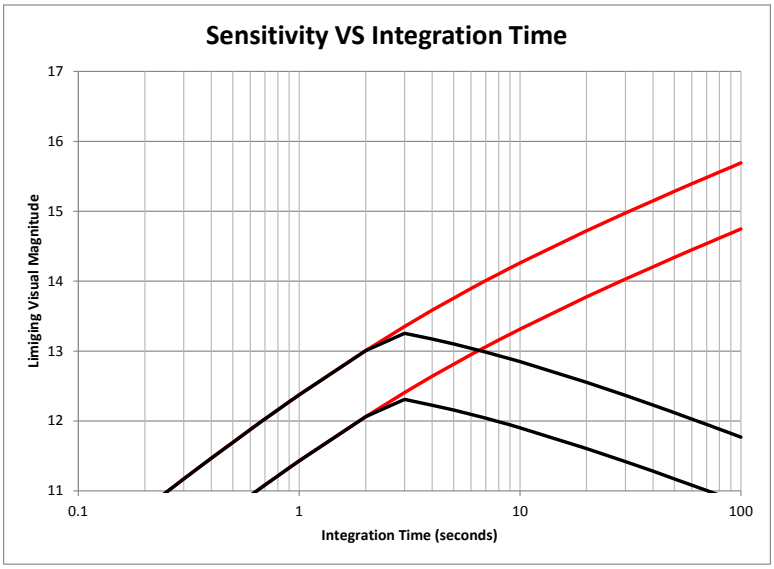

Figure 57. Canon EF 135mm f/2.0L USM, averaged aperture – sidereal tracking.
Comparing sensitivity for centered (upper) VS four-way split PSF positioning.

Another feature of the data in Figure 54 is that we have plotted sensitivity for the average aperture of the lens. Since the lens exhibits strong vignetting at maximum aperture, as seen in Figures 47 and 53, the effective light collection area for objects in the center of the field is greater than for objects near the edge of the field. The average area is calculated from the field-dependent area that is recorded with a given level of vignetting. If we were instead to calculate sensitivity at both the center of the field, where there is no vignetting, and at the edge of the field, where there is significant vignetting, the sensitivity plots would appear as seen in Figure 58. This plot clearly shows the impact of vignetting on limiting magnitude for

this lens system. While not entirely accurate, it is easiest to report sensitivity for the average effective aperture, but it is important to realize that vignetting produces a field-dependent sensitivity. The solution, of course, is to design lens objectives that do not exhibit vignetting.

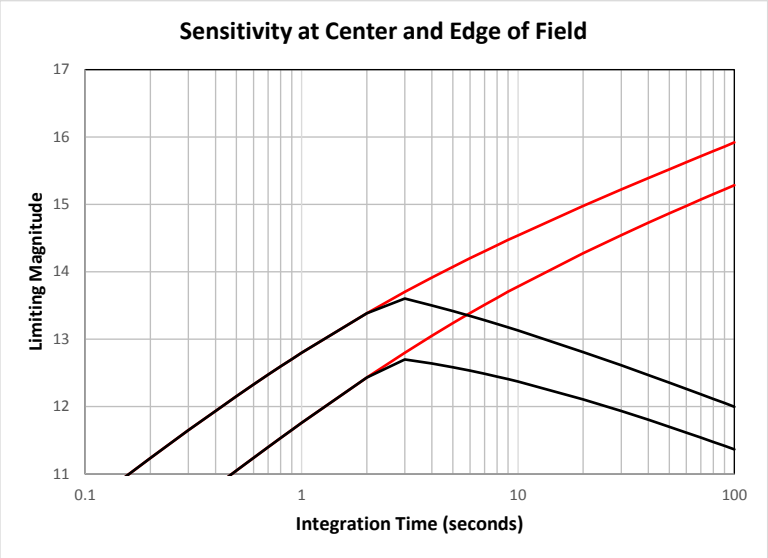

Figure 58. Canon EF 135mm f/2.0L USM, sidereal tracking.
Sensitivity at center and edge of field.

The data presented in Figures 54, 57, and 58 were for a system that was tracking at the sidereal rate. If instead, we turn the drives off and allow the stars to drift by, a geostationary satellite will produce a spot on the focal plane, but a geosynchronous satellite with some orbital inclination will produce a short streak. Since many plans for surveying the GEO region call for observing all objects in a band from 15 degrees above the equator to 15 degrees below, the worst-case satellite one should expect to see would have an inclination of 15 degrees. The satellite is still moving at a rate of 15 arc sec/sec across the sky, but the effect of inclination and having the telescope drifting at a rate of 15 arc sec/sec west to east results in this inclined satellite moving at a rate of 3.92 arc sec/sec relative to the telescope. The geometry of this situation is shown in Figure 59.

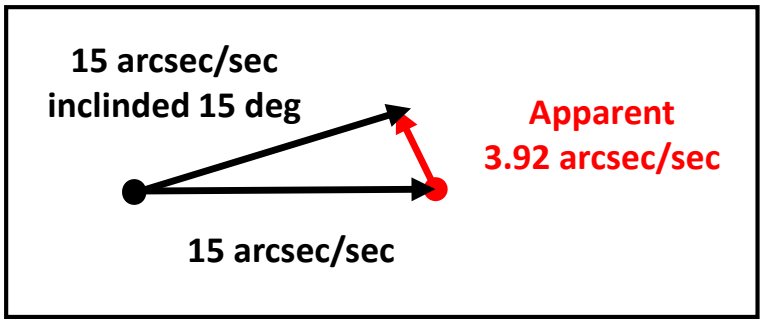

Figure 59. Relative motion for 15-degree inclined GEO satellite when observed from earth with a non-tracking sensor system.

For the situation depicted in Figure 59, we can calculate expected sensitivity values for the 135mm, f/2.0 Canon lens. These results are seen plotted in Figure 60. The red curve is now for a geostationary satellite,

while the black curve is for the 15-degree inclined geosynchronous satellite. Note that the sensitivity for this system has now increased to approximately 14.25 visual magnitudes with an optimum integration time of approximately 10 seconds. When operated in this "drives off" mode, sensitivity increases significantly, but at the expense of all stars now forming streaks on the focal plane, thereby complicating automated data reduction.

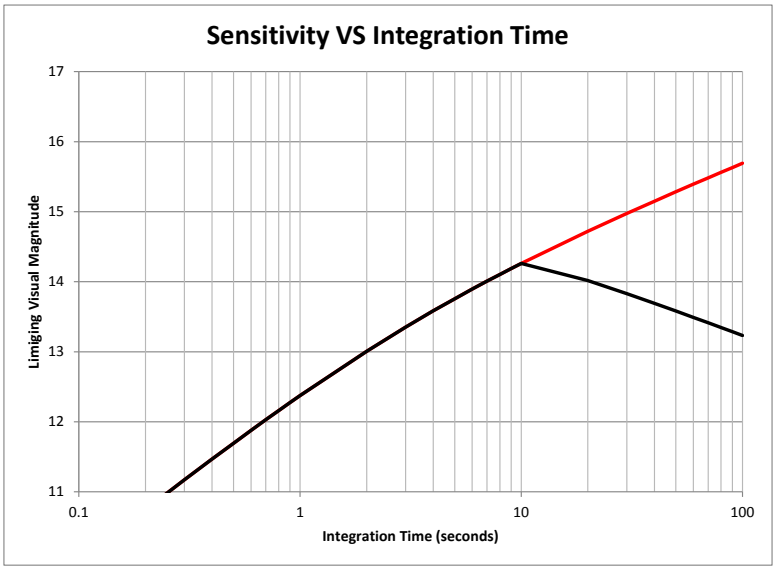

Figure 60. Canon EF 135mm f/2.0L USM, averaged aperture, no tracking – drives off.

To summarize the impact of the various effects discussed above, we present the data in Table 3. There we see the limiting visual magnitude for the lens and camera for targets at the center, edge, and 70% of field; for the PSF centered on either a single pixel or four pixels; for both geostationary and 15-degree inclined geosynchronous satellites, observed with sidereal tracking or without tracking.

Table 3. Summary of sensitivity calculations for 135mm, f/2.0 Canon lens for detecting satellites in GEO.

		Sidereal Tracking All GEO Targets	Without Tracking GEO, 15 deg Inclined
Centered	Center of Field	13.60	14.54
	70% of Field	13.24	14.24
	Edge of Field	12.70	13.78
4X Split	Center of Field	12.66	13.60
	70% of Field	12.30	13.29
	Edge of Field	11.75	12.84

4.4 Impact of Commercial Lens Limitations on Sensitivity

In Section 4.3, we examined the performance of a real lens, similar to one that is presently in use for sky survey work. There, we saw how vignetting could impact sensitivity. Here, we will use an imaginary, ideal lens, known as a paraxial lens, to explore more fully the impact of lens limitations on sensitivity. Specifically, we will examine examples of how chromatic bandpass, vignetting (again), and overall image quality impact limiting magnitude when using lenses for detection satellites in GEO. All results presented are for sidereal tracking only. No results for stationary optics are given in this section.

Presented in Table 4 are the limiting magnitude values for the ideal 135mm, f/2.0 lens. A total of five variations of the ideal lens are examined. The variations are as follows:

1. ideal lens diffraction limited PSF no vignetting wavelengths 350-1100 nm
2. ideal lens diffraction limited PSF no vignetting wavelengths 400-700 nm
3. ideal lens diffraction limited PSF real vignetting wavelengths 350-1100 nm
4. ideal lens realistic PSF no vignetting wavelengths 350-1100 nm
5. ideal lens realistic PSF real vignetting wavelengths 350-1100 nm

Table 4. Results for ideal lens with KAI-16000 CCD, 1x1 binning, 7.4 µm, pixels.

		Ideal Lens	Ideal Lens	Diff Lim PSF with Vig	Real PSF, No Vig	Real PSF, with Vig
		350-1100 nm	400-700 nm	350-1100 nm	350-1100 nm	350-1100 nm
Centered	Center of Field	14.84	14.73	14.84	14.84	14.84
	70% of Field	14.84	14.73	14.47	14.79	14.44
	Edge of Field	14.84	14.73	14.17	14.77	14.13
4X Split	Center of Field	13.80	13.69	13.80	13.80	13.80
	70% of Field	13.80	13.69	13.43	13.78	13.43
	Edge of Field	13.80	13.69	13.13	13.82	13.18

The limiting magnitudes are for a GEO target moving across the focal plane while the optical system tracks at the sidereal rate. The CCD was a KAI-16000, front-illuminated, interline transfer detector with 7.4-um pixels. The observation conditions are as mentioned above in Section 4.3.

For the ideal lens with a real CCD, we see that changing the chromatic bandpass significantly increases sensitivity only by 0.11 magnitudes. Variation of the PSF across the field resulted in loss of only 0.07 magnitudes at the edge of the field, while typical vignetting results in a loss of 0.67 magnitudes. Combining realistic PSF and vignetting characteristics resulted in a reduction 0.71 magnitudes between the center and edge of the field.

For reference, Figures 61 and 62 present the RMS spot radius and vignetting characteristics as a function of field angle for certain variations of this lens. For examples where there was no variation in PSF across the field, the system had diffraction limited ray-traced spots.

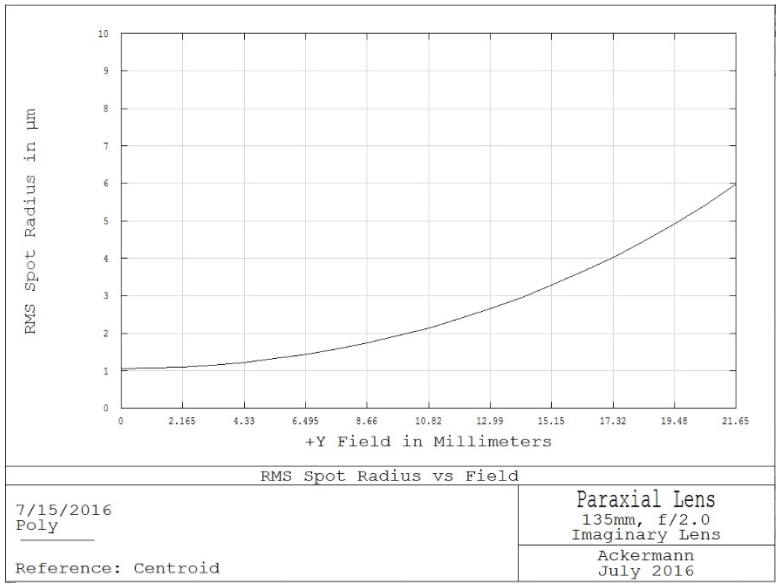

Figure 61. RMS spot radius for ideal lens with realistic variation in PSF.

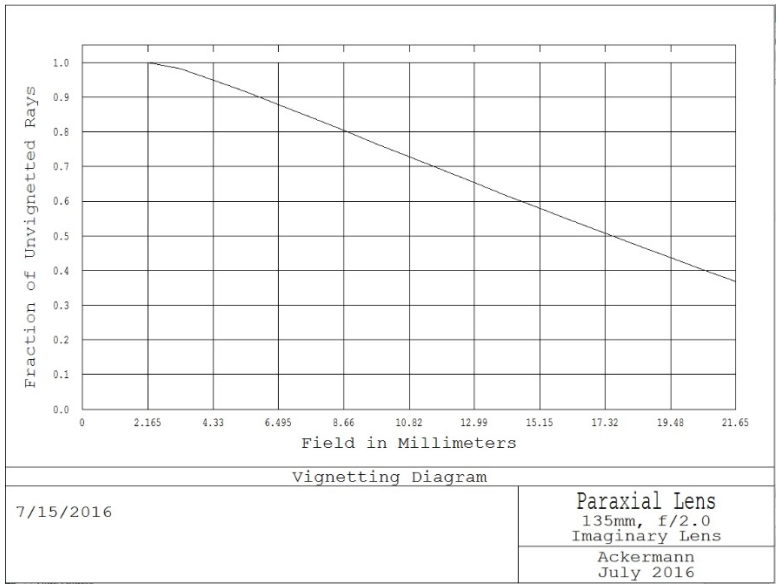

Figure 62. Transmission characteristics for ideal lens with realistic vignetting.

The particular CCD used for the calculations has limited sensitivity at wavelengths longer than about 750 nm. As a result, a lens that is designed for imaging between 400 and 750 nm is almost as sensitive as our ideal lens imaging between 350 and 1100 nm. If we were to repeat the calculations with a deep depletion CCD, designed for high quantum efficiency at longer wavelengths, the results change somewhat as seen in Table 5. These data show that with a more sensitive CCD, a lens designed for a wider spectral

bandpass, provides a significant increase in sensitivity. Also, the overall higher quantum efficiency of the back-illuminated device resulted in an increase detection threshold of 0.56 magnitudes when compared to the front-illuminated, interline transfer CCD. For reference purposes, the quantum efficiency of each CCD is plotted in Figures 63 and 64.

Table 5. Results for ideal lens with generic deep depletion CCD, 1x1 binning, 7.4 µm, pixels.

		Ideal Lens	Ideal Lens	Diff Lim PSF with Vig	Real PSF, No Vig	Real PSF, with Vig
		350-1100 nm	400-700 nm	350-1100 nm	350-1100 nm	350-1100 nm
Centered	Center of Field	15.40	15.09	15.40	15.40	15.40
	70% of Field	15.40	15.09	15.07	15.34	15.01
	Edge of Field	15.40	15.09	14.79	15.31	14.73
4X Split	Center of Field	14.35	14.05	14.35	14.35	14.35
	70% of Field	14.35	14.05	14.02	14.32	14.00
	Edge of Field	14.35	14.05	13.75	14.36	13.77

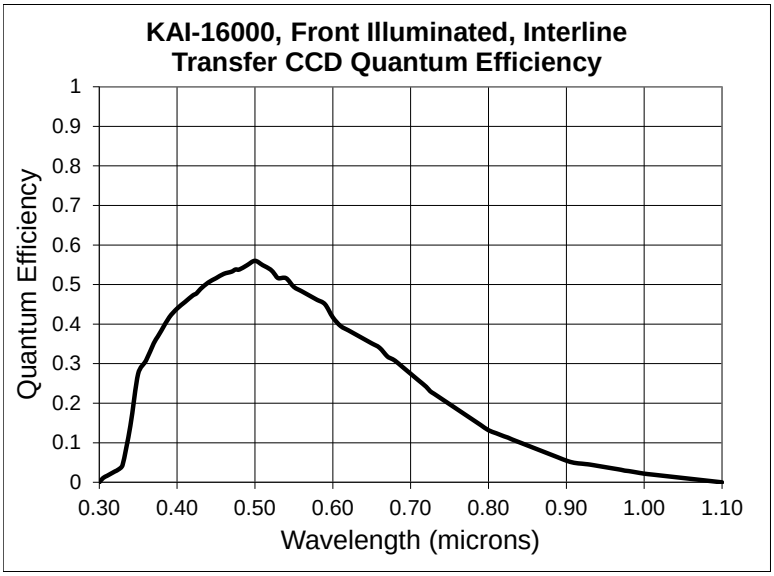

Figure 63. Quantum efficiency of front-illuminated, interline transfer CCD.

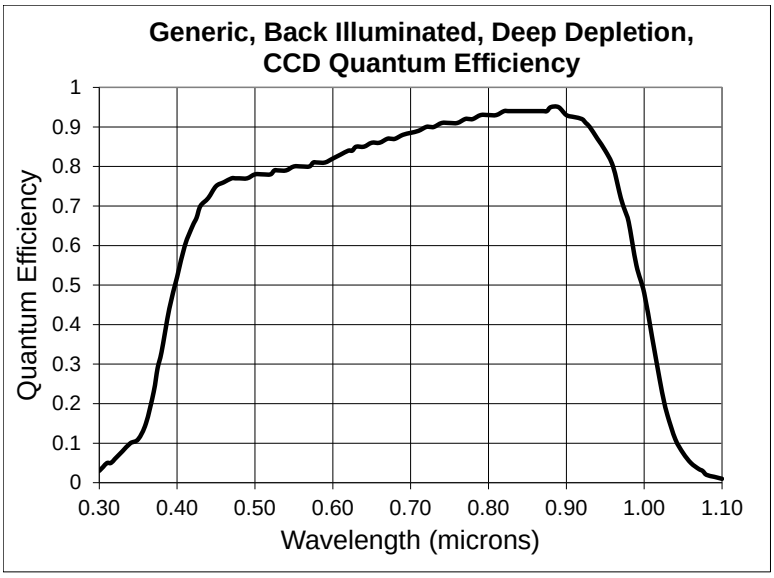

Figure 64. Quantum efficiency of generic back-illuminated, deep depletion CCD.

4.5 The Performance of Custom Lenses

Custom lenses are built frequently for a wide range of uses, from star sensors on satellites to spectrometers on large telescopes. Unfortunately, very few have been designed and used specifically for space surveillance. Three such lenses are mentioned in the literature, but few details are available. Two of the systems were mentioned in Table 1: the lens for The Amateur Sky Survey and the Sova-5 lens of the Russian Pritsel system. The third lens is used at four sites but does not appear to have been part of a lens array project.

The Amateur Sky Survey, at one point, built a small number of 100mm aperture, f/4 lenses for what they referred to as their Mark IV system. Earlier versions used commercial camera lenses, but the final systems were equipped with this custom optic. A few details of the project are available in reference [107].

A very recent satellite surveillance system built in Russia is known as Pritsel which translates to “Sight.” The system includes two telescopes of 750mm aperture, two of 250mm aperture and two lenses, Sova-5, of 50mm aperture [37]. A picture of the complete Pritsel system is shown in Figure 65. The two Sova-5 units are barely visible on the far left. An image of the Sova-5 by itself is seen in Figure 66.

Figure 65. The Pritsel system [37].

Figure 66. The Sova-5 lens.

As with the TASS Mark IV lens, few details of the Sova-5 lens are available. However, from information that has been published and the data in Figure 66, the Sova-5 objective is understood to have the following characteristics:

- focal length: 100 mm
- field of view: 40 degrees
- focal ratio: f/2.0
- aperture: 50 mm
- image circle: 72.3 mm diameter
- bandpass: 450-850 nm
- 80% encircled energy: 24 µm diameter

No information on layout or optical configuration is available. The Sova-5 lens qualifies as being part of a lens array project, as two units are mounted to a larger telescope in the Pritsel system and Russia has plans to duplicate Pritsel at a number of locations around the world.

The final custom lens identified was the VT-53e objective in use with the International Scientific Optical Network (ISON) [108]. This lens was designed by the master Russian optical physicist, Dr. Valery Terebizh, who is responsible for most of the optical designs in use with ISON. The VT-53e is not used in a lens array survey project and only four copies were built for use at different locations within the ISON program. The lens is, however, important to mention as it demonstrates some of the characteristics that can be achieved with custom optical systems.

The VT-53e has the following characteristics:

- focal length: 204 mm
- field of view: 20 degrees
- focal ratio: f/1.632
- aperture: 125 mm
- image circle: 70 mm diameter
- bandpass: 450-850 nm
- 80% encircled energy: ~12 µm diameter

Terebizh designed the VT-53e to use all spherical lens surfaces, and it does not rely on CaF2 for color correction. The lens was designed for a 400 nm wide color band, but it is offset from the normal visible range by 50 nm. The lens vignettes slightly towards the outer edge of the field and the design was optimized with the wavelengths weighted to match the quantum efficiency of typical CCD detectors [109]. The vignetting characteristics of the lens are shown in Figure 67 with a spot diagram in Figure 68. This spot diagram is actually for a follow-on design, the VT-53x, but it is similar to that for the VT-53e. A picture of the VT-53e lens is shown in Figure 69.

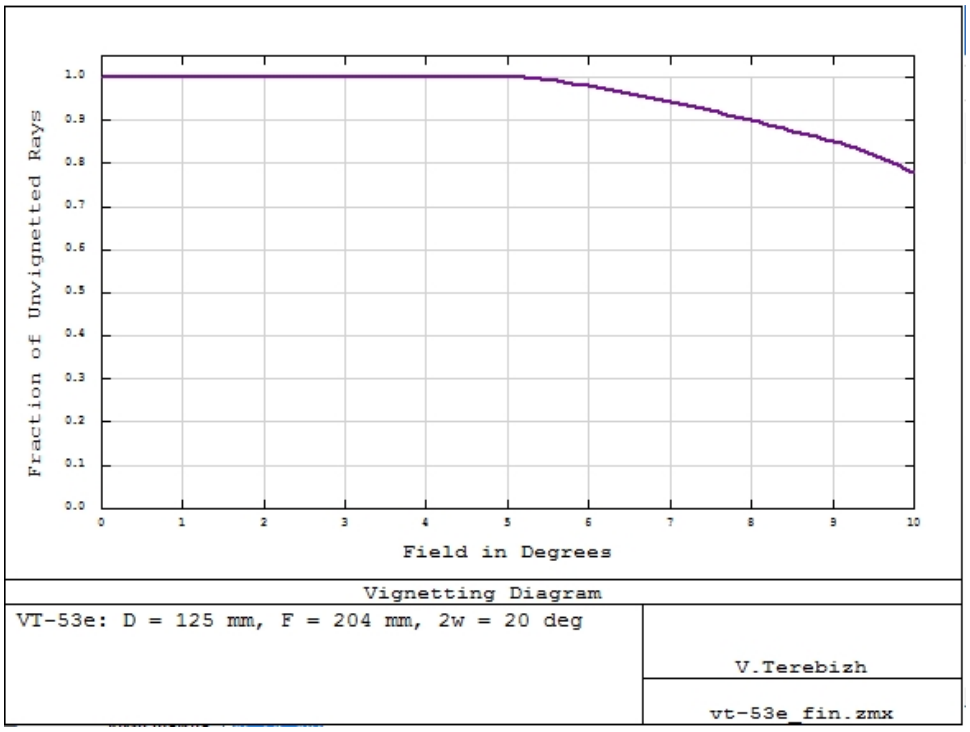

Figure 67. Vignetting plot for the VT-53e.

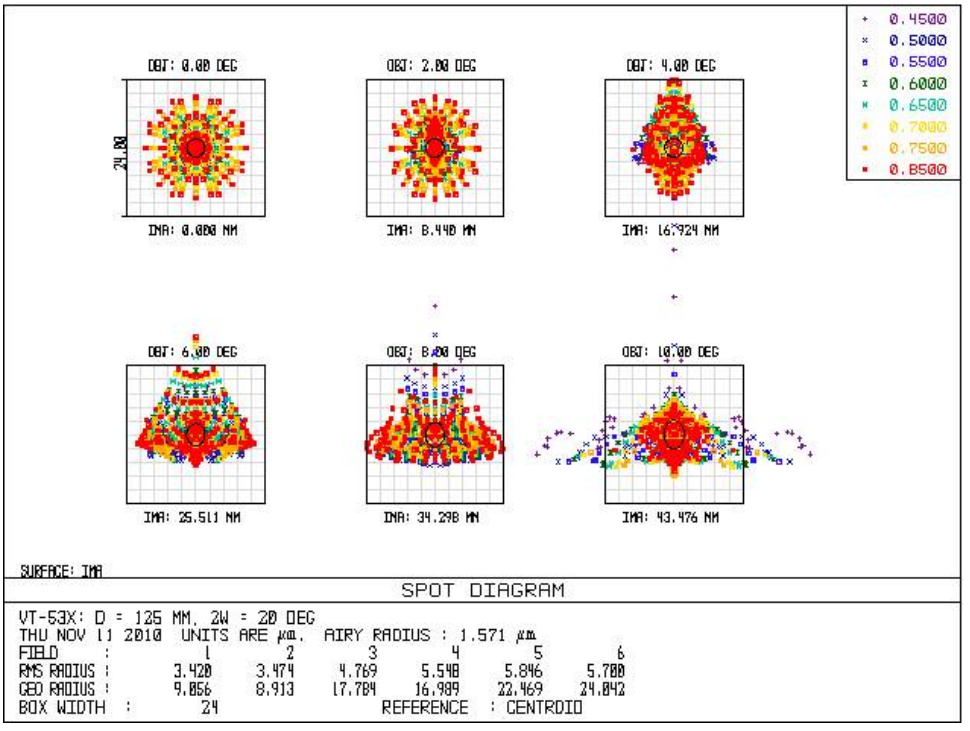

Figure 68. Spot diagram for the VT-53x design.

Figure 69. The VT-53e lens [110].

A description of the VT-53e was included because it demonstrates the potential for custom lenses used for astronomical research. We can use the previously discussed techniques to calculate sensitivity for a sensor with the VT-53e lens and a front-illuminated CCD. A plot of sensitivity VS integration time for sidereal tracking and GEO targets is presented in Figure 70. The CCD used for the calculation was the KAF-4320, 2k x 2k sensor with 24 µm pixels. The lens and sensor combination is able to detect GEO targets of 14.7 magnitudes with an SNR=6. The larger aperture of the VT-53e lens, combined with its lower vignetting, results in greater sensitivity when compared to the Canon 135mm f/2.0 lens (see Figure 54).

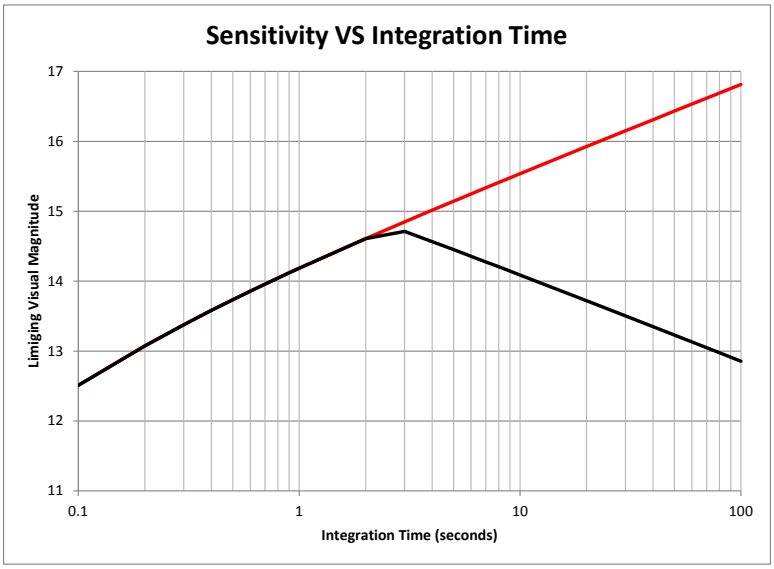

Figure 70. Sensitivity calculation for VT-53e lens, KAF-4320 sensor, sidereal tracking.

4.6 The Performance and Sensitivity of APOs

APO refractors are important tools in astronomy, but to date, have not been widely used as part of lens and camera arrays for survey work. The miniWasp project is, in fact, the only current project using a mixture of APO refractors and commercial camera lenses. Commercial APOs and camera lenses are available in similar apertures. The greatest differences between the two types of system are focal length and vignetting. Camera lenses traditionally are available with shorter focal lengths but they usually come with the disadvantage of light falloff towards the edge of the field. Having longer focal lengths for similar apertures, APO refractors are less capable of detecting satellites in GEO, but would have a similar sensitivity for detecting the more slow moving asteroids and comets.

As an example, we take a slightly closer look at the commercial Vixen VSD100 APO. This is a relatively new optical system brought out by Vixen, based on a modification of an older design by Pentax [111]. The Pentax APO used four lenses and was well respected by amateur astronomers, but was eventually withdrawn from the market. More recently, Vixen introduced the VSD100 with five lenses, including two made from low dispersion glass, as seen in Figure 38. The additional lens improves performance, but the telescope really performs midway between a traditional APO and a camera lens. It is capable of imaging wider fields than a traditional APO, but does not have as high of image quality. At the same time, it cannot image fields as wide as true camera lenses.

When used for detection of earth-orbiting satellites, the longer focal length causes the target spot to move across the focal plane at a higher rate, thereby reducing sensitivity somewhat. The calculated sensitivity is seen in Figure 71. When compared to a fast lens, such as the VT-53e, it is less sensitive. The lowered sensitivity is due partly to the smaller aperture and partly due to the longer focal length.

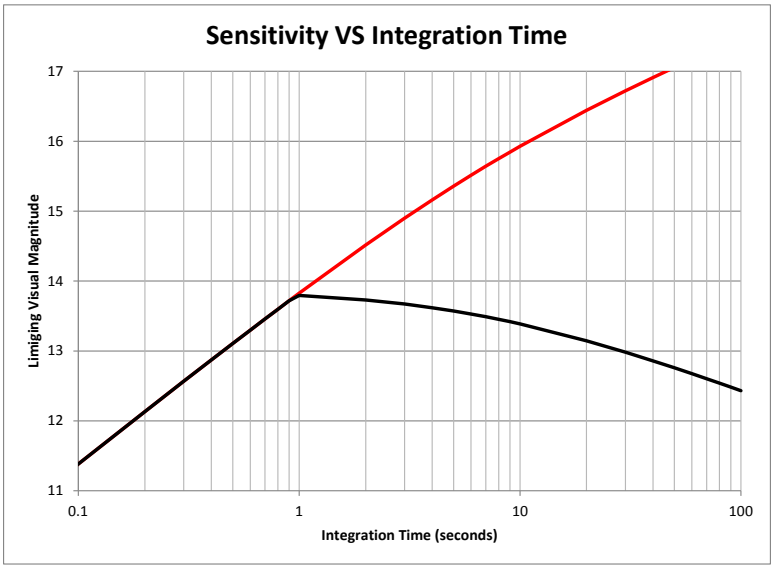

Figure 71. Calculated sensitivity for Vixen VSD100 APO with KAI-16000 CCD.

5 The Potential of Custom Lens Systems

In Section 4.5, we briefly examined three custom lenses that were, or presently are, being used for satellite detection and tracking. Little information was available to accurately assess their performance and potential. In this section, we consider what characteristics the ideal, yet practical, lens should have if specifically designed for some type of sky surveillance mission. While commercial lenses are inexpensive and readily available, when sensitivity is more important than cost, custom optical designs should be considered in the system design trade space.

5.1 Characteristics of the Ideal, Yet Practical, Lens

In previous sections, we saw how the limitations of commercial lenses ultimately lead to lower sensitivity. In some cases, the reduction in sensitivity was small, while in other cases, it was more significant. Before designing a custom lens, we must first determine the design parameters. Ideally, we want a wide field and short integration times as this combination will result in completing one survey of the sky more quickly. A problem, however, is that for a given size CCD, wider fields require shorter focal lengths, and shorter integration times require larger apertures. These two characteristics combine to produce the requirement for a fast lens, or one with a small focal ratio. Fast lenses are significantly more difficult to design, and their image quality is usually lower, resulting in reduced sensitivity. In general, lenses faster than f/2 are very difficult to design, while lenses faster than f/1.4 are extremely difficult to design. For the moment, we will concentrate on a lens of 135mm focal length and an f/2.0 focal ratio as this matches the Canon lens discussed above.

Next, we want the custom lens to overcome many of the limitations seen in commercial camera lenses. To accomplish this, the following general characteristics are recommended:

- focal length 135mm
- focal ratio f/2.0
- field of view 18 degrees
- aperture 67.5 mm
- image circle 43 mm diameter
- bandpass 400-800 nm
- wavelength weighting uniform
- overall image quality best achievable
- image quality variation uniform across field
- vignetting none
- lens surfaces all spherical
- glass selection standard catalog glass types

5.2 Custom Lens Design Examples

Following some extensive design work, a lens design was realized that essentially meets the above requirements. The lens layout is shown in Figure 72, with the ray-traced spot diagram in Figure 73, and a vignetting plot shown in Figure 74. Note that this lens differs significantly from the traditional double gauss [112] lens design seen in many of the more expensive, commercial camera lenses.

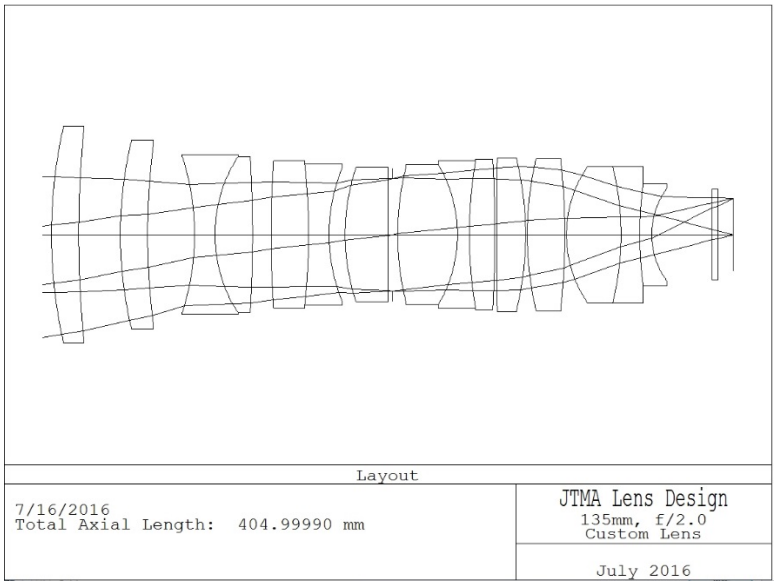

Figure 72. Layout for custom design 135mm, f/2.0 lens [113].

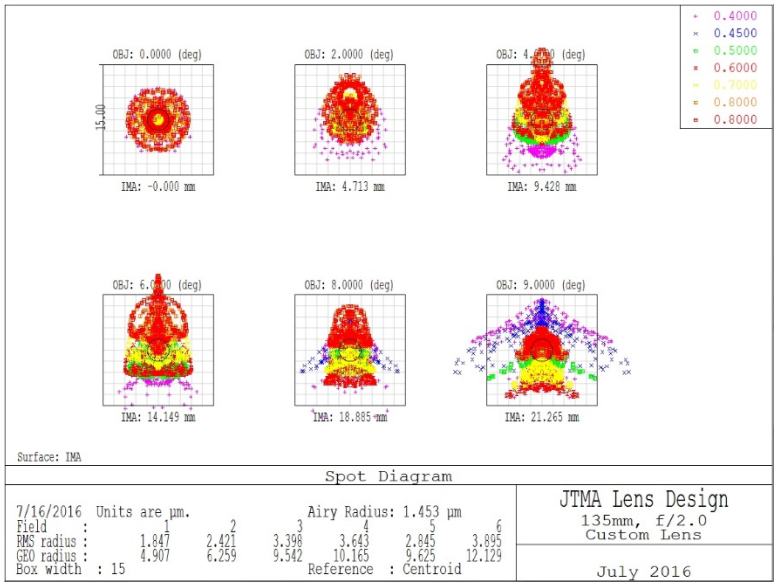

Figure 73. Spot diagram for custom design 135mm, f/2.0 lens [113].

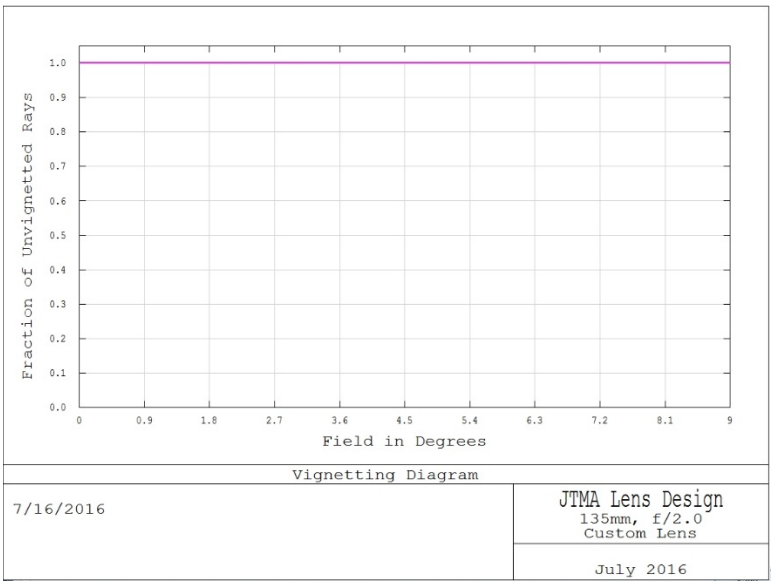

Figure 74. Vignetting plot for custom design 135mm, f/2.0 lens [113].

Comparing the spot diagrams in Figures 48 and 73, we see that the custom optical design exhibits significantly higher image quality while being corrected over a wider optical band, and while exhibiting no geometric vignetting. All lenses are specified from available glass and all lens diameters are small enough to easily be fabricated from readily available glass blanks (which are normally limited to 160-mm diameter).

In Figure 75, we plot the sensitivity for this lens, using the same KAI-16000 CCD as before. Comparing the plot to the sensitivity plot for the Canon 135mm f/2.0 lens seen in Figure 54, we see that the custom design with its wider bandpass and no vignetting improves detection thresholds, in the aperture averaged case, by 0.41 visual magnitudes. In Table 6, we compare the sensitivity of the commercial and custom f/2.0 lenses for detection of a GEO target while the lens is in sidereal track. The significant advantage of the custom lens is at large field angles. When averaged over the full field, this gives the custom lens the edge for random satellite detections, but, in the center of the field, both lenses are essentially equal in performance. The slight improvement in sensitivity for the custom lens results from its wider spectral bandwidth.

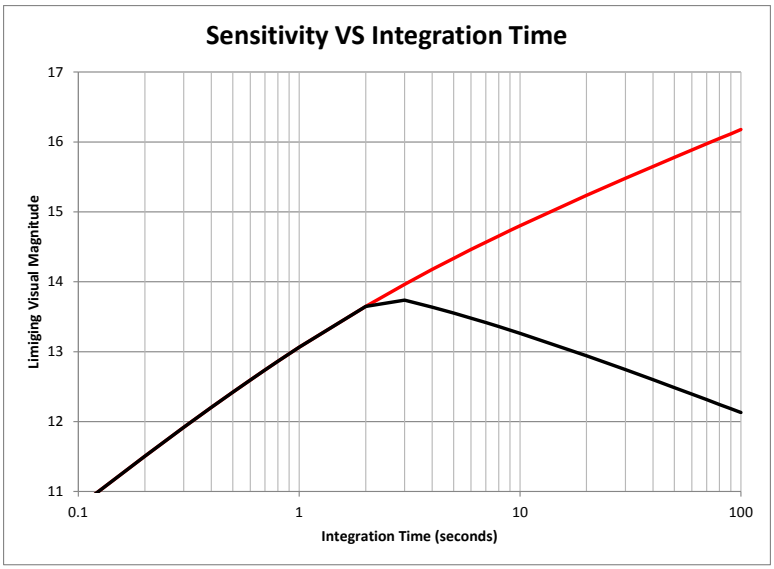

Figure 75. Custom 135mm f/2.0, averaged aperture – sidereal tracking

Table 6. Comparing sensitivity of commercial and custom 135mm focal length, f/2.0 lenses.

		Sidereal Tracking Commercial 135/2.0 Lens	Sidereal Tracking Custom 135/2.0 Lens
Centered	Center of Field	13.60	13.66
	70% of Field	13.24	13.66
	Edge of Field	12.70	13.66
4X Split	Center of Field	12.66	12.65
	70% of Field	12.30	12.65
	Edge of Field	11.75	12.65

The custom 135mm, f/2.0 lens performs well, but it requires 15 lens elements and would therefore be more expensive to produce. The Nikon 135mm, f/1.8 lens seen in Figure 30 also requires 15 lens elements, but as seen in Figure 31, its image quality is roughly one half that of our custom lens. The Nikon patent design is faster at f/1.8, but it also exhibits vignetting and was designed for a narrower optical bandpass. Still, the data in Table 6 demonstrate only a modest improvement in sensitivity for what is likely to be an expensive lens to build in small quantities.

If one is going to the trouble of designing a custom lens, it might just as well be designed to operate with as large an aperture as reasonably possible. Once again, following what turned out to be some extremely lengthy design and optimization work, the custom optical design has been modified to operate at a focal ratio of f/1.4. The optical layout for this lens is seen in Figure 76 with the ray-traced spot diagram seen in Figure 77.

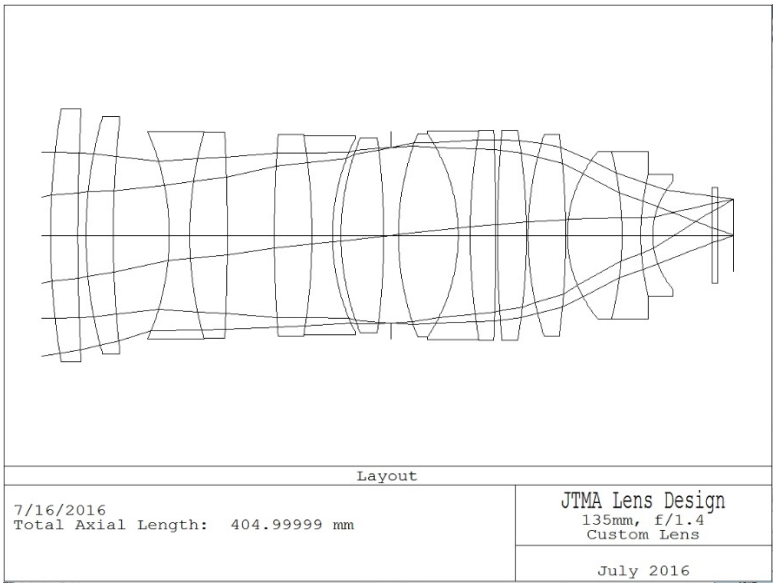

Figure 76. Layout for custom design 135mm, f/1.4 lens [113].

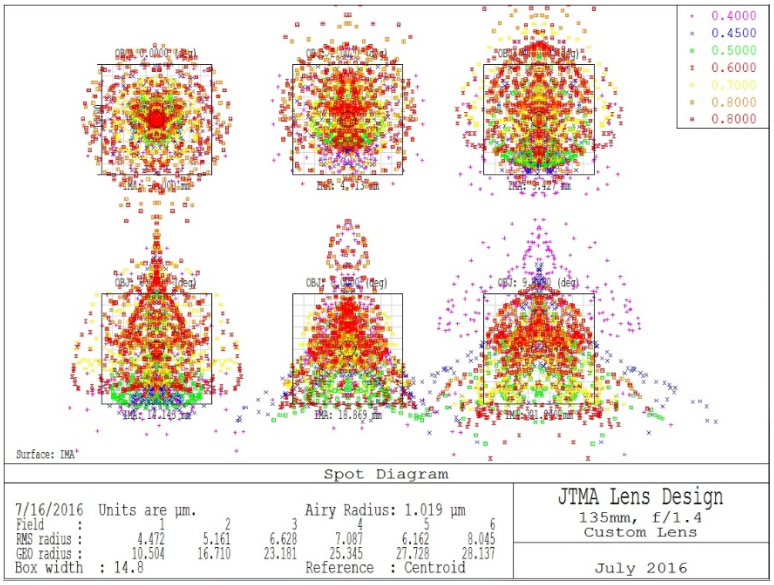

Figure 77. Spot diagram for custom design 135mm, f/1.4 lens [113].

The spot diagram for the 135mm, f/1.4 lens is noticeably worse than that for the custom 135mm, f/2 lens, but of roughly the same quality as the commercial Canon 135mm, f/2.0 lens. The f/1.4 lens does, however, pass more than twice the light of the commercial lens (due to both aperture and vignetting), and essentially twice the light of the f/2.0 custom lens. The layout for the two custom lenses appear to have some similarities, but there are important internal differences nonetheless.

A plot of sensitivity for the 135mm, f/1.4 lens is seen in Figure 78. At 14.17 visual magnitudes across the full field, this lens is 0.92 magnitudes more sensitive than the aperture averaged performance of the commercial Canon f/2.0 lens. In Table 7, we compare performance for the two lenses at the center, 70%,

and edge field points. With its 97-mm diameter aperture and zero vignetting, the custom f/1.4 design simply collects a lot more light than the alternatives, and has a resulting higher sensitivity.

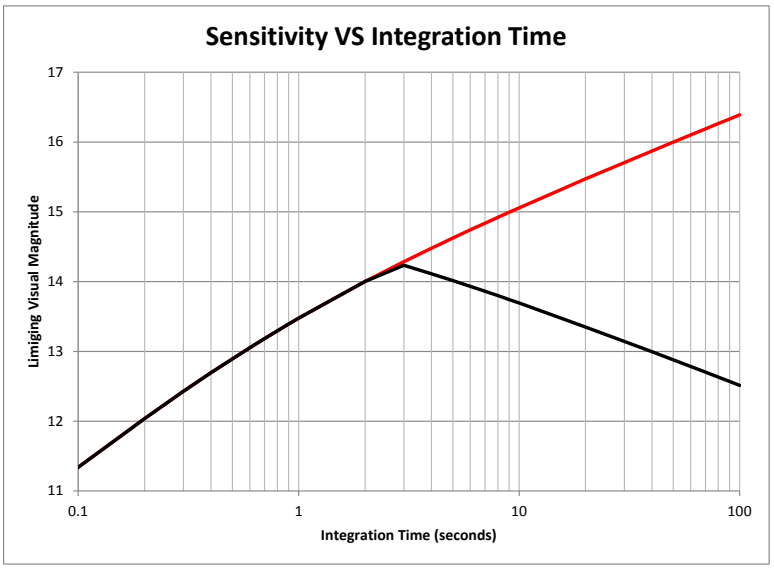

Figure 78. Custom 135mm f/1.4, averaged aperture – sidereal tracking

Table 7. Comparing sensitivity of commercial and custom 135mm focal length, f/2.0 and f/1.4 lenses.

		Sidereal Tracking Commercial 135/2.0 Lens	Sidereal Tracking Custom 135/1.4 Lens
Centered	Center of Field	13.60	14.17
	70% of Field	13.24	14.17
	Edge of Field	12.70	14.17
4X Split	Center of Field	12.66	13.22
	70% of Field	12.30	13.22
	Edge of Field	11.75	13.22

5.3 Larger Custom Lens Examples

The 135mm focal length custom lens designs presented in the previous section had apertures of 67.5 mm and 97 mm. The lenses were designed with an internal aperture stop, placing some lenses in front of the stop and some to the rear. While this is not a fully symmetrical arrangement, the fore and aft placement of elements helps to reduce optical aberrations. The problem with this approach is that it results in lens diameters that are larger than the system aperture. The extra lens element diameter is necessary to prevent vignetting for off axis field points. As an example, consider again, the 135mm, f/1.4 lens as shown in

Figure 76. We present the same layout again in Figure 79, but this time we show only light rays that enter the system with an angle of zero degrees relative to the optical axis. These are often referred to as being "on axis" light rays. Note how the light bundle entering the first element does not fill the entire aperture. This image, of course, shows only the rays that actually pass through the aperture stop and contribute to the image. There are light rays outside this bundle that enter the first lens but eventually fail to pass through the aperture; these are not shown.

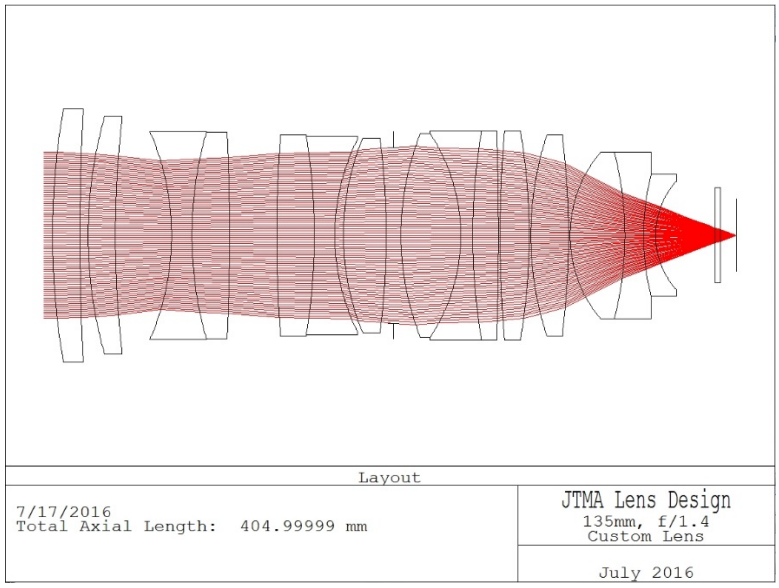

Figure 79. Layout for custom design 135mm, f/1.4 lens, showing on-axis light rays only [113].

In more traditional configurations, the designer would limit the diameter of the first lens element to be only slightly larger than the diameter required to accommodate the on-axis light bundle. Other lens element diameters are adjusted as required to produce an acceptable light falloff at the edge of the field. This adjustment reduces weight and cost, and has the added benefit of significantly simplifying the optical design.

For our two custom 135mm focal length lenses, the diameter of the largest lens elements were:

- f/2.0 design 134 mm
- f/1.4 design 148 mm

As most standard production, optical glass is available only in strips of 40 mm thickness and 160 mm width, these two lenses are nearing the practical limits of manufacturability. A smaller number of glass types are available in larger blanks as standard production, and a modest number of glasses can be special ordered in larger blanks. An example of larger glass materials comes from the Ohara I-Line catalog [114]. These are special glasses with improved ultraviolet transmission. Most are available in blanks up to 300 mm diameter. This catalog is, however, limited in the number and types of glass available.

As a result of glass limitations, the largest practical aperture for lens designs employing catalog glass materials is about 150 mm. For traditional commercial designs that exhibit vignetting, this limits one to

lenses ranging from a 400mm, f/2.8 lens to a 200mm, f/1.4 system. For custom lenses with an internal aperture stop, designed for zero vignetting, we are limited to roughly a lens of 250mm focal length with an f/2.0 focal ratio. An alternate optical design places the aperture stop on the first lens element, similar to how a refractor is designed. In such cases, we can increase aperture slightly and achieve a lens of 300mm focal length with an f/2.0 focal ratio, but the field of view is not quite as wide as that achieved by designs with an internal aperture stop. An example 300mm, f/2.0 lens is shown in Figure 80. This lens has excellent image quality, as seen in Figure 81, but only achieves this with a field of 10 degrees.

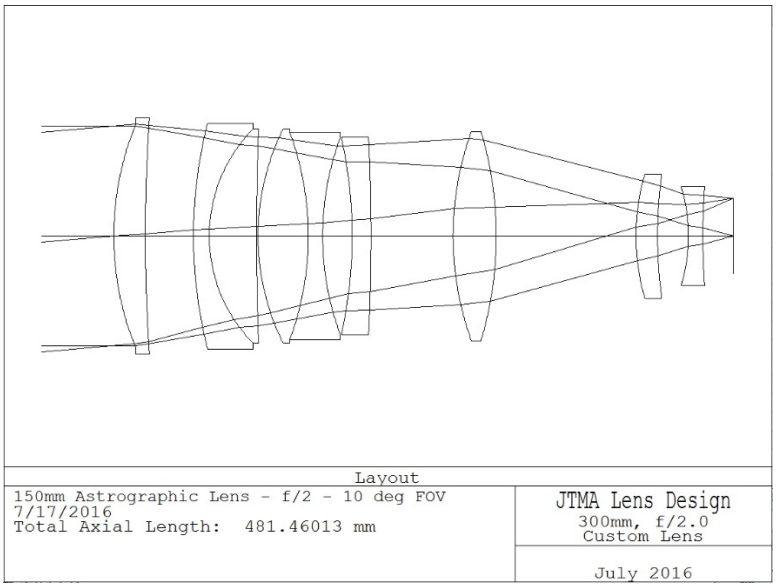

Figure 80. Layout for custom design 300 mm, f/2.0 lens [113].

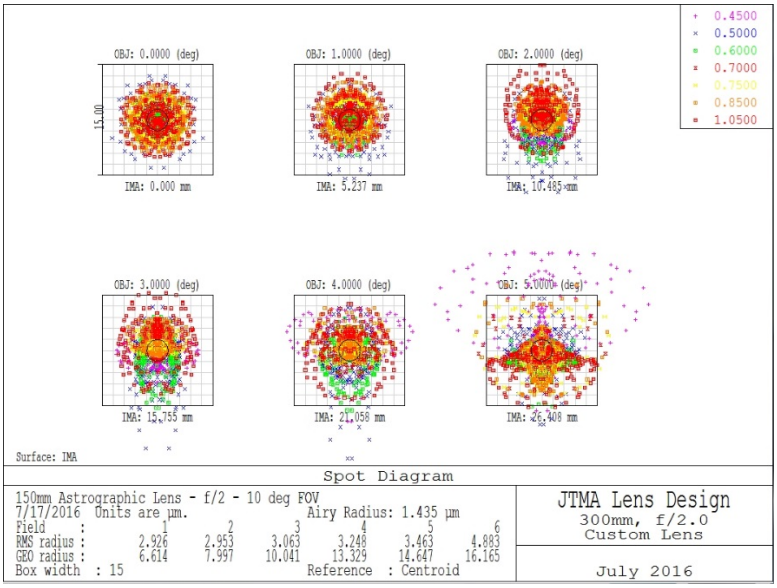

Figure 81. Spot diagram for custom design 300 mm, f/2.0 lens [113].

For lenses much larger than the above examples, the design approach must change, and two techniques are available. First, we could use conventional types of glass, available in large diameter blanks, design the equivalent of a large auxiliary wide-angle lens to sit out front of a smaller aperture lens system. From the world of commercial photographic equipment, auxiliary wide-angle lenses were negative power, afocal Galilean telescopes that were attached to the front of camera lenses. They maintained the designed aperture ratio of the camera lens, but reduced the focal length to result in a wider image field. We can use the same concept to maintain focal ratio while increasing aperture and focal length. This approach has optical limits and is useful for pushing apertures to about 175 mm diameter, but not much larger. Rather than being an afocal attachment, the front focal reducer is optimized together with the rear lens to produce an integrated, higher performance design. An example of this concept is seen in Figure 82. This lens has a 175 mm aperture, a 268mm focal length, and images a field of 15 degrees diameter producing a 70-mm diameter image circle. The first four lenses are all of BK7 and F2 type glass. The remaining nine lenses are all small enough to be made from catalog glass types.

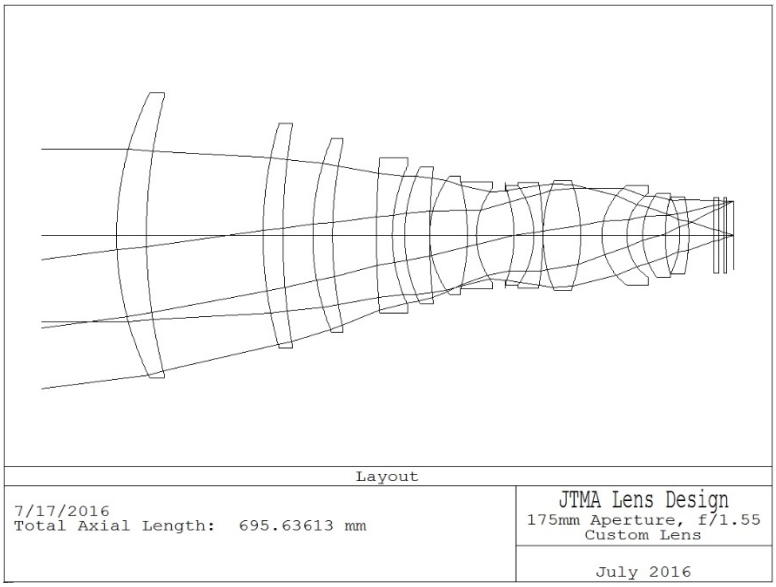

Figure 82. Layout for custom 175 mm aperture, f/1.55lens [113].

The other approach to realizing larger lenses without custom ordering special types of glass, is to use only materials that are available in large diameters. For our purposes, these include Schott types BK7, F2, and LLF1, along with fused silica and crystalline calcium fluoride. The limiting material here is the CaF_2, which is normally only available up to about 320-mm diameter without special production efforts. This is a greatly reduced set of materials to work from, but fortunately CaF_2 is renowned for its extremely low chromatic dispersion.

As an example of such a lens design, consider the optical layout shown in Figure 83. This lens was designed to duplicate the aperture and focal length of the famed Zeiss BMK-75 ballistic camera lens [1], but was optimized for a much wider chromatic bandpass and designed to use a flat CCD photon detector. The aperture is 300 mm while the focal length is 750mm. The system is designed to image a field of 10.2 degrees onto an STA-1600 CCD, having a diagonal measurement of 134 mm. Image quality, represented by the ray-traced spot diagram, is seen in Figure 84.

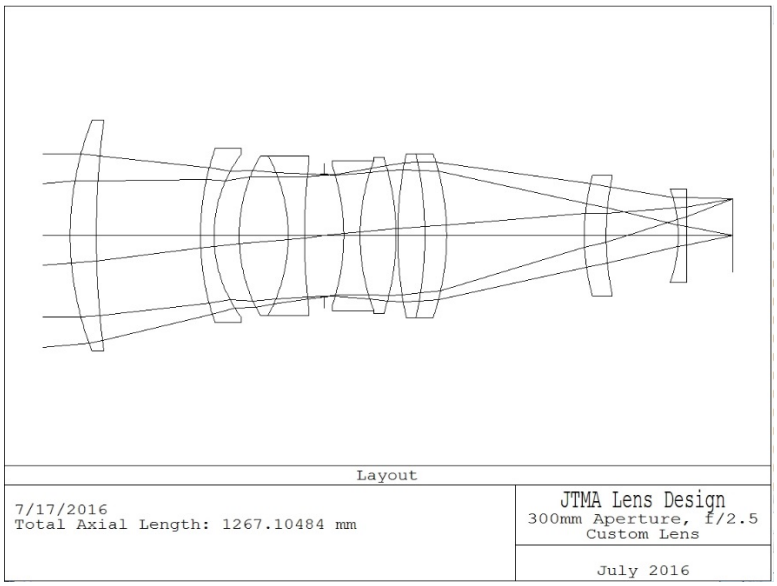

Figure 83. Layout for custom 300 mm aperture, f/2.5lens [113].

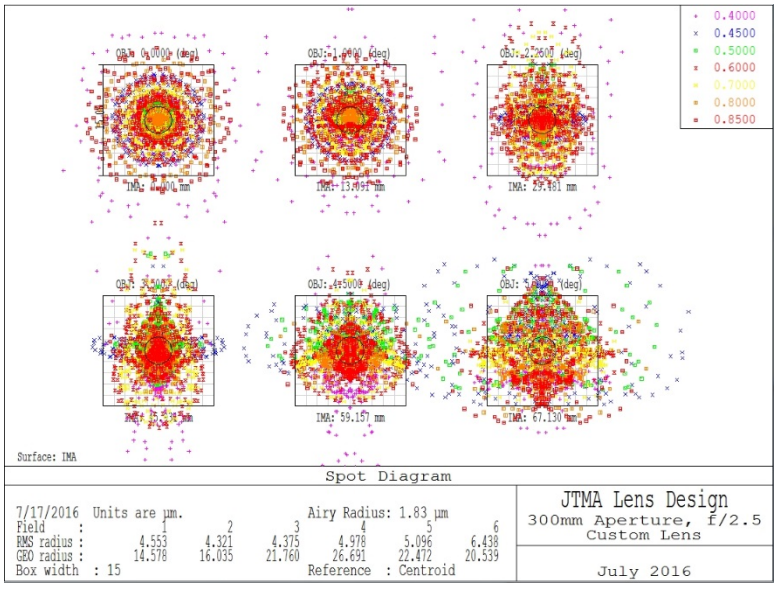

Figure 84. Spot diagram for custom 300 mm aperture, f/2.5lens [113].

Using the optical materials available in large sizes, a variety of lens designs are possible. Parameters for a few such designs are presented in Table 8.

Table 8. Parameters for select large lenses.

Aperture (mm)	Focal Length (mm)	Focal Ratio	Field of View (deg)	Limiting Magnitude
200	500	2.5	15.6	15.88
200	425	2.1	18.0	16.00
200	400	2.0	19.2	16.05
250	750	3.0	17.0	16.40
250	500	2.0	10.0	16.25
300	750	2.5	10.2	16.50

The primary reason for going to larger aperture lenses is to increase the limiting magnitude for the survey instrument. Table 8 also includes calculated limiting magnitudes of GEO targets for each of these six lenses, assuming sidereal tracking. Each of these lenses, with the proper CCD, is capable of detecting targets more than 2 magnitudes fainter than the commercial 135mm focal length lens, and in one case, almost 3 magnitudes fainter. Clearly, there is no substitute for effective aperture.

5.4 Custom APO Refractors

Well-designed traditional APOs have near diffraction limited performance, but this is usually on a curved focal surface. For imaging applications, these telescopes normally require a field flattening optic, usually with two or three lens elements. The newer APOs designed specifically for imaging normally have the field flattening elements designed into and optimized with the overall optical system, thereby providing some improvement in image quality. The potential for improving image quality with traditional APOs is quite limited due to their current performance. Dedicated imaging APOs, as mentioned above, are beginning to look more like camera lenses and often rely on some reduction in optical performance to achieve wider fields of view. These systems can be improved upon with the right optical design.

As APOs see limited use in lens array-based survey work, we will not dedicate much space to the topic, but will provide a single comparison of a custom imaging APO to the approximated performance for a commercial, 102 mm aperture, f/5.1, sextuplet APO. Available information indicated the commercial APO was optimized for a bandpass of 490 to 680 nm and had six lenses in two groups. The front group included S-FPL53 glass by Ohara, while the rear group included H-FK61 glass from CDGM. The optical layout for the approximated commercial APO is seen in Figure 85, with its corresponding spot diagram seen in Figure 86. The approximated design was optimized to closely match published spot diagrams for the commercial APO [115].

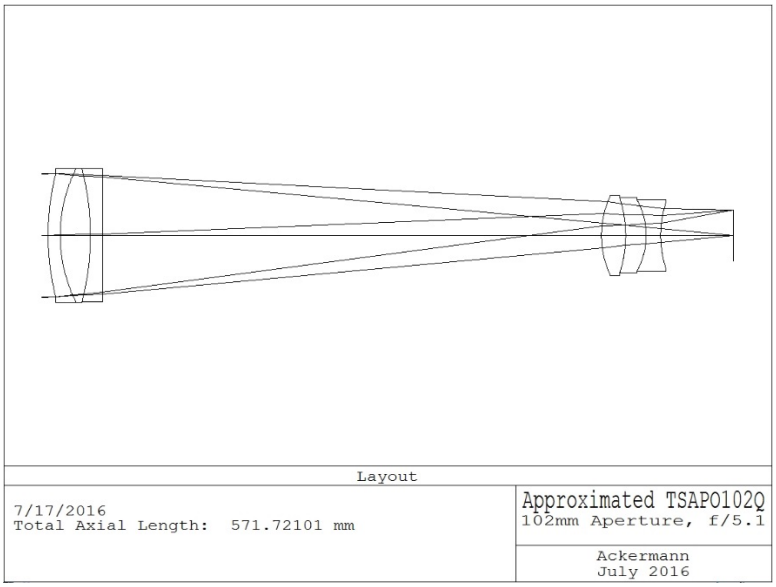

Figure 85. Layout for approximated 102 mm aperture, f/5.1 APO [113].

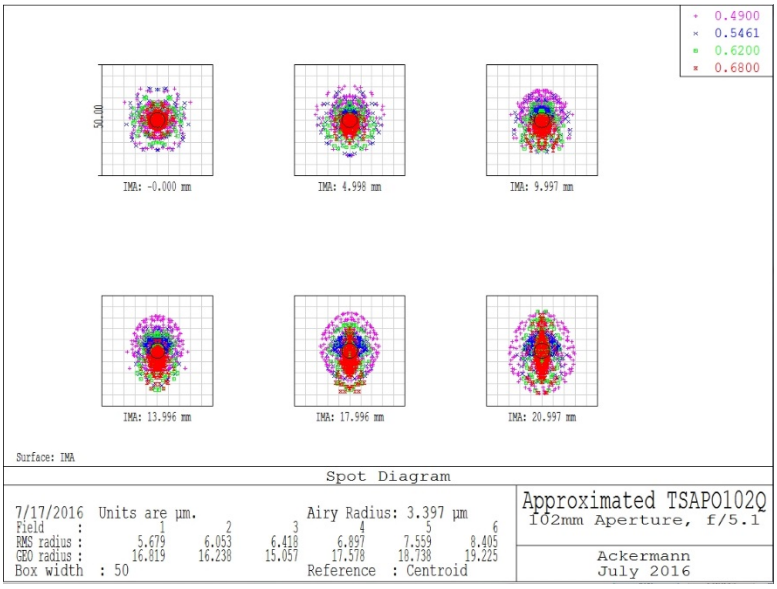

Figure 86. Spot diagram for approximated 102 mm aperture, f/5.1 APO [113].

The custom APO was designed to match the aperture, focal ratio, and field of view of the commercial unit, but was optimized for near diffraction limited performance over a bandpass of 375 to 900 nm. The spot diagram for the custom APO is shown in Figure 87. Note the scale difference between Figures 86 and 87. Details of the custom APO optical design were not available, but it was mentioned to contain only a single element of low dispersion glass and has a flat image surface with significant back focus.

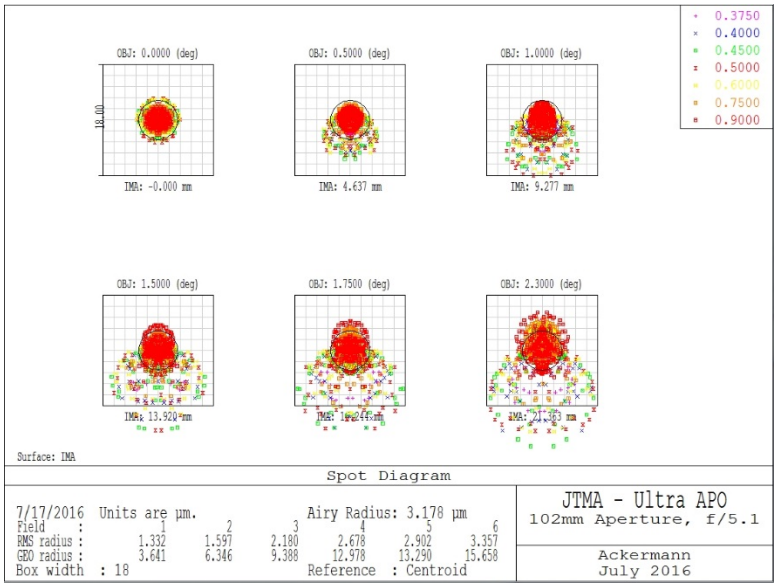

Figure 87. Spot diagram for custom 102 mm aperture, f/5.1 APO [113].

When comparing the sensitivity for GEO targets while engaged in sidereal tracking, we find that the commercial APO achieves 13.18 visual magnitudes, while the custom design can reach 13.88 magnitudes, both with an SNR=6, using a KAI-16000 CCD. The tighter spots and wider bandpass of the custom APO result in 0.7 visual magnitudes more sensitivity from the same aperture optical system.

6 Lenses vs. Telescopes: Cost and Performance

The previous sections were all dedicated to wide-field, large aperture lens systems for space surveillance. When evaluating the effectiveness and efficiency of these systems, it is important to compare them to telescopes to gain a better understanding of where each type of optical system offers the best combination of coverage and sensitivity, with the lowest overall cost. In this section, we compare lenses with modern versions of traditional reflecting telescopes, catadioptric telescopes, and medials.

6.1 General Characteristics of Optical Systems

Lens systems are limited in aperture to something less than approximately 300 mm. There are examples of refractive ballistic cameras with larger aperture lenses, but these are rare instruments with performance suitable for film but limited by present standards. The three great advantages of lens systems are that they (1) do not have reflecting surfaces, with 7% to 9% loss of light for each reflection; (2) do not suffer from obscuration; and (3) generally can produce wider fields of view than reflective systems. The disadvantages include complex designs with multiple elements, many air-to-glass interfaces, weight, cost, and chromatic aberration. Lenses are best used in applications requiring wide fields of view, where their more limited apertures will not hinder the collection goals.

Reflective systems require a mirror and, in all but a very few cases, the designs include obscuration, which reduces their effective collection aperture. The earliest reflective systems used only mirrors, but almost all modern reflecting telescopes include a combination of lenses and mirrors to widen their field of view, flatten the image plane, widen the chromatic bandpass, and improve image quality. Most modern systems are based on the prime focus corrector [116], dating to 1913, and corrected Cassegrain systems [117], similarly dating to 1913.

Reflective systems have the advantage of being available with much larger apertures than refractive systems, but they often come with much more narrow fields of view. The one exception is the three-mirror anastigmat system by Paul [118], dating to 1935. The Paul system is capable of much wider fields than either the prime focus or Cassegrain systems, but it comes with significant obscuration, light losses from three reflections, and it still requires refractive correcting lenses.

While Sampson, later followed by Ross and Wynne, attempted to correct and widen the field of traditional reflecting telescopes, a great improvement in wide-field systems was introduced by Schmidt in 1930 [119]. The system combined a thin aspheric corrector plate located at both the aperture stop and center of curvature for a spherical mirror. The Schmidt camera had a field of view significantly wider than any optical system of its time. The full aperture aspheric corrector plate introduced essentially zero optical power while correcting the optical aberrations of the spherical mirror. Schmidt introduced the concept of the full-aperture catadioptric optical system.

It is interesting to note that Schmidt also developed a similar system that used three spherical mirrors instead of the aspheric corrector plate [120]. This contribution of Schmidt is not well known, but is essentially identical to the three-lens system patented by Houghton in 1944 [121].

What is known today as the Houghton system uses either two or three spherical lenses forming what is essentially an afocal, full-aperture corrector for a spherical mirror telescope. The optical system is also

known as the Richter-Slevogt [122], mostly in eastern-Europe and Russia. The Richter-Slevogt optical system has been extensively studied by the master Russian designer, Terebizh [123], who introduced modifications that significantly widen the field of view.

Medial optical systems are much less well known than any of the designs mentioned above. The medial combines the functions of a lens with that of a mirror. These designs feature full aperture refractive elements, like a catadioptric, but the lens contributes approximately half the total optical power. The best known medial system is based on the British patent of Hamilton [124] dating to 1814, but the design approach, was in fact, anticipated by Sir Isaac Newton as described in his, previously unpublished, notes of 1673 [125]. Medials are capable of very wide fields and are relatively simple optical designs.

Catadioptric systems, such as the Schmidt, can image fields as wide as 20 degrees or more, but the image is produced on a curved focal surface. When modifying these systems for flat-field imaging, fields of view are much closer to 5 degrees diameter. There are no hard and fast rules, or limits, for how wide a field can be produced by a given optical system, but in general, reflective systems with flat fields wider than 10 degrees are either non-existent or suffer from poor image quality. Terebizh has prepared a masterful work comparing the performance of ten different optical systems [126], but the work did not concentrate on lens systems. Typical limits on fields of view for different optical systems are given in Table 9. These are not absolute limits, but are based on experience with typical optical systems.

Table 9. Field limits of typical optical systems.

Optical System	Typical Field (deg)
Medium-Aperture, High-Speed Lens Systems	40
Large-Aperture, High-Speed Lens Systems	20
Prime Focus Corrected Reflectors	6
Corrected Cassegrain Reflectors	5
Schmidt-Camera Catadioptric	6
Houghton-Camera Catadioptric	5
Richter-Slevogt-Terebizh Cassegrain	10
Houghton-Terebizh Cassegrain	10
Hamilton Medial	10

6.2 Comparison Criteria

The only useful comparison of dissimilar optical systems is an examination of how well, and economically, they help fulfill a given observing mission. If we restrict our interests to a search for satellites in GEO, from a given site, we need to surveil a patch of sky 120 degrees wide and 30 degrees tall. The 120 degree requirement comes from viewing to within 30 degrees of the horizon on either side of the zenith, while the 30 degree tall requirement comes from the expectation that most GEO satellites have inclinations less than 15 degrees. Given this area of 3600 square degrees, the important performance parameters are sensitivity, search rate (or coverage rate), and cost.

Sensitivity was discussed extensively in previous sections. For search, we want to design an observing program that guarantees that no satellite bright enough to be seen can escape detection resulting from incomplete coverage of the sky. With this in mind, two observing strategies need to be evaluated. One strategy is to use enough optical systems to continuously observe the entire 3600 square degrees of sky (or very close to that value). These systems are fixed and do not require repositioning or any type of tracking. We refer to these as staring systems.

The other strategy uses one or more systems on a moving mount to continuously tile the sky with small observing patches. The mounts need to reposition the optical systems quickly, and then execute a sidereal track while the cameras record. We refer to these as tracking systems.

The key parameter is the search rate, which can be calculated in one of two ways. One simple view of search rate is to take the image area of a system and multiply it by the number of fields that can be exposed each hour, giving a value of square degrees per hour. The time required for each field depends upon the integration time, image download time, number of frames per field, and move time. We assume the move time is 5 seconds, with exposure times determined by the optical system and read times of 3 seconds per frame. The final frame for any field can be read out while the system is moving to the next field position. A total of three frames are recorded at each field point. This approach gives a raw search rate, but it does not guarantee a leak proof search strategy.

The second way to calculate search rate is to determine how long it takes a satellite to cross the image field for each optical system. This value is then used as the maximum interval between revisits by the optical system. While a telescope and drive might be able to cover more square degrees each hour, the requirement for revisit effectively limits the useful search rate. This approach produces a lower search rate, thereby requiring more optical systems to cover the 3600 square degree patch of sky.

To calculate total system cost, we use published prices for telescopes, where available, or estimate the cost based on commercial optics for the lens systems. Each optical system requires a camera and a computer. For the step and track search strategy, each optical system also requires a mount and drive. Other than the optical systems, the estimated cost of components used for this study are shown in Table 10.

Table 10. Estimated cost of system components.

Item	Cost
43mm CCD Camera	$10,000
52mm CCD Camera	$15,000
61mm CCD Camera	$20,000
70mm CCD Camera	$20,000
87mm CCD Camera	$150,000
135mm CCD Camera	$200,000
Mount/Drive Cost	$10,000
Computer Cost	$5,000

6.3 Cost vs. Sensitivity

6.3.1 Commercial Lens Arrays

As the primary topic of this report is lens arrays, we examine the cost vs. performance trades first. Table 11 presents the characteristics of ten commercial lens systems ranging from 24 to 400 mm focal length. Each lens is based on available information for a commercial product. Prices are based on published values for current similar products. Performance is reported in terms of limiting visual magnitude with an associated total cost per site for both staring and tracking systems. These data are presented in Table 12 and shown graphically in Figure 88. Note that the costs for the lenses are presented in dollars, while the cost for a site is given in thousands of dollars.

Table 11. Characteristics of commercial lens systems.

Commercial Lenses		Aperture	Focal Length		CCD Diagonal	FOV	Limiting Magnitude	Limiting Magnitude	Typical Cost
Manufacturer	Model	(mm)	(mm)	f/#	(mm)	(deg)	Staring	Tracking	($)
Commercial	L 24/1.4 - Aspheric	17.5	24.5	1.4	43	82.54	12.0	11.1	$4,999
Commercial	L 28/1.4 - Aspheric	20	28	1.4	43	75.04	12.2	11.4	$4,999
Commercial	L 35/1.4 - Aspheric	25	35	1.4	43	63.12	12.5	11.6	$999
Commercial	L 50/1.2 - Aspheric	41.5	50	1.2	43	46.54	12.9	12.0	$1,349
Canon	L 85/1.2 - Aspheric	71	85	1.2	43	28.39	13.3	12.4	$1,899
Commercial	L 100/2.0 - Aspheric	50	100	2.0	43	24.27	14.0	13.1	$499
Canon	L 135/2.0	67.5	135	2.0	43	18.10	14.3	13.3	$999
Canon	L 200/1.8	111	200	2.0	43	12.27	15.2	14.1	$5,699
Canon	L 300/2.8	107	300	2.8	43	8.20	15.0	13.7	$6,099
Canon	L 400/2.8	143	400	2.8	43	6.15	15.4	14.1	$9,999

Table 12. Performance vs. cost for commercial lens array sites.

Commercial Lenses		Staring			Tracking		
Manufacturer	Model	Number Required	Sensitivity	Total Site Cost (k$)	Number Required	Sensitivity	Total Site Cost (k$)
Commercial	L 24/1.4 - Aspheric	2	12.0	$40	1	11.1	$30
Commercial	L 28/1.4 - Aspheric	2	12.2	$40	1	11.4	$30
Commercial	L 35/1.4 - Aspheric	2	12.5	$32	1	11.6	$26
Commercial	L 50/1.2 - Aspheric	3	12.9	$49	1	12.0	$26
Canon	L 85/1.2 - Aspheric	10	13.3	$169	1	12.4	$27
Commercial	L 100/2.0 - Aspheric	12	14.0	$186	1	13.1	$25
Canon	L 135/2.0	24	14.3	$384	1	13.3	$26
Canon	L 200/1.8	48	15.2	$994	1	14.1	$31
Canon	L 300/2.8	119	15.0	$2,511	1	13.7	$31
Canon	L 400/2.8	207	15.4	$5,175	3	14.1	$105

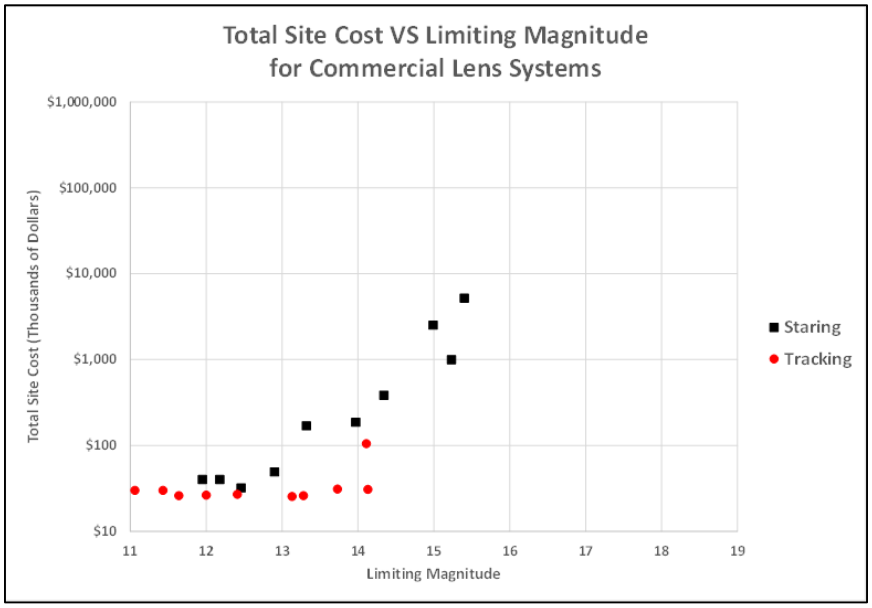

Figure 88. Limiting magnitude vs. cost for commercial lens arrays.

6.3.2 Custom Lens Arrays

Data for arrays of custom lenses are presented in Tables 13 and 14 and in Figure 89.

Table 13. Characteristics of custom lens systems.

Custom Lenses		Aperture (mm)	Focal Length (mm)	f/#	CCD Diagonal (mm)	FOV (deg)	Limiting Magnitude Staring	Limiting Magnitude Tracking	Estimated Cost ($)
Manufacturer	Model								
JTMA Design	Non Vignetting 135/2	67.5	135	2.0	43	18.10	14.9	13.9	$5,573
JTMA Design	Non Vignetting 135/1.4	97	135	1.4	43	18.10	15.2	14.3	$9,956
JTMA Design	Non Vignetting 200/2	100	200	2.0	52	14.81	15.6	14.7	$16,000
JTMA Design	Non Vignetting 400/2.8	143	400	2.8	87	12.41	16.4	15.4	$20,000
JTMA Design	Non Vignetting 300/2	150	300	2.0	52	9.91	16.4	15.4	$19,998
JTMA Design	NVNon Vignetting	200	400	2.0	135	19.16	16.9	16.0	$31,688
JTMA Design	Non Vignetting 425/2.125	200	425	2.1	135	18.05	17.0	16.0	$31,688
JTMA Design	Non Vignetting 500/2.5	200	500	2.5	135	15.38	17.0	15.9	$31,688
JTMA Design	Non Vignetting 500/2	250	500	2.0	87	9.94	17.2	16.3	$45,284
JTMA Design	Non Vignetting 750/2.5	300	750	2.5	135	10.29	17.6	16.5	$60,623

Table 14. Performance vs. cost for custom lens array sites.

Custom Lenses		Staring			Tracking		
Manufacturer	Model	Number Required	Sensitivity	Total Site Cost (k$)	Number Required	Sensitivity	Total Site Cost (k$)
JTMA Design	Non Vignetting 135/2	24	14.9	$494	1	13.9	$31
JTMA Design	Non Vignetting 135/1.4	24	15.2	$599	1	14.3	$35
JTMA Design	Non Vignetting 200/2	33	15.6	$1,188	1	14.7	$46
JTMA Design	Non Vignetting 400/2.8	42	16.4	$7,350	1	15.4	$185
JTMA Design	Non Vignetting 300/2	68	16.4	$2,720	1	15.4	$50
JTMA Design	NVNon Vignetting	18	16.9	$4,260	1	16.0	$247
JTMA Design	Non Vignetting 425/2.125	18	17.0	$4,260	1	16.0	$247
JTMA Design	Non Vignetting 500/2.5	33	17.0	$7,811	1	15.9	$247
JTMA Design	Non Vignetting 500/2	68	17.2	$13,619	1	16.3	$210
JTMA Design	Non Vignetting 750/2.5	64	17.6	$17,000	1	16.5	$276

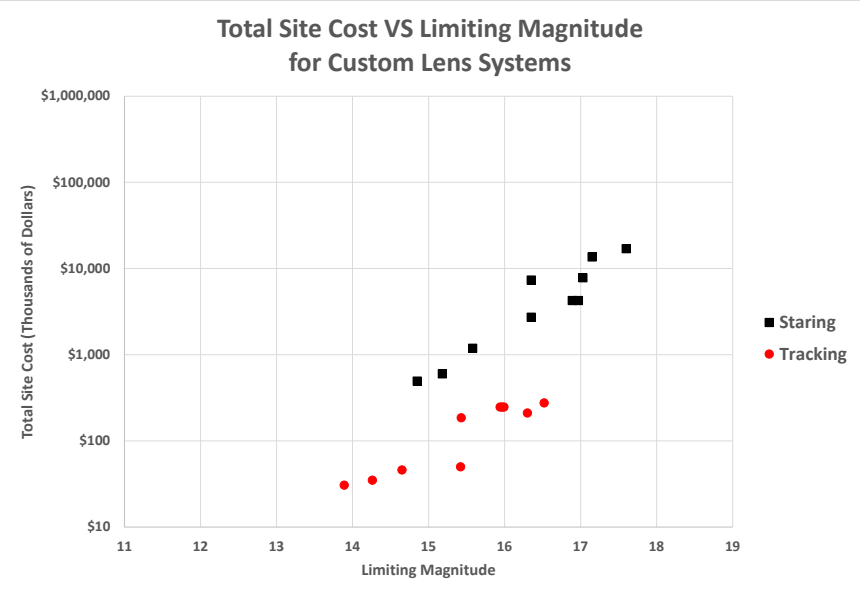

Figure 89. Limiting magnitude vs. cost for custom lens arrays.

6.3.3 Arrays of Reflecting Telescopes

This section reports data for fast, commercial, reflecting telescopes of 600 mm aperture and smaller.

Table 15. Characteristics of reflecting telescope systems.

Reflecting Telescopes		Aperture (mm)	Focal Length (mm)	f/#	CCD Diagonal (mm)	FOV (deg)	Limiting Magnitude Staring	Limiting Magnitude Tracking	Optical System Cost ($)
Manufacturer	Model								
APM	Large Prime Focus Astrograph	560	1120	2.0	87	4.45	18.0	17.1	$101,250
APM	Wynne-Riccardi-Astrograph	305	850	2.8	87	5.86	17.4	16.3	$20,250
APM	Wynne-Riccardi-Astrograph	406	1130	2.8	87	4.41	17.8	16.9	$50,625
APM	Wynne-Riccardi-Astrograph	560	1400	2.5	87	3.56	18.2	17.3	$101,250
APM	Wynne-Riccardi-Astrograph	600	1500	2.5	87	3.32	18.4	17.4	$118,100
Astro Systeme Austria	ASA Astrograph 8H	200	560	2.8	52	5.32	15.7	14.5	$12,200
Officina Stellare	RiFAst 300	300	1150	3.8	61	3.04	16.7	15.4	$26,995
Officina Stellare	RiFAst 400	400	1550	3.8	70	2.59	17.1	15.8	$26,995
Officina Stellare	RiFAst 500	500	1900	3.8	87	2.62	17.9	16.7	$49,695
Officina Stellare	Ultra CRC 300	300	1620	5.4	61	2.16	16.6	15.2	$16,475
Officina Stellare	Veloce RH 200AT	200	600	3.0	43	4.10	15.3	14.0	$7,795
Officina Stellare	Veloce RH 300	300	900	3.0	61	3.88	16.2	14.9	$24,395
Officina Stellare	Veloce RH 350	350	980	2.8	61	3.57	16.4	15.1	$40,695
Takahashi	Epsilon 130D	130	430	3.3	43	5.72	15.0	13.7	$2,995
Takahashi	Epsilon 180	180	500	2.8	43	4.92	15.7	14.3	$5,400
TS Boren-Simon	PowerNewton Astrograph	200	560	2.8	25	2.56	15.7	14.5	$2,160
TS Boren-Simon	PowerNewton Astrograph	254	711	2.8	25	2.01	15.9	14.6	$2,575

Table 16. Performance vs. cost for reflecting telescope array sites.

Reflecting Telescopes		Staring			Tracking		
Manufacturer	Model	Number Required	Sensitivity	Total Site Cost (k$)	Number Required	Sensitivity	Total Site Cost (k$)
APM	Large Prime Focus Astrograph	380	18.0	$97,375	6	17.1	$1,598
APM	Wynne-Riccardi-Astrograph	203	17.4	$35,576	3	16.3	$556
APM	Wynne-Riccardi-Astrograph	380	17.8	$78,138	6	16.9	$1,294
APM	Wynne-Riccardi-Astrograph	576	18.2	$147,600	11	17.3	$2,929
APM	Wynne-Riccardi-Astrograph	663	18.4	$181,065	14	17.4	$3,963
Astro Systeme Austria	ASA Astrograph 8H	256	15.7	$8,243	4	14.5	$169
Officina Stellare	RiFAst 300	784	16.7	$40,764	19	15.4	$1,178
Officina Stellare	RiFAst 400	1056	17.1	$54,907	30	15.8	$1,860
Officina Stellare	RiFAst 500	1040	17.9	$212,883	28	16.7	$6,011
Officina Stellare	Ultra CRC 300	1580	16.6	$65,531	52	15.2	$2,677
Officina Stellare	Veloce RH 200AT	455	15.3	$10,372	9	14.0	$295
Officina Stellare	Veloce RH 300	484	16.2	$23,907	9	14.9	$535
Officina Stellare	Veloce RH 350	576	16.4	$37,840	12	15.1	$908
Takahashi	Epsilon 130D	225	15.0	$4,049	3	13.7	$84
Takahashi	Epsilon 180	319	15.7	$6,508	5	14.3	$152
TS Boren-Simon	PowerNewton Astrograph	1122	15.7	$19,254	34	14.5	$923
TS Boren-Simon	PowerNewton Astrograph	1764	15.9	$31,002	66	14.6	$1,820

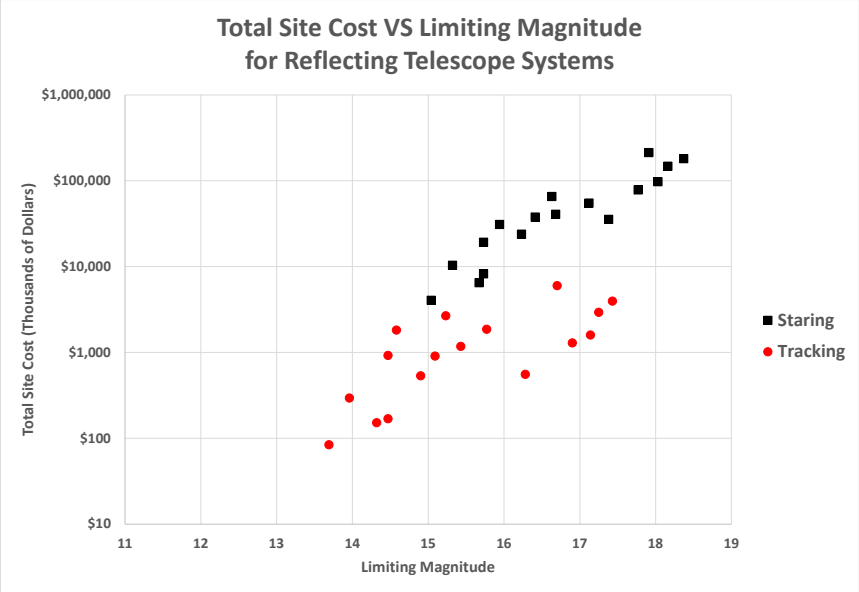

Figure 90. Limiting magnitude vs. cost for reflecting telescope arrays.

6.3.4 Arrays of Medial and Catadioptric Telescopes

Medial and catadioptric optical systems proved to be the most challenging as only a few are made for the commercial market. To augment the number of systems used for comparison, we included nine Russian systems used with ISON [127], the Sova-25 system from the Russian Pritsel Space Surveillance facility [37], and two Chinese systems (the CSTAR [128] and AST3 [129]). The three systems by Officina Stellare are actually Cassegrain form medials, while the four Celestron systems are all based on the Schmidt-camera. As there are no published cost figures for the Russian and Chinese systems, we arbitrarily assigned them a per unit cost of $20,000. The specific foreign optical systems include the following:

- GAS-250 250 mm aperture Hamilton optical system
- ORI-25 250 mm aperture Hamilton optical system
- ORI-40 400 mm aperture Hamilton optical system
- Santel-400 400 mm aperture Hamilton optical system
- Santel-500 500 mm aperture Hamilton optical system
- VT-78a 192 mm aperture Houghton-Terebizh optical system
- Genon Max 300 mm aperture Houghton-Terebizh optical system
- RST-220 220 mm aperture Richter-Slevogt-Terebizh optical system
- VT-52c 180 mm aperture Richter-Slevogt-Terebizh Cassegrain
- Sova-25 250 mm aperture Richter-Slevogt-Terebizh Cassegrain
- CSTAR 145 mm aperture Houghton-Cassegrain optical system
- AST3 500 mm aperture Baker/Schmidt/Wright optical system

The optical system of the Chinese AST3 telescope is a bit more difficult to categorize. It uses an aspheric Schmidt-type plate, combined with a hyperbolic primary mirror, followed by a lens corrector group located just before the focal plane. It includes elements of a Schmidt camera, a Wright camera [130], and a Baker Reflector Camera [131], but does not fit perfectly into any single design family. The characteristics and sensitivity of various medial and catadioptric optical systems are seen in Tables 17 and 18, with a plot of cost as a function of sensitivity in Figure 91.

Table 17. Characteristics of catadioptric and medial systems.

Catadioptrics and Medials		Aperture	Focal Length		CCD Diagonal	FOV	Limiting Magnitude	Limiting Magnitude	Optical System Cost
Manufacturer	Model	(mm)	(mm)	f/#	(mm)	(deg)	Staring	Tracking	($)
ISON	GAS-250	250	740	3.0	52	4.02	16.5	15.2	$20,000
ISON	ORI-25	250	625	2.5	52	4.76	16.6	15.4	$20,000
ISON	ORI-40	400	915	2.3	52	3.26	17.3	16.2	$20,000
Sankovich	Santel-400	400	1000	2.5	52	2.98	17.2	15.9	$20,000
Sankovich	Santel-500	500	1250	2.5	52	2.38	17.7	16.5	$20,000
Officina Stellare	Veloce RH 200AT	200	600	3.0	43	4.10	15.3	14.0	$7,795
Officina Stellare	Veloce RH 300	300	900	3.0	61	3.88	16.2	14.9	$24,395
Officina Stellare	Veloce RH 350	350	980	2.8	61	3.57	16.4	15.1	$40,695
ISON	VT-78a	192	300	1.6	52	9.91	16.0	15.0	$20,000
Borisov	Genon Max (VT-99c)	300	450	1.5	52	6.61	16.7	15.7	$20,000
ISON	RST-220 (Terebizh)	220	507	2.3	52	5.87	16.3	15.3	$20,000
ISON	VT-52c	180	294	1.6	52	10.11	15.9	14.8	$20,000
Russia	Sova-25 (VT-51d)	250	410	1.6	72	10.04	16.3	15.4	$20,000
China	CStar (sCMOS)	145	174	1.2	21	6.91	15.5	14.6	$20,000
Celestron	C-11 with HyperStar	279.4	560	2.0	28	2.86	16.1	14.9	$2,794
Celestron	RASA-11	279.4	620	2.2	43	3.97	16.4	15.2	$3,499
Celestron	C-14 with HyperStar	355.6	684	1.9	43	3.60	16.6	15.4	$5,598
Celestron	RASA-14	355.6	790	2.2	61	4.42	16.8	15.5	$9,995
China	AST3	500	1866	3.7	106	3.25	18.1	16.7	$20,000

Table 18. Performance VS cost for catadioptric and medial array sites.

Catadioptrics and Medials		Staring			Tracking		
Manufacturer	Model	Number Required	Sensitivity	Total Site Cost (k$)	Number Required	Sensitivity	Total Site Cost (k$)
ISON	GAS-250	462	16.5	$18,480	8	15.2	$400
ISON	ORI-25	324	16.6	$12,960	5	15.4	$250
ISON	ORI-40	676	17.3	$27,040	15	16.2	$750
Sankovich	Santel-400	798	17.2	$31,920	19	15.9	$950
Sankovich	Santel-500	1278	17.7	$51,120	38	16.5	$1,900
Officina Stellare	Veloce RH 200AT	455	15.3	$10,372	9	14.0	$295
Officina Stellare	Veloce RH 300	484	16.2	$23,907	9	14.9	$535
Officina Stellare	Veloce RH 350	576	16.4	$37,840	12	15.1	$908
ISON	VT-78a	68	16.0	$2,720	1	15.0	$50
Borisov	Genon Max (VT-99c)	156	16.7	$6,240	2	15.7	$100
ISON	RST-220 (Terebizh)	203	16.3	$8,120	3	15.3	$150
ISON	VT-52c	68	15.9	$2,720	1	14.8	$50
Russia	Sova-25 (VT-51d)	68	16.3	$3,060	1	15.4	$55
China	CStar (sCMOS)	150	15.5	$7,500	2	14.6	$120
Celestron	C-11 with HyperStar	885	16.1	$15,748	26	14.9	$723
Celestron	RASA-11	486	16.4	$8,991	9	15.2	$256
Celestron	C-14 with HyperStar	600	16.6	$12,359	13	15.4	$398
Celestron	RASA-14	380	16.8	$13,298	6	15.5	$270
China	AST3	861	18.1	$193,725	20	16.7	$4,700

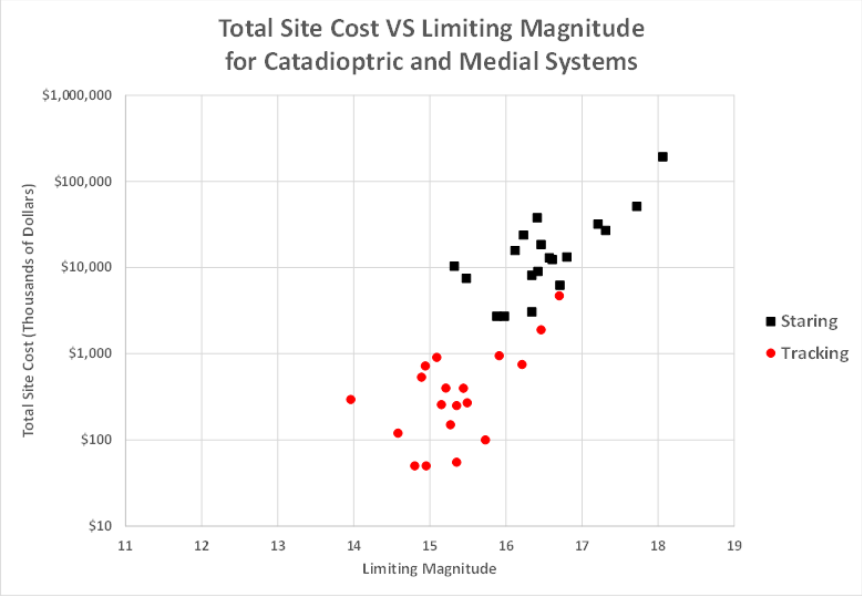

Figure 91. Limiting magnitude VS cost for catadioptric and medial arrays.

6.4 Results of Comparisons

The data presented in Section 6.3 provide for some interesting conclusions. For high sensitivity, there is no substitute for aperture. Lens systems with apertures larger than approximately 150 mm diameter are simply not available as commercial items. For high sensitivity, reflecting telescopes are the answer, but due to their size and cost, they are not suitable for staring applications where one requires continuous observation of an area covering thousands of square degrees. Reflecting telescopes are more suited to being mounted on drive mechanisms that allow for rapid repositioning and tracking.

For applications requiring continuous surveillance of wide areas of the sky, lens systems are the obvious choice, but they come with the limitation of lower sensitivity in any single frame. Lenses have sufficiently wide fields that a modest number of systems can be used to tile a significant area of the sky. With continuous surveillance, multiple frames can be stacked and processed together to improve sensitivity. Custom lenses help to improve sensitivity and utility, and can even offer wider fields with larger apertures than commercial lenses, but they still cannot approach the capabilities of reflecting telescopes.

Between reflecting telescopes and photographic lenses are the interesting optical designs known as catadioptrics and medials. These systems offer wider fields than traditional reflecting telescopes, but are limited to roughly 10 to 12 degrees total field and therefore cannot replace photographic lenses. Medials and catadioptrics, however, can easily be produced with apertures much larger than most lens systems and at a fraction of the price. Similar to reflecting telescopes, these systems do suffer from obscuration and some designs have vignetting, but it is much easier to increase the aperture of a medial or catadioptric, than to increase the aperture of a lens system. It is interesting to note that project ISON, which is perhaps the largest global assembly of telescopes performing space surveillance, uses significant numbers of medial and catadioptric telescopes of the Hamilton, Richter-Slevogt, and Houghton-Terebizh configurations.

Combined with the selection of optical system, one must also consider whether to image while staring or in sidereal track. For fixed camera arrays, the only choice is to stare. The staring system has advantages in sensitivity but disadvantages in image processing. However, if one keeps the exposures sufficiently short, the stars will not streak more than a single pixel, and image processing and data reduction are fairly simple. Tracking systems result in well-defined star fields, making data reduction much easier, but the streaking targets result in a lower sensitivity without the application of other techniques such as streak integration, image stacking, and multiple hypothesis tracking.

7 All-Sky, Whole-Sky, Meteor, Aurora and Fisheye Cameras

As discussed in previous sections, staring arrays of lens systems are useful for continuous imaging of very wide fields at low to moderate sensitivity, while a smaller number of tracking telescopes (reflectors, medials, or catadioptrics) can image the same area with higher sensitivity but without continuous coverage. To provide a more complete treatment of the overall topic, it is necessary to examine the utility of optical systems intended to capture all, or at least most, of the sky with a single image. Such systems are described by a number of different names, usually somewhat related to their intended application. They are, at times, known as all-sky cameras; whole sky cameras; cloud, meteor, canopy, or aurora cameras; and fisheye cameras. Some people simply refer to these systems as hemisphere cameras.

7.1 Development of Whole-Sky Imaging Systems

A review of the technical literature suggests that the first use of wide-field cameras to image all, or most, of the sky occurred in 1896 when Koppe used multiple cameras and parallax to measure the height of clouds [132]. In 1905, Mueller was working with a camera that rotated to collect a hemispheric image of the sky. The work was reported by Fassiq in 1915, but Fassiq states that he watched a demonstration of the camera 10 years before [133]. The camera was inclined at a 45-degree angle. It would rotate about a vertical axis, while the film inside also rotated. A picture of the camera is seen in Figure 92, with a sample image shown in Figure 93.

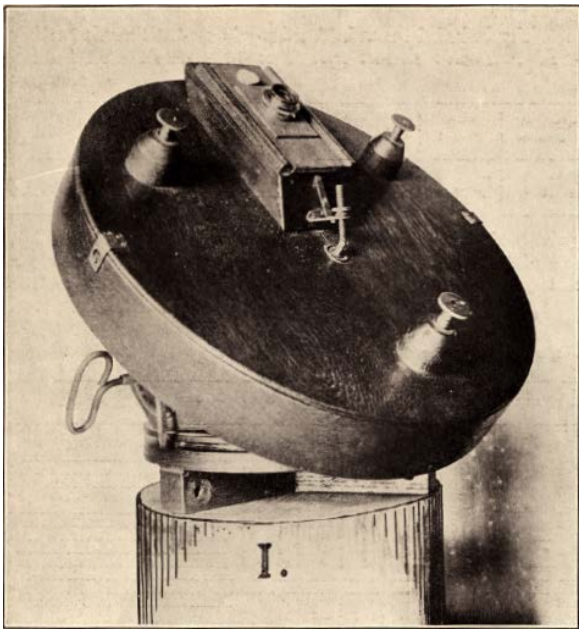

Figure 92. Mueller whole sky camera (circa 1905).

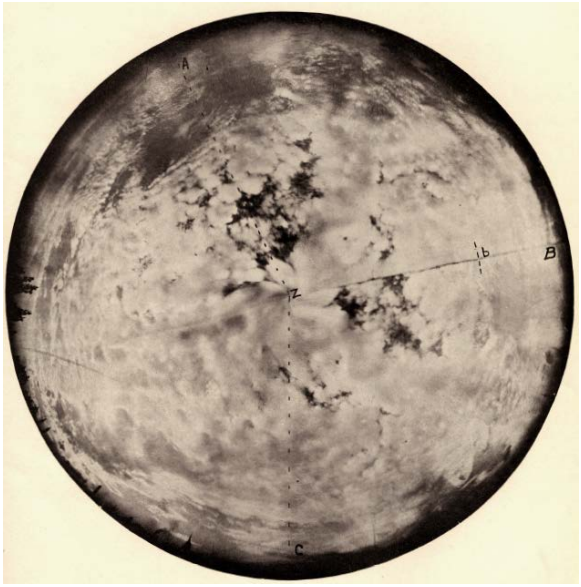

Figure 93. Hemispheric cloud image from Mueller's camera.

In 1905, Wood hinted at the concept of a fisheye camera [134], but did not explicitly describe the concept until the second edition of his text in 1914 [135]. Wood not only described how a fish views the above-water world, but also demonstrated the concept, presenting sample images recording a full 180-degree hemisphere. An image from Wood's camera is shown in Figure 94.

Figure 94. Image from fisheye camera by Wood (circa 1914).

In 1922, Bond published details of how he eliminated the water from the Wood's fisheye camera, replacing it with a hemisphere of glass [136]. A problem with this design was that the image was produced on a hemispheric surface, making the camera less than useful at the time. Bond's optical concept is seen in Figure 95.

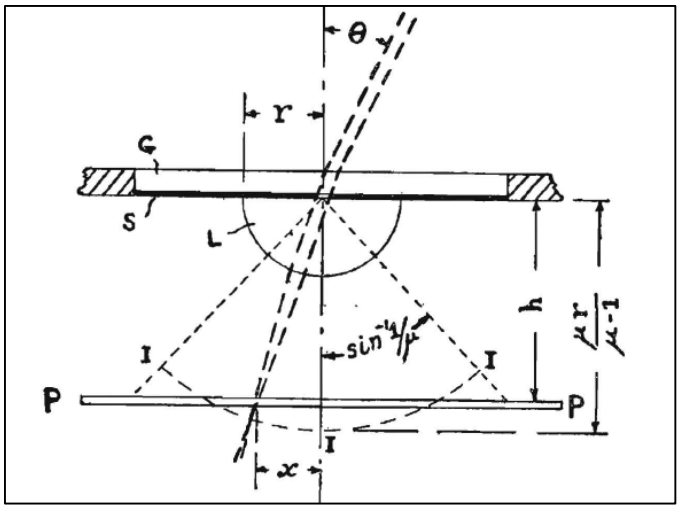

Figure 95. Bond's 1922 fisheye camera concept.

The greatest surprise found in the literature for fisheye lenses and whole sky imaging systems comes from 1923, when Bernhard Schmidt, who later would invent the famous Schmidt Camera, patented a lens systems with a 120-degree field of view [137]. The basic lens consisted of a plano concave, crown glass negative element mated with a convex flint glass positive element. The two lenses could fit together to form a planar slab of glass, but Schmidt realized that he could separate the lenses and put a unitary power relay optical system in between the two major elements to lengthen the lens and make the optical system more useful [138]. A drawing of Schmidt's near fisheye lens is seen in Figure 96.

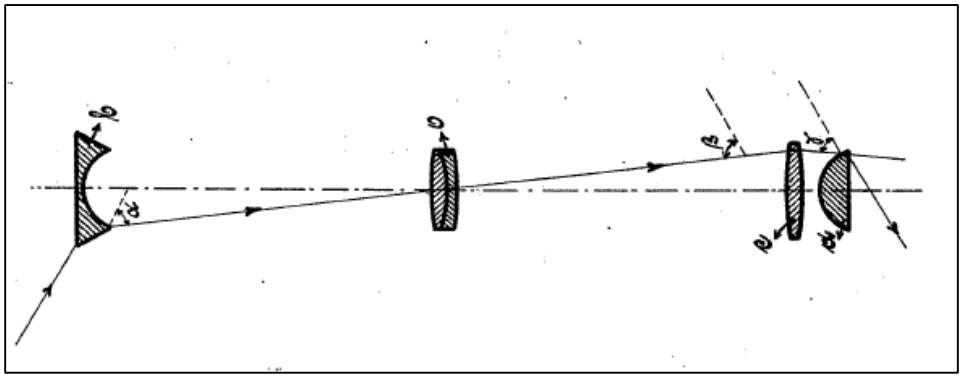

Figure 96. Schmidt's 120-degree lens of 1923 [137].

In 1924, Hill patented the design for the first true fisheye lens [139]. It could record an image of a full hemisphere and project it onto a flat focal surface, making it compatible with film and photographic plates. Hill describes the optical system and mentions the intended use for recording images of clouds [140]. An illustration of the Hill design is seen in Figure 97. From 1924 forward, the optical designs for many different fisheye lenses are found in the technical and patent literature. The first complex fisheye

design is seen in German patent 620,538 from 1935 [141]. This design more closely resembles modern fisheye lens layouts and imaged a field of 160 degrees. Since their invention, fisheye lenses have been used for everything from forest canopy studies [142] to satellite detection and tracking [143].

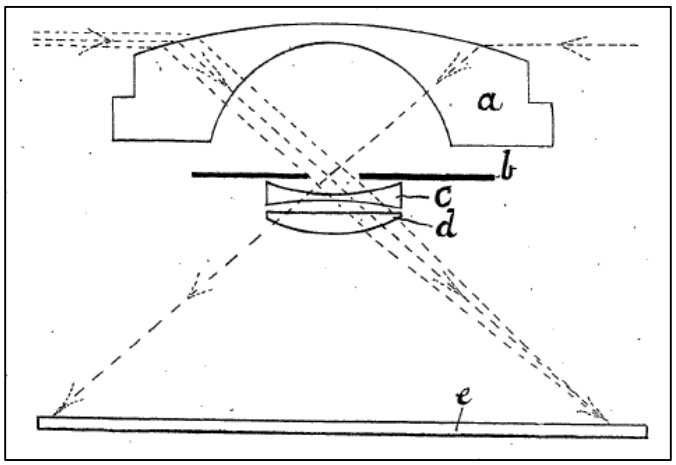

Figure 97. Optical design for Hill's fisheye lens [139].

The other approach to imaging the whole sky, or most of the visible sky, is to use a combination of lenses and mirrors. Reflective all-sky cameras come in three basic forms: one using a single concave mirror, another using a single convex mirror, and a third using two convex mirrors. The first mention of a wide field camera using a reflective mirror dates to 1911. This device was designed to capture a panoramic, but not a hemispherical image. It used a conventional camera pointed at a conical mirror [144].

The first mention of a whole sky imager using a convex mirror was during a 1929-1930 expedition to Greenland where Georgi required an optical system to capture images of the aurora [145]. The system used a conventional camera with a mirrored convex surface. A similar device was used in 1947 by Gartlein to photograph the aurora from multiple northern latitude sites. A picture of Gartlein's camera is seen in Figure 98.

Figure 98. Convex mirror whole sky camera used by Gartlein in 1947 [146].

In 1945, Henyey and Greenstein developed a 140-degree sky imager using a conventional camera lens pointed into a concave spherical mirror [147]. This device and several copies were used to record everything from meteor showers and the aurora, to simple star fields. A picture of the Henyey-Greenstein camera is shown in Figure 99, with an image from the camera shown in Figure 100.

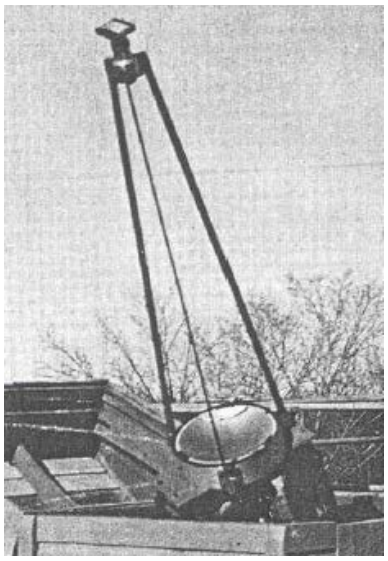

Figure 99. Concave reflecting all-sky camera by Henyey and Greenstein [148].

Figure 100. Image made with Henyey and Greenstein camera [148].

The whole sky camera based on a two convex mirrors was patented by Young in 1947 [149]. This system uses a conventional camera pointed up through a hole in the convex primary mirror. The camera stares into the convex secondary mirror. This approach is more compact than either of the single mirror concepts and has the advantage of minimizing the image of the camera seen in each frame. A drawing of the Young design is shown in Figure 101, with an image of an actual system seen in Figure 102.

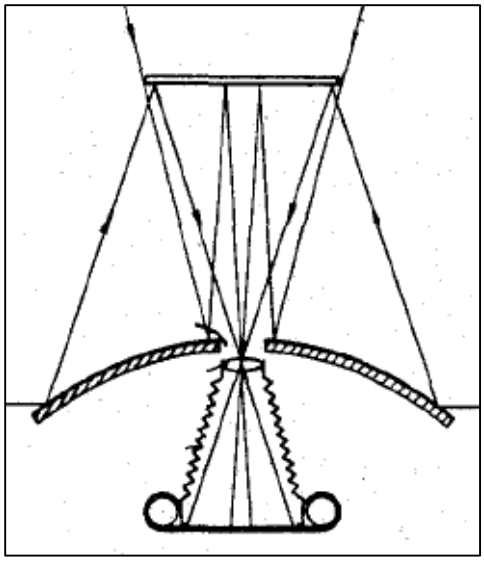

Figure 101. Young two-mirror whole sky camera [149].

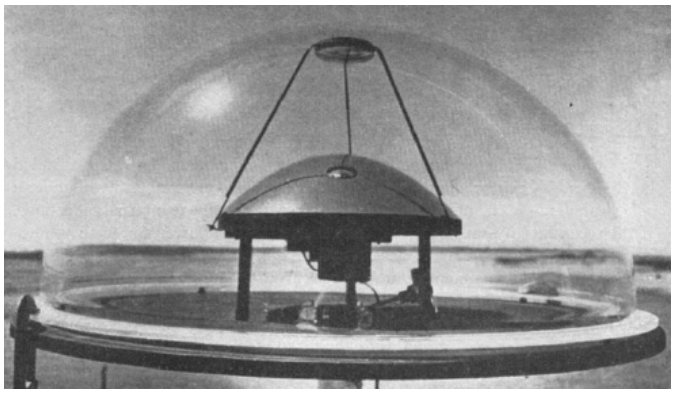

Figure 102. A functional example of a Young two-mirror whole sky camera [150].

Since the work of Georgi, Henyey and Greenstein, and Young, there have been many modifications of the reflective all-sky camera concept, but all of them are based on these three pioneering works. Most of the recent work has been focused on unfolding the highly distorted images to produce orthographic projections for sections of the hemispheric image.

A significant problem with fisheye lenses and reflective whole sky imagers is that their effective apertures are quite small. A typical fisheye lens will have an effective aperture of 10 mm or less, while reflective systems with large diameter mirrors will similarly have entrance pupils on the order of 10 mm. These systems simply do not admit much light. An alternate approach is to use a small array of wide angle camera lenses to cover all, or most, of the visible sky. The best example of such a system is the RAPTOR-Q developed at Los Alamos National Laboratory [6]. This system uses five 24 mm f/1.4 camera lenses with effective apertures of 17.14 mm, admitting nearly three times as much light as a typical fisheye lens or reflective whole sky camera. The individual images need to be stitched together, but with modern digital image processing, this task is trivial. A sample image from the RAPTOR-Q system is shown in Figure 103.

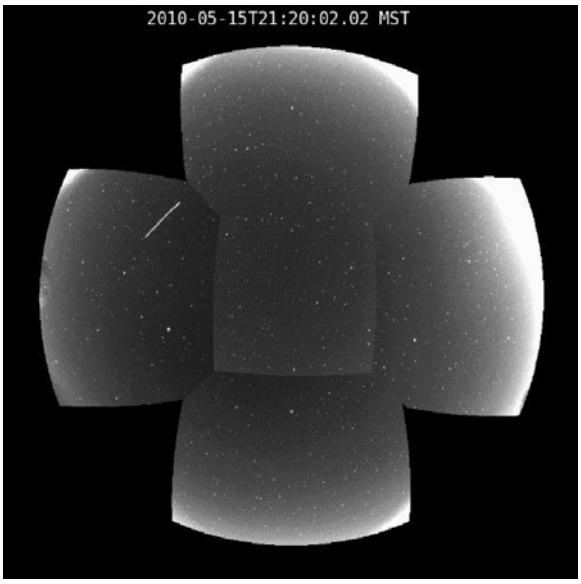

Figure 103. Image from the RAPTOR-Q system [151].

7.2 Cameras for Meteor and Aurora Photography

Phenomena such as meteor showers and aurora displays cover large parts of the sky, but they do not require a whole sky imaging system to record them. A number of optical systems were developed specifically for meteor photography, and a number of commercial wide-field lenses have been pressed into service for recording both meteors and the aurora. Perhaps the best known meteor camera is the Baker Super Schmidt with a 12.25-inch aperture and an 8-inch focal length [152]. These cameras could record a field of 53 degrees diameter with image quality higher than any comparable lens, but with the disadvantage of producing images onto a highly curved spherical surface. These cameras were optically faster and recorded a wider field than the Baker-Nunn satellite cameras, but had a smaller aperture and a more highly curved focal surface, making them more difficult to work with. The optical layout for a Baker Super Schmidt is shown in Figure 104. The achromatic Schmidt plate in the center of the system is aspheric, though not as much so as required for a classic Schmidt camera of equivalent aperture and focal ratio.

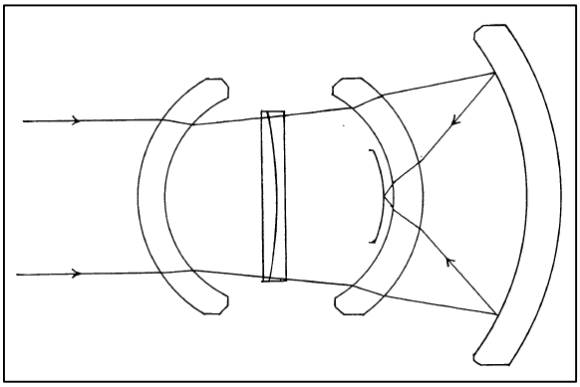

Figure 104. Optical layout of the Baker Super Schmidt meteor camera [153].

While the Baker Super Schmidt system has a respectable aperture for satellite tracking, the camera could not easily be adapted due to the highly curved focal surface. Past efforts to adapt CCD imagers to Baker-Nunn [154] and Schmidt cameras [155] with their more gentle curved focal surfaces have resulted in significant reductions in the useful field of view, to the point where other optical approaches are less expensive and more efficient. A recent optical system developed by Terebizh [156] can image a 45-degree field onto a spherical surface at f/2.5. While the spherical surface is still a problem for CCDs, the slower focal ratio eases the problem of locally flattening the image so that a mosaic of CCDs with different orientations could still capture a high quality image. The Terebizh design also has the advantage of requiring only one type of glass, and all spherical surfaces. At present, the Terebizh design has not been built.

The other approach for imaging large parts of the sky, without a whole sky camera, utilizes lenses. As meteors are fleeting targets, they require either large apertures or fast optical systems to render useful images on film. With CCD sensors, these restraints can be relaxed somewhat, but given the small size of pixels, modern systems require higher image quality from their lenses. When using film, two popular lenses were the Super Farron [157], with a 76 mm aperture, 30-degree field of view and a relative aperture of f/0.87; and the commercial Ross Xpress lens of 1.5-inch aperture, a 60-degree field of view and an f/4 relative aperture [153, 158]. Neither of these lenses produces sufficient image quality to justify adapting them to CCD sensors. Attempts to develop designs for modern lenses with parameters similar to those of the Super Farron result in only slight improvement.

7.3 Whole Sky Imaging Systems for Space Surveillance

Whole sky cameras do not need to be deployed in arrays. A single system can image the entire visible sky from a given site. Instead of arrays, we find networks of individual systems employed for fireball (meteor) monitoring and weather observations. The utility of such systems for space surveillance is just beginning to be explored.

One of the significant limitations of whole sky imagers is their small effective aperture. For space surveillance and satellite tracking, the small effective aperture results in lower sensitivity as individual pixels viewing wide areas of sky collect lots of background signal while faint targets contribute very little signal of their own. Optical models for a fisheye lens and a Henyey-Greenstein camera, both with 20 mm focal length and 10 mm aperture, were developed in Zemax and then used to assess the resulting sensitivity on a conventional DSLR class sensor. The results are essentially as one should expect. The fisheye lens performs slightly better than the reflective camera. The fisheye lens has more optical surfaces and air-to-glass interfaces to contend with, while the reflective camera suffers from a 10% loss of photons due to the single reflection. The results of simulations for both sidereal tracking (which makes no sense for a whole sky imaging system) and untracked staring mode are shown in Table 19.

Table 19. Sensitivity calculations for 10 mm aperture whole sky cameras.

		Limiting Magnitude	Exposure Time (s)
Fisheye Lens	Sidereal Track	10.37	20
	Untracked	11.19	100
H-G Camera	Sidereal Track	10.36	20
	Untracked	11.18	100

One point of interest in Table 19 are the exposure times. These result from the time it would require a target spot to move across a single pixel. These long times tend to greatly reduce the overall data rate from a single site, but have no other real benefit. Shorter exposures are possible, but with a loss of sensitivity, unless some form of frame stacking is employed. The exposure times are an average across the field, as stars near the center move very slowly while stars near the edge will move more rapidly.

The huge advantage of a whole sky imaging system is that any target above its detection threshold is guaranteed to be observed. The disadvantage is that most of the targets observed are less than interesting. Lens arrays, while requiring more systems to capture an appreciable percentage of the sky, are significantly more sensitive and, hence, more useful for space surveillance.

8 Summary

Lens arrays offer many small observing programs the opportunity to put significant quantities of equipment into operation at a very low cost. As a result, we have seen a proliferation of observing projects using arrays of commercial cameras equipped with commercial photographic lenses. These systems perform well, but the convenience of low initial price and rapid availability comes with limitations. Unlike APO refractors, photographic lenses are not designed for the special demands of astrophotography. The designs are optimized for the multitude of demands required for general photography rather than serving as point designs for astronomy. Design compromises—including vignetting, bandpass narrowing, and chromatic weighting—all conspire to reduce sensitivity. The significant advantage of lens systems, however, is their ability to image fields wider than most, if not all, reflecting telescopes.

One alternative to commercial photographic lenses is to develop custom lenses specifically optimized for wide-field astronomical observation. These lenses can be designed with higher image quality, larger apertures, smaller relative apertures, and overall wider fields of view. Combining these improvements in a single optical system results in a significant improvement in sensitivity, with only a modest increase in cost.

While lens systems are attractive due to their small size and relative ruggedness, they are not the solution for all observing missions. When high sensitivity is required and continuous surveillance is not, arrays composed of smaller numbers of telescopes based on either catadioptric or medial designs appear to provide the most cost-effective solution. Specifically, many of the Russian designs developed by the master Russian optical physicist, Dr. Valery Terebizh, for the ISON program offer very wide fields of view with apertures larger than available commercial lens systems. These designs provide higher sensitivity without a significant increase in the number of systems necessary to cover the celestial region of interest.

References

[1] J.T. McGraw et al., “Lens Systems for Sky Surveys and Space Situational Awareness,” *Proceedings of the 2013 AMOS Technical Conference*, September 2013.

[2] D. Vukobratovich et al., “Design and Construction of an Astrometric Astrograph,” *Proceedings of the SPIE*, vol. 1752, ed. R. E. Fischer, W.J. Smith (December 1992).

[3] S. Vasilevskis, “Precision Obtainable with the 20-inch Carnegie Astrograph,” *Astronomical Journal*, vol. 62, no. 1248, number 4 (1957).

[4] D. Pollacco, “WASP Hunts Planets,” *Astronomy & Geophysics*, vol. 46, issue 1 (2005).

[5] *The Progressive Astro Imaging Group*, http://www.progressiveastroimaging.com, accessed May 2016.

[6] W.T. Vestrand et al., “The RAPTOR Experiment: A System for Monitoring the Optical Sky in Real Time,” *Proceedings of the SPIE*, vol. 4845 (2002).

[7] R.G. Abraham and Pieter van Dokkum, “Ultra-Low Surface Brightness Imaging with the Dragonfly Telephoto Array,” *Publications of the Astronomical Society of the Pacific (PASP)*, vol. 126, issue 935 (2014).

[8] Pamphlet from the Zijinshan Astronomical Observatory, Honghe Station, Purple Mountain Observatory, under the Chinese Academy of Sciences, 紫金山天文台中国科学院 (2011).

[9] I. Takahashi et al., “AROMA (AGU Robotic Optical Monitor for Astrophysical Objects),” *Advances in Astronomy*, vol. 2010 (2010).

[10] G. Pojmanski, “The All Sky Automated Survey,” arXiv:astro-ph/9712146v1 11 Dec 1997.

[11] *All-Sky Automated Survey for Supernovae*, http://www.astronomy.ohio-state.edu/~assassin/index.shtml, accessed May 2016.

[12] N.M. Law, “Exoplanets from the Arctic: The First Wide-Field Survey at 80 Degrees North,” arXiv:1211.1972, *The Astronomical Journal*, vol. 145, issue 3, id 8 (2013).

[13] A.J. Castro-Tirado et al., “The Burst Observer and Optical Transient Exploring System (BOOTES),” *Astronomy and Astrophysics Supplement Series* 138(3), 583–585 (1996).

[14] P. Jenniskens et al., “CAMS: Cameras for Allsky Meteor Surveillance to Establish Minor Meteor Showers,” *Icarus*, vol. 216, issue 1, 40-61 (2011).

[15] N.M. Law et al., “New Exoplanet Surveys in the Canadian High Arctic at 80 Degrees North,” *Ground-based and Airborne Telescope IV. Proceedings of the SPIE*, vol. 844, id 84445C (2012).

[16] W.T. Vestrand, Los Alamos National Laboratory (LANL), personal communication, July 2016.

[17] R. Rutten, “CONCAM - ING's All-Sky Camera,” *Newsletter of the Isaac Newton Group of Telescopes (ING Newsletter)*, no. 7 (2003).

[18] N.M. Law et al., “The Evryscope: The First Full-Sky Gigapixel-Scale Telescope,” *Proceedings of the SPIE*, vol. 9145, article id 91450Z (2014).

[19] S. Karpov et al., “FAVOR (FAst Variability Optical Registration) - Two-Telescope Complex For Detection And Investigation Of Short Optical Transients,” *Astronomische Nachrichten*, vol. 325, issue 6 (2004).

[20] A. Pal, “Design Concepts of the ‘Fly’s Eye’ All-Sky Camera System,” http://flyseye.net/static/tmp/doc/flydc-v02.pdf, accessed May 2016.

[21] *The HATNet Exoplanet Survey*, hatnet.org, accessed May 2016.

[22] И.Е. Молотов, НАУЧНАЯ СЕТЬ ОПТИЧЕСКИХ ИНСТРУМЕНТОВ ДЛЯ АСТРОМЕТРИЧЕСКИХ И ФОТОМЕТРИЧЕСКИХ НАБЛЮДЕНИЙ, «Известия Главной астрономической обсерватории в Пулкове» № 219, выпуск 1 (2009).

[23] J. Pepper et al., “The Kilodegree Extremely Little Telescope (KELT): A Small Robotic Telescope for Large-Area Synoptic Surveys,” *Publications of the Astronomical Society of the Pacific*, vol. 19, issue 858, arXiv:0704.0460 [astro-ph] (2007).

[24] H-S. Park et al., “Instrumentation of LOTIS--Livermore Optical Transient Imaging System: A Fully Automated Wide-Field-Of-View Telescope System Searching for Simultaneous Optical Counterparts of Gamma-Ray Bursts,” *Proceedings of the SPIE, Optical Astronomical Instrumentation*, ed. S. D’Odorico, vol. 3355 (1998).

[25] J.F.P Spronck et al., “MASCARA: Opto-Mechanical Design and Integration,” *Proceedings of the SPIE* vol. 9147, id 914756 (2014).

[26] E. Gorbovskoy et al., “Transient Detections and Other Real-Time Data Processing From Wide-Field Chambers MASTER-VWF Wide-Field Cameras,” *Advances in Astronomy*, arXiv:0907.1118 [astro-ph.IM] (2010).

[27] G. Beskin et al., “From TORTORA to MegaTORTORA—Results and Prospects of Search for Fast Optical Transients,” *Advances in Astronomy*, vol. 2010, id 171569 (2010).

[28] S. Karpov et al., “Wide and Fast. Status Update on FAVOR Project and MegaTORTORA System,” *Astronomical Society of India Conference Series*, vol. 7 (2012).

[29] S. Karpov et al., “Massive Photometry of Low-Altitude Artificial Satellites on Mini-MegaTORTORA,” *RevMexAA* (2015).

[30] O. Guyon et al., “The PANOPTES Project: Discovering Exoplanets with Low-Cost Digital Cameras,” *Proceedings of the SPIE* vol. 9145 (2014).

[31] H.J. Deeg, “PASS, a Permanent All Sky Survey for the Detection of Transits,” *Proceedings of the First Eddington Workshop on Stellar Structure and Habitable Planet Finding*, ESA SP-485 (2002).

[32] N. Risinger, “Photopic Sky Survey,” http://www.skysurvey.org/survey/, accessed May 2016.

[33] L. Mankiewicz et al., “Pi of the Sky Full System and the New Telescope,” *Revista Mexicana de Astronomía y Astrofísica (Serie de Conferencias)*, vol. 45 (2014).

[34] K.A. Alsubai et al., “The Qatar Exoplanet Survey,” *Acta Astronomica*, vol. 63, no. 4 (2013).

[35] *Robotic Optical Transient Search Experiment (ROTSE)* website, http://www.rotse.net/information/, accessed May 2016.

[36] *Sky Sentinel* website, http://goskysentinel.com/, accessed May 2016.

[37] Е.А. Гришин, Потенциальная роль оптико-электронных средств ОАО «НПК «СПП» в обнаружении и мониторинге опасных небесных тел, Presentations at the conference "Methods For Detection Of Dangerous Celestial Bodies," Moscow (2015).

[38] J. Dick et al., “Surveying for Debris in MEO with Optical Sensors,” 5th ESA Space Debris Conference (2009).

[39] R.A. Street et al., “SuperWASP: Wide Angle Search for Planets,” *Scientific Frontiers in Research on Extrasolar Planets, ASP Conference Series*, vol. 294 (2003).

[40] A. Finkbeiner, “Astronomy: Amateur Sky Survey Keeps It Simple,” *Science*, vol. 278, issue 5340 (1997).

[41] R. Alonso et al., “The Transatlantic Exoplanet Survey (TrES): A Review,” *Transiting Extrasolar Planets Workshop ASP Conference Series*, vol. 366 (2007).

[42] S.R. Kane et al., “Recent Results from the Wide Angle Search for Planets (WASP) Prototype,” *Scientific Frontiers in Research on Extrasolar Planets ASP Conference Series*, vol. 294 (2003).

[43] K. Onda et al., “Ultra Wide-Field Telescope WIDGET for Observing GRB,” *Nuovo Cimento-Societa Italiana di Fisica Sezione B*, vol. 121, issue 12 (2006).

[44] P.R. McCullough et al., “The XO Project: Searching for Transiting Extrasolar Planet Candidates,” *The Publications of the Astronomical Society of the Pacific*, vol. 117, Issue 834 (2005).

[45] I.S. Glass, “The Beginnings of Astronomical Photography at the Cape,” *Monthly Notes of the Astronomical Society of Southern Africa*, vol. 48 (1989).

[46] *English Mechanic and World of Science*, vol. 36, no. 922, 24 November 1887.

[47] D. Gill, “On photographs of the Great Comet (b) 1882,” *Monthly Notes of the Royal Astronomical Society*, vol. 43 (1882).

[48] The Royal Observatory at the Cape of Good Hope, https://www.facebook.com/Royal.Observatory.Cape/photos/, accessed July 2016.

[49] E. E. Barnard, “Photographs of the Milky Way and of Comets,” *Publications of Lick Observatory*, vol. 11 (1913).

[50] P. Ré, *E.C.* [sic] *Barnard's Photographs of the Milky Way and Comets*, http://www.astrosurf.com/re/barnard_book_1913.pdf, accessed July 2016.

[51] E.E. Barnard, "On Some Celestial Photographs Made with a Large Portrait Lens at the Lick Observatory," *Monthly Notes of the Royal Astronomical Society*, vol. 50 (1890).

[52] "The BRUCE Photographic Telescope," *Publications of the Astronomical Society of the Pacific*, vol. 5, no. 32 (1893).

[53] http://dasch.rc.fas.harvard.edu/telescopes/Aseries9.jpg, accessed July 2016.

[54] F.E. Ross, "A Wide-Angle Astronomical Doublet," *Journal of the Optical Society of America*, vol. 5, issue 2 (1921).

[55] W.F. van Altena, "The Double Astrograph of the Yale Southern Observatory," http://www.astro.yale.edu/vanalten/Astrograph.html, accessed July 2016.

[56] C.P. Goerz, "Photographic Objective," US Patent 635,472 (1899).

[57] W.L. Elkin, "The Velocity of Meteors from Photographs," *Astronomical Journal*, vol. 20, issue 469 (1899).

[58] W.L. Elkin, "Photographic Observations of the Leonids at the Yale Observatory," *Astrophysical Journal*, vol. 9 (1899).

[59] R. Hudec et al., "The Optical Transient Search in the Bamberg Southern Sky Survey: Preliminary Results," *Acta Polytechnica* vol. 52, no. 1 (2012).

[60] The Damon Telescopes from The Patrick Moore Collection, http://www.patrickmoorecollection.com/viewSlide.php?id=7007&gallerypage=1&category=134&search=harvard, accessed May 2016.

[61] *The Dutch Meteor Society* website, https://dmsweb.home.xs4all.nl/, accessed July 2016.

[62] R. Haas, "New Camera Battery," https://dmsweb.home.xs4all.nl/photo/haas_array.html, accessed July 2016.

[63] R. Reeves, "A Camera Cluster for Meteor Photography," http://www.robertreeves.com/cluster.htm, accessed July 2016.

[64] D.A. Kerr, "Derivation of the 'Cosine Fourth' Law for Falloff of Illuminance Across a Camera Image," issue 4 (2007), http://dougkerr.net/Pumpkin/articles/Cosine_Fourth_Falloff.pdf, accessed May 2016.

[65] M. Aggarwal et al., "On Cosine-fourth and Vignetting Effects in Real Lenses," *Proceedings of the Eighth IEEE International Conference on Computer Vision*, vol. 1 (2001).

[66] P. Angenieux, "Large Aperture Six Component Optical Objective," US Patent 2,701,982 (1955).

[67] A. Bravnicar, “The Light Giant – A Lens That Made History,” *Photo Journal*, September 4, 2012.

[68] T. Smith, “Principles and Methods of Calculating Telescope Objectives,” *Transactions of the Optical Society*, vol. 18, no. 4 (1917).

[69] K. Momiyama, “Large Aperture Ratio Photographic Lens,” US Patent 4,364,643 (1982).

[70] *Zemax, LLC*, http://www.zemax.com/, accessed May 2016.

[71] G.H. Smith et al., “Optical Designs for the Mars ’03 Rover Cameras,” *Proceedings of the SPIE, Current Development in Lens Design and Optical Engineering II*, vol. 4441, id 10.1117/12.449558 (2001).

[72] T. Steinich and B. Blahnik, “Optical Design of Camera Optics for Mobile Phones,” *Advanced Optical Technologies*, vol. 1, issue 1-2 (2012).

[73] *FLI (Finger Lakes Instrumentation)* website, http://www.flicamera.com, accessed May 2016.

[74] Leica Noctilux-M 50 mm f/0.95 ASPH, Leica Camera AG.

[75] S. Matsui, “Telephoto Lens System,” US Patent 4,062,630 (1977).

[76] T. Ito, “Optical System, Optical Apparatus, and Method for Manufacturing Optical System,” US Patent Application Publication, US 2012/0050872 (2012).

[77] F. Faedi et al., “New Transiting Exoplanets from the Superwasp-North Survey,” *Proceedings IAU Symposium No. 276*, ed. A. Sozzetti, M.G. Lattanzi, A.P. Boss (2010).

[78] F. Faedi and D. Pollacco, *SuperWASP*, http://www.mpe.mpg.de/events/ropacs-2012/Talks/Pollacco_SWASP_RoPACS.pdf, accessed May 2016.

[79] H.D. Taylor, “Description of a Perfectly Achromatic Refractor,” *Monthly Notes of the Royal Astronomical Society*, vol. 54 (1894).

[80] H.D. Taylor, “Object Glass for Telescopes,” US Patent 540,339 (1895).

[81] H.D. Taylor, “Telescope Objectives for Photographic Purposes,” *Monthly Notes of the Royal Astronomical Society*, vol. 53 (1893).

[82] H.F. Newall, “Notes on Some Photographs Taken with a Visual Telescope,” *Monthly Notes of the Royal Astronomical Society*, vol. 54 (1894).

[83] E.C. Pickering, “New Form of Construction of Object-Glasses Intended for Stellar Photography,” *Nature*, October 13, 1887.

[84] P. Moore, “Refracting Telescopes,” *Encyclopedia of Astronomy and Astrophysics*, Nature Publishing Group and Institute of Physics Publishing (2001)

[85] H.D. Taylor, “Lens,” US Patent 568,052 (1896).

[86] Celestron, LLC, personal communication, January 2016.

[87] Dallmeyer, “Improvements Relating to Photographic Lenses,” British Patent 24,720 (1900).

[88] L.M. Rutherford, “Astronomical Photography,” *American Journal of Science and Arts*, Second Series, Vol. 39, May 1865.

[89] A. Nagler, “Multi-Purpose Telescope,” US Patent 4,400,065 (1983).

[90] FSQ-106, *Quadruplet Fluorite Apochromatic Refractor, Instruction Manual*, Takahashi.

[91] A. Ashford, “Telescope Service 65mm f/6.5 Quadruplet Astrograph Refractor,” ScopeTest.com, http://www.nightskies.net/scopetest/scopes/telescope_service/apo65q.html, accessed May 2016.

[92] http://blogs.yahoo.co.jp/fmasa_database/38275989.html, accessed May 2016.

[93] http://www.vixenoptics.com/Vixen-VSD-100mm-f-3-8-Astrograph-p/26145.htm, accessed May 2016.

[94] http://www.stjarnhusetonline.se/magnify/1932.3.html, accessed May 2016.

[95] Borg ED f/4 Focal Reducer [7704], http://www.sciencecenter.net/hutech/borg/techdocs/7704.pdf, accessed May 2016.

[96] http://www.astronomyalive.com.au/quickview/index/view/path/telescopes/professional/sky-rover-ult-80-ed-glass-sextuplet-fully-flat-field-apo-astrograph-refractor-telescope.html, accessed July 2011.

[97] http://www.stellarvue.com/stellarvue-130-mm-f-5-apo-sextuplet-astrograph-3-tcf-3-focuser-svs130-tcf3/, accessed July 2016.

[98] Apochromatic Objective, WO 2008/002188 A1 (2008).

[99] S. Kharusi, Shoot-out: TV-60is vs Canon 400mm/5.6L, http://www.samirkharusi.net/tv60_canon.html, accessed May 2016.

[100] S. Kharusi, Televue APO Refractor vs Canon Supertele, http://www.samirkharusi.net/televue_canon.html, accessed May 2016.

[101] Canon 135mm f/2 L EF L USM (1996-today), http://kenrockwell.com/canon/lenses/135mm-f2.htm, accessed June 2016.

[102] S. Takahashi, “Telephoto Lens of Large Aperture Ratio,” US Patent 4,852,984 (1989).

[103] J.T. McGraw & Associates, June 2016.

[104] J. Tonry, University of Hawaii, Institute for Astronomy, personal communication, March 2016.

[105] M.R. Ackermann et al., “Blind Search for Micro Satellites in LEO: Optical Signatures and Search Strategies,” *Proceedings of the 2003 AMOS Technical Conference*, also published as SAND2003-3225C, Sandia National Laboratories, Albuquerque, NM (2003).

[106] T.P. Grayson, “Curved Focal Plane Wide Field of View Telescope Design,” *Proceedings of the SPIE*, vol. 4849 (2002).

[107] M.W. Richmond et al., “TASS Mark III Photometric Survey of the Celestial Equator,” *Publications of the Astronomical Society of the Pacific*, vol. 112 (2000).

[108] http://lfvn.astronomer.ru/news/2008/10/0001/index.htm, accessed July 2016.

[109] V.Yu. Terebizh, personal communication, July 2016.

[110] V.Yu. Terebizh, personal website, http://www.terebizh.ru/V.Yu.T/pictures/vt-53e/, accessed July 2016.

[111] Japanese Patent 1992078805, 100 SDUF APO Refractor Telescope (1992).

[112] A.G. Clark, “Photographic Lens,” US Patent 399,499 (1889).

[113] Lens design courtesy of J.T. McGraw & Associates, Placitas NM (2016).

[114] *Ohara I-Line Optical Glass*, http://www.oharacorp.com/iline.html, accessed July 2016.

[115] *Pierro-Astro*, http://www.pierro-astro.com/tsoptics/lunette-astrographe-ts-imaging-star-102_detail, accessed July 2016.

[116] R.A. Sampson, “On Correcting the Field of a Newtonian Telescope,” *Monthly Notes of the Royal Astronomical Society*, vol. 73 (1913).

[117] R.A. Sampson, “On a Cassegrain Reflector with a Corrected Field,” *Proceedings of the Royal Society of London, Series A, Containing Papers of a Mathematical and Physical Character* 88.602 (1913).

[118] M. Paul, *Revue d’Optique Théorique Instrumentale*, vol. 14, no. 5, p. 169 (1935).

[119] B. Schmidt, *Mitteilungen Hamburger Sternwarte in Bergedorf*, 7 (36), 15 (1930).

[120] A.A. Wachmann, *Sky & Telescope*, vol. 15, no.1, 4 (1955).

[121] J.L. Houghton, “Lens System,” U.S. Patent 2.350,112 (1944).

[122] R. Richter, *Deutsche Patentanmeldung* (Zeiss) Z 26 592 IXa 42h (5.9.1941).

[123] V.Yu. Terebizh, *Bulletin of the Crimean Astrophysical Observatory*, vol. 97 (2001).

[124] W.F. Hamilton, British Patent 3781, February 12, 1814.

[125] I. Newton, *The Correspondence of Isaac Newton, Volume I, 1661-1675*, ed. H.W. Turnbull and J.F. Scott, Cambridge University Press, Cambridge (1959).

[126] V.Yu. Terebizh, “On the Capabilities of Survey Telescopes of Moderate Size,” preprint (arXiv:1602.02904), pending publication in the *Monthly Notes of the Royal Astronomical Society* (2016).

[127] I. Molotov et al., “Recent Developments within the ISON Project,” Scientific and Technical Subcommittee: 2016, 53rd session (15-26 February 2016), Vienna, Austria.

[128] X. Yuan et al., “Chinese Small Telescope ARray (CSTAR) for Antarctic Dome A,” *Proceedings of the SPIE*, vol. 7012 (2008).

[129] X. Yuan and D.-Q. Su, “Optical System of the Three Antarctic Survey Telescopes,” *Monthly Notes of the Royal Astronomical Society*, 424 (2012).

[130] F. Wright, “An Aplanatic Reflector with a Flat Field Related to the Schmidt Telescope,” *Publications of the Astronomical Society of the Pacific*, vol. 47, no. 280 (1935).

[131] C.K. Seyfert, “The Baker-Schmidt Telescope of the Arthur J. Dyer Observatory,” *Mitteilungen der Astronomischen Gesellschaft*, vol. 7 (1956).

[132] C. Koppe, Photogrammetrie und Internationale Wolkenmessung, Braunschweig, Germany: Druck und Verlag von Friedrich Vieweg und Sohn. (1896).

[133] Q.L. Fassig, “A Revolving Cloud Camera,” *Monthly Weather Review*, 43 (1915).

[134] R.W. Wood, *Physical Optics*, MacMillan, New York (1905).

[135] R.W. Wood, *Physical Optics*, MacMillan, New York (1914).

[136] W.N. Bond, “Wide Angle Lens for Cloud Recording,” *Philosophical Magazine and Journal of Science*, vol. 44, Sixth Series (1922).

[137] B. Schmidt, German Patent 384,879 (1923).

[138] W. Busch, “A Little-Known 3-Lens Catadioptric Camera by Bernhard Schmidt,” *Journal of Astronomical History and Heritage*, 16 (2013).

[139] R. Hill, Improvements in Photographic Lenses, GB Patent 225,398 (1924).

[140] R. Hill, “A Lens for Whole Sky Photographs,” *Quarterly Journal of the Royal Meteorological Society*, vol. 50 (1924).

[141] German Patent 620,538 (1935).

[142] H.E. Brown, *The Canopy Camera*, Colorado State University, Fort Collins, No. 72 (1962).

[143] W.J. Mandeville, “Visible Cloud Imager for Autonomous Telescopes,” *Proceedings of the AMOS Technical Conference* (2015).

[144] L.H. Kleinschmidt, Apparatus for Producing Topographic Views, US Patent 994,935 (1911).

[145] J. Georgi, “The Photographic Sky-Mirror,” *Weather*, vol. 12 (1933).

[146] C.W. Gartlein, “Unlocking Secrets of the Northern Lights,” *National Geographic* (1947).

[147] L.G. Henyey, *Miscellaneous Optical Designs*, OSRD Report No. 4505, Yerkes Optical Bureau. University of Chicago (1945).

[148] W. Sheehan, “W.W. Morgan and the Discovery of the Spiral Arm Structure of our Galaxy,” *Journal of Astronomical History and Heritage*, vol. 11 (2008).

[149] W.A. Young, Wide Angle Optical System, US Patent 2,403,595 (1947).

[150] W.S. von Arx, “Synoptic Photography,” *Weather*, Vol. 13 (1958).

[151] J. Wren, “A Portable Observatory for Persistent Monitoring of the Night Sky,” *Proceedings of the SPIE*, vol. 7737 (2010).

[152] J.G. Baker, Schmidt Image Former with Spherical Aberration Corrector, US Patent 2,458,132 (1949).

[153] J. Davis, “The Design and Performance of Three Meniscus Schmidt Meteor Cameras,” *Quarterly Journal of the Royal Astronomical Society*, vol. 4 (1963).

[154] O. Fors, “The Fabra-ROA Baker-Nunn Camera at Observatori Astron`omic del Montsec: A Wide-Field Imaging Facility for Exoplanet Transit Detection,” arXiv:0912.0796v1 (2009).

[155] J.A. Snyder, “QUEST Camera I: A 67 Megapixel CCD Camera Optimized for a Driftscan Quasar Search,” *Proceedings of the SPIE*, vol. 3355 (1998).

[156] V.Yu. Terebizh, “All-Spherical Telescope with Extremely Wide Field of View,” arXiv:1602.02370 (2016).

[157] G.A. Harvey, *A Description of Four Fast Slitless Spectrographs*, NASA TN D-4145 (1967).

[158] R. Kingslake, *A History of the Photographic Lens*, Academic Press (1989).

Distribution

External Distribution:

Max Williams, Colorado Springs, CO — cmaxwilliams@msn.com (electronic copy)

Dr. John Tonry, University of Hawaii — jt@IfA.Hawaii.Edu (electronic copy)

ODNI/ICSSG
- MGen (ret) Richard O'Lear, ODNI/ICSSG — RICHAJO3@ucia.gov (electronic copy)
- George Graveson, ODNI/ICSSG — george.graveson@dni.gov (electronic copy)

Mr. Chris Higgins, AFSMC/SYGO — james.higgins@us.af.mil (electronic copy)

Dr. Robert Peterkin, AFRL/RD — robert.peterkin@us.af.mil (electronic copy)

Dr. Susan Lederer, NASA JSC — susan.m.lederer@nasa.gov electronic copy)

LtCol Andy Dills, AFSPC/STA — anthony.dills@us.af.mil (electronic copy)

Mitre Corp.
- Mr. Mike Dearborne, Mitre Corp — mdearborn@mitre.org (electronic copy)
- Mr. Derek Ho, Mitre Corp — derekho@mitre.org (electronic copy)

LtCol Brian Smith, USAFA/DFP — brian.smith@usafa.edu (electronic copy)

Internal Distribution

1	MS0421	Jon Rogers	0153 (electronic copy)
1	MS0980	Prabal Nandy	5553 (electronic copy)
1	MS0980	Drew Woodbury	5553 (electronic copy)
1	MS0980	Steve Gianoulakis	5550 (electronic copy)
1	MS0899	RIM-Reports Management	9532 (electronic copy)


Sandia National Laboratories